SIMULATING THE LOW-PRESSURE DIRECT INJECTION SYSTEM OF A HYDROGEN-FUELED ENGINE

WENCHAO JIAO

Department of Maritime and Transport Technology
Faculty of Mechanical Engineering
Delft University of Technology (TU Delft)

August 2024

Wenchao Jiao: *Simulating the low-pressure direct injection system of a hydrogen-fueled engine* © August 2024

SUPERVISORS:
Prof.dr.ir. P. de Vos & Ir. E. S. Van Rheenen

LOCATION:
Delft, South Holland, the Netherlands

TIME FRAME:
November 2021 – August 2024

The thesis is typeset in LaTeX 2ε with hypertext to prepare the references, abbreviations, figures and tables.

An electronic version of the thesis is available at TU Delft Repository.

SIMULATING THE LOW-PRESSURE DIRECT INJECTION SYSTEM OF A HYDROGEN-FUELED ENGINE

WENCHAO JIAO

in partial fulfillment of the requirements for the degree of

Master of Science
in Marine Technology

with the specialization
of Marine Engineering

at the Delft University of Technology;

to be defended publicly on
Wednesday August 28st, 2024 at 12:45 p.m. (CEST).

Student number:	5494370	
Report number:	MT.23/24.043.M	
Thesis Committee:	Prof.dr.ir. P. de Vos,	TU Delft, chair
	Ir. E. S. Van Rheenen,	TU Delft, supervisor
	Prof.dr.ir. H. Polinder,	TU Delft, member

This page intentionally left blank

ABSTRACT

To more effectively reduce carbon emissions from ships during operation, utilizing hydrogen as a fuel for ship engines has emerged as a promising direction. Given the unique physical properties of hydrogen, targeted modifications to existing engines are necessary for adaptation. In hydrogen-fueled engines, the injection system is a critical component. This study aims to adjust the design parameters of a novel injector to match large two-stroke ship engines and to theoretically demonstrate the feasibility of this novel injector for use in large two-stroke engines fueled by hydrogen.Currently, the majority of hydrogen-fueled engines are four-stroke engines, typically employing high-pressure injection. However, high-pressure injection tends to shorten the lifespan of the injection system, consequently reducing the overall lifespan of the engine. Therefore, this study proposes a low-pressure injection scheme, combined with in-cylinder direct injection, to mitigate the risk of unintended ignition. Given the high autoignition temperature of hydrogen, spark ignition is employed to facilitate ignition. A critical step in evaluating feasibility is determining the appropriate injection timing.Initially, it was established that hydrogen should be injected after the commencement of the compression stroke to achieve optimal mixing. Subsequently, the study analyzed the in-cylinder pressure variations during the compression stroke to identify the feasible injection window. Finally, the design parameters of the injector were configured to align with these conditions. The findings theoretically demonstrate that this injector can achieve low-pressure direct injection in large two-stroke hydrogen engines.Due to time constraints, the study did not investigate the effects of different injection angles and positions on the engine. Nonetheless, the theoretical analysis confirms the feasibility of employing low-pressure direct injection in large two-stroke hydrogen engines.

Keywords: Hydrogen,Injection strategy,Low Pressure Injection,Direct Injection,Crank Angle,Two Stroke Engine,Pneumatic Valve

CONTENTS

LIST OF FIGURES

This page intentionally left blank

LIST OF TABLES

This page intentionally left blank

NOMENCLATURE

Latin symbols

P	pressure	[bar]
R	specific gas constant of hydrogen	$[J/kg \cdot K]$
T	temperature of hydrogen	[K]
V_0	the initial volume of the actuator cylinder	$[cm^3]$
V_1	the volume after the valve plate lifted to the maximum value	$[cm^3]$
m	mass of hydrogen	[kg]
t	time	[ms]
$\dot{m}_{in}$	the mass flow passing the refilling orifice	[kg/ms]
$\dot{m}_{out}$	the mass flow passing the ball valve	[kg/ms]
$\dot{m}_{static}$	the static mass flow	[kg/ms]
$A_{eff,RO}$	the cross-sectional area of the refilling orifice	$[mm^2]$
$A_{eff,BV}$	the cross-sectional area of the ball valve	$[mm^2]$
P_{sup}	the supply pressure	[bar]
P_{cyl}	the cylinder pressure	[bar]
d_1	the diameter of the actuator cylinder	[mm]
D	the diameter of the curtain area	[mm]
F_{sup}	the pressure difference between the supply pressure and the actuator cylinder pressure	[N]
$F_{suction}$	the suction force	[N]
F_{spring}	the spring force	[N]
s	the spring force	[N]
k	the spring stiffness	[N/m]
L_0	the compressed spring length to maintain the preload force	[N/m]

h	the lift height of the valve plate	[mm]
h_{max}	the maximum lift height of the valve plate	[mm]
V_h	the displacement per cylinder	[m^3]
H_u	the lower heating value of hydrogen	[MJ/kg]
$\triangle t_{inj}$	the available injection window time	[ms]
n	the engine speed	[rpm]
A_{ref}	the reference flow cross-sectional area	[mm^2]
C_D	the discharge coefficient	[−]
$A_{curtain}$	the curtain area	[mm^2]
d	the nozzle diameter	[mm]
$\triangle r$	the radial width of the contact area	[mm]
P_b	the brake power of the engine	[kw]
$\dot{Q}_f$	the heat flow of the fuel	[kJ]
h^L	the lower heat value of the fuel	[kJ/kg]
$\dot{m}_f$	the fuel flow	[kg/h]
W_e	the efficiency work	[kJ]
f	the cycle frequency of the engine	[Hz]
V_s	the stroke volume	[m^3]
V_{TDC}	the stroke volume of top dead center	[m^3]
V_{BDC}	the stroke volume of bottom dead center	[m^3]
r_C	the effective compression ratio of the engine	[−]

Greek symbols

α	engine crank angle	[dCA]
ψ	the isentropic flow function	[−]
ψ_{max}	the maximum isentropic flow function	[−]
κ	the specific heats ratio of hydrogen	[−]
ω_i	the indicated specific piston work	[kJ]
η_i	the indicated engine efficiency	[−]
$\triangle \alpha_{inj}$	the available injection crank angle	[dCA]
η_e	the effective engine efficiency	[−]

ϵ	the geometric compression Ratio of the engine	$[-]$

This page intentionally left blank

MAIN BODY

1

INTRODUCTION

1.1 BACKGROUND

As an essential mode of cargo transportation, maritime transportation has profoundly affected human industrial and economic development, with 90% of global trade completed[1]. Although the carbon emissions caused by maritime transport are smaller than those of other industries on land, as the scale of shipping expands, the amount of carbon emissions it brings becomes increasingly difficult to ignore. At the same time, the International Maritime Organization (IMO) has carried out many studies to reduce and control carbon emissions during ship transportation. It has proposed a goal of reducing carbon emissions to near zero by 2050. Figure 1.1 shows the distribution of carbon emissions generated by transportation in 2022.

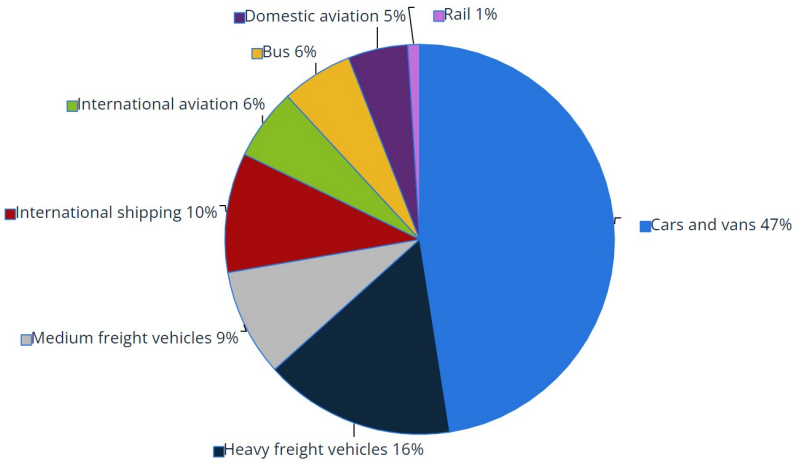

Figure 1.1: Distribution of carbon dioxide emissions produced by the transportation sector worldwide in 2022[2]

It can be seen that the carbon emissions generated by ship transportation account for 10%, and with the end of COVID-19, which indicates world trade is recovering. Presumably, shipping activities will also increase, and carbon emissions will also increase. At the same time, major shipowners and ports have also established their own decarbonization goals. For example, Maersk has set the goal of achieving carbon neutrality by 2050 and placed orders for several LNG container ships this year to demonstrate its decarbonization[3]. Mediterranean Shipping Company has decided to have 14 new ships adapted to various low-carbon fuels by 2022[4]. It can be observed that the low-carbon measures taken by several shipping giants in the world involve using new clean fuel, as can be seen from the Figure 1.2 and Figure 1.3: the optimization of ship power systems, such as the use of all-electric propulsion or low-carbon fuels, can significantly reduce carbon emissions caused by shipping. This reduction is crucial because the main component of greenhouse gases produced by ships during shipping is carbon dioxide. So, to achieve the goal of carbon neutrality in 2050, using LNG ships is a good way, but there will eventually be carbon emissions, and the most effective way is to use carbon-free fuels, such as hydrogen.

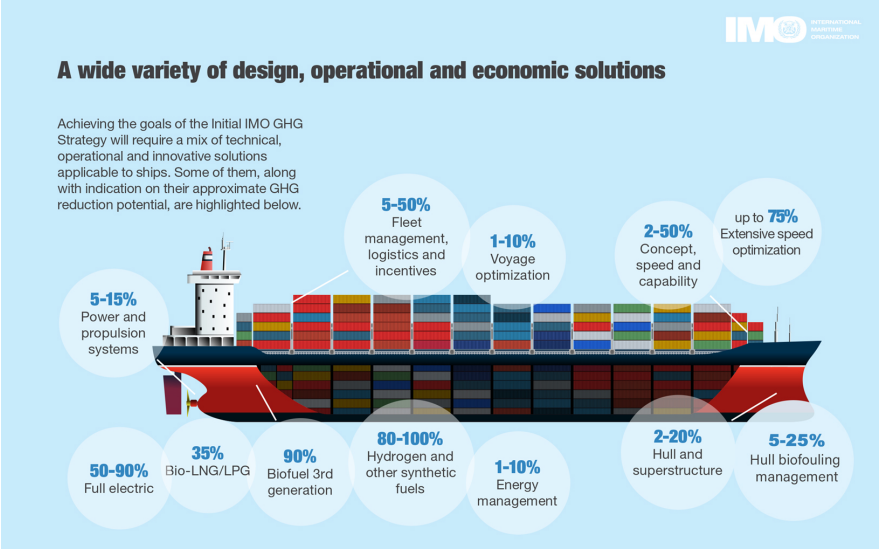

Figure 1.2: IMO's work to cut GHG emissions from ships[5]

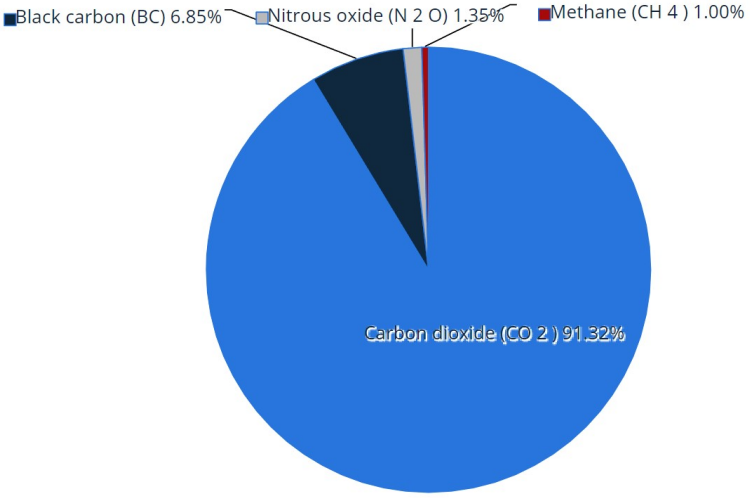

Figure 1.3: GHG emissions produced by the global shipping industry[2]

The benefits of using hydrogen as a fuel are apparent. The most significant advantage is that hydrogen does not produce carbon emis-

sions. The product is only H_2O when hydrogen is used in a fuel cell[6]. Moreover, hydrogen contains a lot of energy. Under the same unit mass of energy, hydrogen has a LHV of 120 $120 MJ/Kg$ and higher than other traditional fuel.[7], which can meet the demand for power and the requirements of environmental regulations. However, when hydrogen is used in fuel cells, some shortcomings prevent hydrogen fuel cells from being accepted by the public. The main reason is that compared with hydrogen fuel cells, internal combustion engines have better stability, secondly, they have higher energy density, and finally, and most importantly, they are more cost-effective.[8]. Moreover, PEM fuel cells have incredibly high hydrogen purity requirements, requiring high purity as high as 99.9%. When hydrogen is used as a fuel for internal combustion engines, mainly when used as a fuel for ship engines, high LHV and zero carbon emissions will show great advantages. Of course, certain modifications to the engine control components are needed to adapt to the properties of hydrogen. Compared to other alternative fuels such as ethanol, methanol, biodiesel, and natural gas, which can all reduce carbon emissions to varying degrees, hydrogen as an energy carrier has the advantage of not producing hydrocarbons. Additionally, its inherently fast combustion rate can enhance engine efficiency. Hydrogen also has a broad flammability range, allowing it to mix with air in different ratios for combustion in engines. This versatility helps in meeting stringent emission regulations more effectively.[9] Still, the zero-carbon emissions of hydrogen fuel and the mature technology of internal combustion engines will undoubtedly become a promising development direction in the future.

1.2 RESEARCH MOTIVATION

> ***"Decarbonizing international shipping is a priority issue for IMO and we are all committed to act together in achieving the highest possible ambition[10]."***

To achieve decarbonization goals, marine diesel engines often have three ways to reduce carbon emissions: alternative fuels, exhaust

gas after-treatment, and in-cylinder purification[11]. It can also be seen from the above that using alternative fuels, such as carbon-free fuels, can more effectively reduce carbon emissions. Hydrogen fuel has better fuel characteristics and does not produce carbon emissions, meeting the requirements of international regulations[12]. There are also many studies on hydrogen fuel engines. Due to the characteristics of hydrogen fuel itself, the current mainstream strategy for hydrogen fuel engines is to use high-pressure port injection and spark plug ignition[13]. This method can achieve higher power density but produces backfiring, knocking, and other undesirable phenomena. To avoid such problems, this study uses a low-pressure direct injection hydrogen fuel engine[14]. Comparing the optimized hydrogen engine with the original engine proves the vast potential of the low-pressure direct injection hydrogen fuel engine.

1.3 RESEARCH OBJECTIVES

The research goal is to simulate the low-pressure direct injection system of a hydrogen-fueled engine, in which the low-pressure direct injection system is the key and the injection process will be the focus of the research. Due to the direct injection strategy, the mixing uniformity of hydrogen and air will be affected, and some parameters will have a more significant impact on the mixing uniformity, such as injection timing, injection pressure, injector location, injector orientation, and injection strategy. However, due to the variety of these parameters, evaluating all permutations and combinations in a short period is almost impossible. To simplify the model and facilitate the research, a fixed injection pressure, injector position, and angle will be used, and the focus will be on the injection timing and strategy.To simulate different injection timing and strategies, the to-be-developed model will simulate the physical processes of hydrogen low-pressure injection into a WinGD x92DF engine, using the results of Wittek paper.[14]

This page intentionally left blank

2

LITERATURE REVIEW

This chapter primarily describes the inherent properties of hydrogen, the ignition and injection methods currently employed when using hydrogen in internal combustion engines, and discusses the advantages and disadvantages of different methods. It also addresses various engine issues encountered during the application process. Subsequently, the chapter explains why the low-pressure direct injection method is adopted in the design of a hydrogen-fueled two-stroke engine.

2.1 THERMOPHYSICAL PROPERTIES OF HYDROGEN AS FUEL FOR INTERNAL COMBUSTION ENGINES

Hydrogen is a colorless and odorless gas that is non-toxic to the human body. When burned, it produces water and a lot of heat and does not produce carbon emissions. Some of the critical properties of hydrogen have a crucial impact on the design of hydrogen fuel engines. The following table compares the properties of hydrogen with other traditional fossil fuels.

Property	Hydrogen	Methane	Gasoline	Diesel
Carbon content(mass%)	0	75	84	86
Lower(net) heating value(MJ/kg)	119.9	45.8	43.9	42.5
Density(at 1 bar & 273K;$\mathrm{kg\,m^{-3}}$)	0.089	0.72	730-780	830
Volumetric energy content(at 1 bar & 273K;MJ/M3)	10.7	33.0	33×10^3	35×10^3
Molecular weight	2.016	16.043	∼110	∼170
Boiling point(K)	20	111	298-488	453-633
Auto-ignition temperature(K)	853	813	∼623	∼523
Minimum ignition energy in air(at 1 bar & at stoichiometry;mJ)	0.02	0.29	0.24	0.24
Stoichiometry air/fuel mass ratio	34.4	17.2	14.7	14.5
Quenching distance(at 1 bar & 298K at stoichiometry;mm)	0.64	2.1	∼2	-
Laminar flame speed in air(at 1 bar & 298K at stoichioemetry;m/s)	1.85	0.38	0.7-0.43	0.37-0.43
Diffusion coefficient in air(at 1 bar & 273K;m^2/s)	8.5×10^{-6}	1.9×10^{-6}	-	-
Flammability limits in air(vol%)	4-76	5.3-15	1-7.6	0.6-5.5
Adiabatic flame temperature(at 1 bar & 298K at stoichiometry;K)	2480	2214	2580	∼2300
Octane number(R+M)/2	130+	120+	86-94	-
Cetane number	-	-	13-17	40-55

Table 2.1: Hydrogen properties compared with gasoline, diesel and methane[9]

As can be seen from the table, compared with other traditional fossil fuels, hydrogen has the following significant differences:

- Zero carbon content
- Extremely high lower heating value
- Extremely high auto-ignition temperature
- Very low density
- Laminar flames speed in air is extremely fast
- High stoichiometric air-fuel ratio
- The diffusion coefficient in the air is extremely high
- The flammability limit in air has a wide range

Hydrogen's zero carbon content and high lower heating value are the fundamental reasons it is used as an alternative energy source. This is also a considerable advantage of hydrogen compared to other fossil fuels. Hydrogen has the highest mass-to-energy ratio among chemical fuels. It is three times that of traditional gasoline and more than five times that of alcohol[15]. Due to the high diffusivity of

hydrogen in the air and the extremely fast laminar flame speed, hydrogen can be burned faster during combustion, thereby providing better combustion efficiency and cycle changes over a wide range within the cylinder.

However, when pure hydrogen is used as fuel, due to its extremely low density, the energy density of the hydrogen and air mixture in the engine cylinder is reduced, which results in a reduction in engine output power, which is unacceptable for heavy-duty. The current measures to eliminate the negative effects of hydrogen's extremely low density are generally to pressurize hydrogen fuel to increase its energy per unit volume and output power[16]. The auto-ignition temperature of hydrogen is 853K, which is significantly higher than other fossil fuels. An external auxiliary ignition device makes the mixture of hydrogen and air easier to ignite. Engines have two main ignition methods: spark ignition and compression ignition. Spark ignition is more suitable, but often, spark ignition requires a control component such as a spark plug, which is an easily damaged component in heavy-duty engines and will increase maintenance and management costs. If compression ignition is selected, the maximum compression ratio of the hydrogen fuel engine needs to be determined by the temperature rise relationship of the compression process and the compression ratio.In this study, spark ignition will continue to be used, while compression ignition will remain under theoretical exploration. This topic will be discussed in the engine verification chapter, where the reasons for not choosing this method will be provided.

2.2 IGNITION METHODS

2.2.1 *Spark ignition*

The purpose of using spark ignition to ignite hydrogen fuel is to avoid the effects of hydrogen's extremely high auto-ignition temperature. In a spark ignition engine, hydrogen has some properties conducive to combustion, which can be better utilized, such as fast laminar

flame speed, low ignition energy, and a wide range of flammability limits, all of which make hydrogen-fueled engines perform better than traditional fossil-fuel engines.

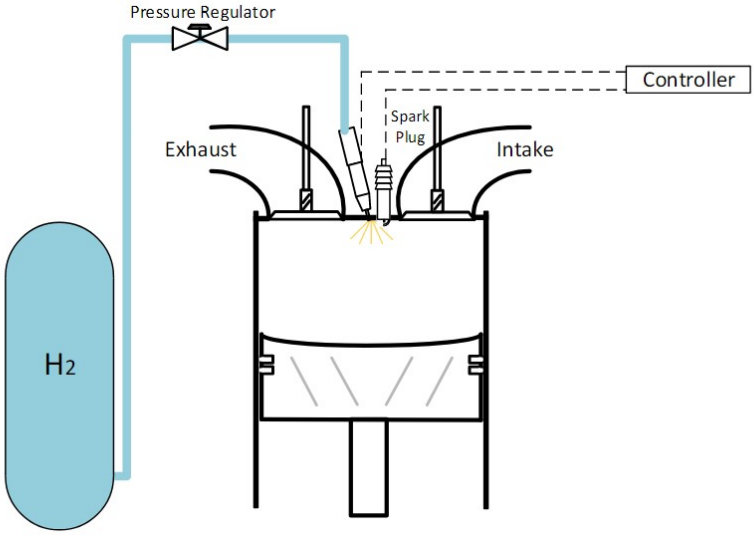

Figure 2.1: Spark-ignited hydrogen fuel internal combustion engine[1]

When hydrogen is mixed with air and injected into a spark-ignited engine cylinder, it can be burned there without requiring significant modifications to the engine. When using hydrogen as the fuel for spark-ignited engines, a homogeneous lean combustion strategy is often adopted, which can fully use hydrogen's wide flammability limit range to obtain a better combustion process. Due to the low density of hydrogen, the charging displacement needs to be increased, which will reduce output power. A turbocharging system needs to be used to pressurize the mixture of hydrogen and air to solve this problem[17].

Due to hydrogen's low ignition energy requirement and high combustion temperature, hydrogen is prone to engine knocking when operating in a spark-ignited engine, which will seriously affect the engine's performance and life[18]. The port injection method is often changed to direct injection, performed after the intake valve is

closed. But using spark ignition engines is not a good choice because the presence of spark plug components will increase the maintenance and management costs of the engine, and it can only be used under high speed and low torque conditions, and for low speed and high torque situations, such as ships engines, spark-ignited engines are not suitable.

2.2.2 *Compression ignition*

Compression ignition engines using pure hydrogen as fuel are still experimental and have not been fully commercialized. Hydrogen is mainly used as a diesel additive to reduce the use of diesel, reduce engine emissions, and improve engine efficiency and power output. There are many reasons for using hydrogen as a diesel additive in compression ignition engines. The fundamental reason is to change the overall C/H ratio of the fuel. Due to the high diffusivity of hydrogen itself, mixing hydrogen with diesel can significantly increase the fuel's diffusivity, making it blend better with the air and is more uniform, providing better conditions for the combustion process[19]. Some studies have pointed out that when hydrogen is mixed with diesel, when the engine is at full load, and the hydrogen enrichment is 50%, the engine will cause knocking. When the optimal hydrogen enrichment of the fuel is 30%, the engine will have the lowest emissions of hydrocarbons and nitrogen oxides[20].In dual-fuel engines, the ignition energy of hydrogen is provided by diesel combustion, and the amount of diesel used to ignite hydrogen accounts for about 30% of the total fuel[21]. The temperature generated by compression in currently widely used compression ignition engines cannot meet hydrogen requirements. The use of compression ignition engines can meet the demand for high torque. Therefore, when hydrogen is used as a compression ignition engine fuel, spark plugs or glow plugs are often needed to help.

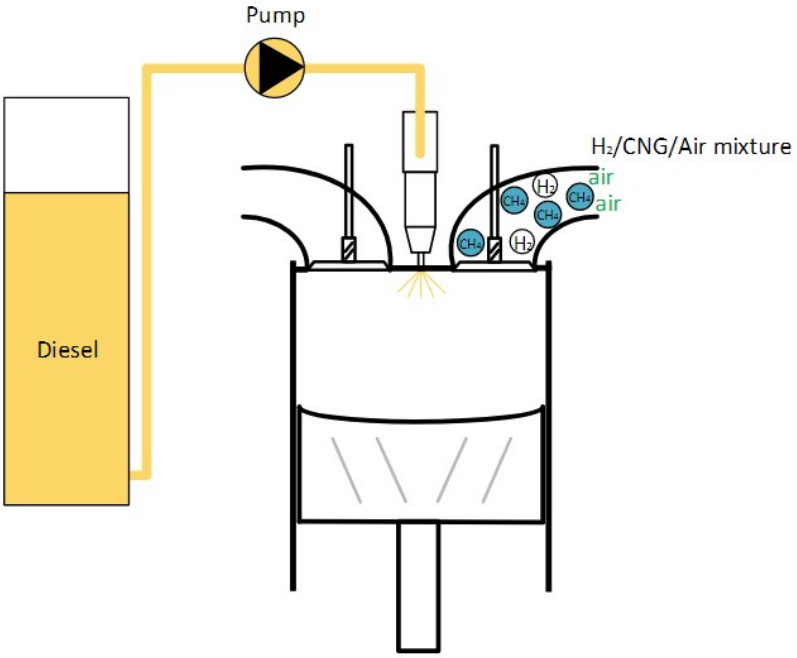

Figure 2.2: Sketch of the dual fuel engine system, blends CNG and hydrogen at intake manifold for IC. [1]

2.3 INJECTION METHODS

Whether spark ignition or compression ignition is used, both primary purpose is to address the high autoignition temperature of hydrogen fuel, but more than one problem needs to be solved. For hydrogen fuel engines, fuel injection technology plays a vital role. Although hydrogen can be used directly in existing engines, the fuel supply and combustion systems need to be modified to obtain a better combustion process. Currently, two fuel injection technologies, port fuel injection and direct injection, are mainly used.

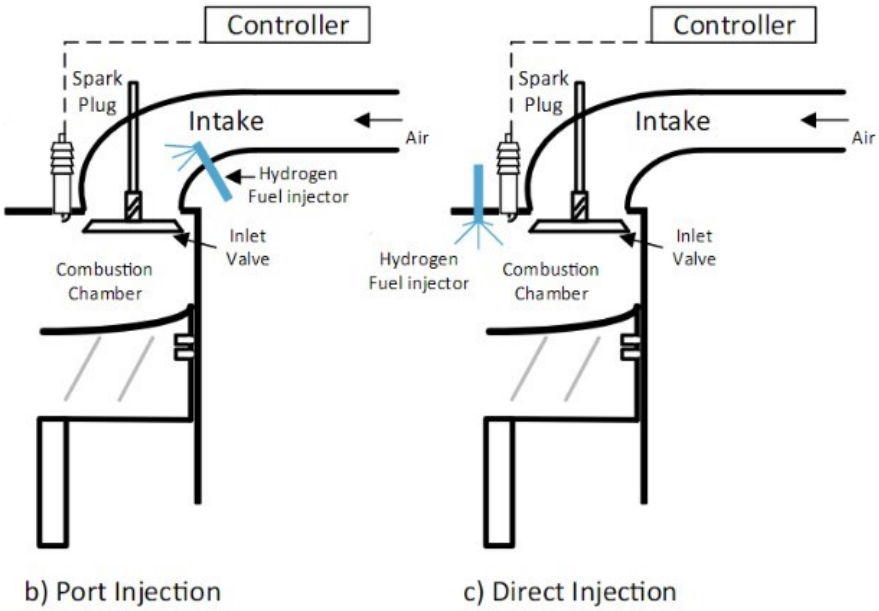

Figure 2.3: Hydrogen injection techniques into an IC engine[1]

2.3.1 *Port Fuel Injection*

Port injection technology injects hydrogen fuel into the port through an electronic injector after the engine's intake stroke begins. Due to the low ignition energy required by hydrogen fuel, if it enters the cylinder prematurely, it will quickly come into contact with the high-temperature mixture left from the previous combustion process. This can cause an ignition event, commonly known as backfire. This event will cause the fuel and air mixture passed into the cylinder to be burned, causing a misfire cycle and knocking. After research, it was found that hydrogen injection timing is a critical factor in avoiding backfire. Suppose the injection time is too early, close to

the stage when the intake valve is opened. In that case, the high-temperature mixture in the cylinder has not been cooled and ignited the hydrogen fuel, which will cause backfire. If the injection time is too late, close to the intake valve closing stage, it will cause part of the mixture of hydrogen fuel and air to remain near the port, causing backfire at the beginning of the next cycle[14]. The optimal injection period should start at the end of the intake stroke or after the exhaust valve is completely closed. This timing ensures that the smallest amount of hydrogen fuel enters the exhaust manifold. Additionally, it prevents the hydrogen fuel from coming into contact with the high-temperature mixture remaining in the combustion chamber, thereby avoiding the risk of backfire.

Port injection technology can achieve a satisfactory injection process by adjusting the timed manifold injection and accurately controlling the injection time and duration[22]. At the same time, the injection of low-temperature hydrogen can help the cylinder cool down so that the output power of the hydrogen fuel engine can be equivalent to that of traditional fuel engines. However, due to the vast air-fuel ratio of hydrogen fuel, the charge volume needs to be bigger, resulting in low power density and limiting the engine's power output. This limits the use of port injection technology in hydrogen fuel engines, and direct injection method is adopted in this study.

2.4 THE DIFFERENCE BETWEEN HIGH PRESSURE AND LOW PRESSURE INJECTION SYSTEM

By comparing port and direct injection technology, direct injection technology is more suitable for hydrogen fuel engines and can effectively reduce the risk of unstable combustion. Although direct injection technology has many advantages, there are still challenges in its commercialization. Hydrogen itself has the characteristics of low density, low lubricity, and low viscosity, which leads to two opposed injection pressure options: high-pressure injection and low-pressure injection.

High-pressure injection uses higher pressure to inject hydrogen fuel into the cylinder. There are two main reasons for choosing this method. One is to solve the problem of low power density of hydrogen. For example, injecting hydrogen at a pressure of 350 bar and a temperature of 263K can increase its density to 31kg/m^3 and boost the volumetric energy to 3700MJ/m^3.[16]; the other is that engines using high-pressure injection often inject near the end of the compression stroke, so high pressure is needed to overcome the cylinder at the end of the compression stroke internal pressure. Choosing high-pressure injection requires more effort in hydrogen engine modification to meet high-pressure requirements, which makes the engine system more complex and costly. The figures below show the hydrogen jet conditions under various ambient pressures when the injection pressure is 3mpa and 5mpa, which can be seen that under the same ambient pressure and time, the injection distance and diffusion effect of the hydrogen jet with high injection pressure are better than those with low injection pressure.

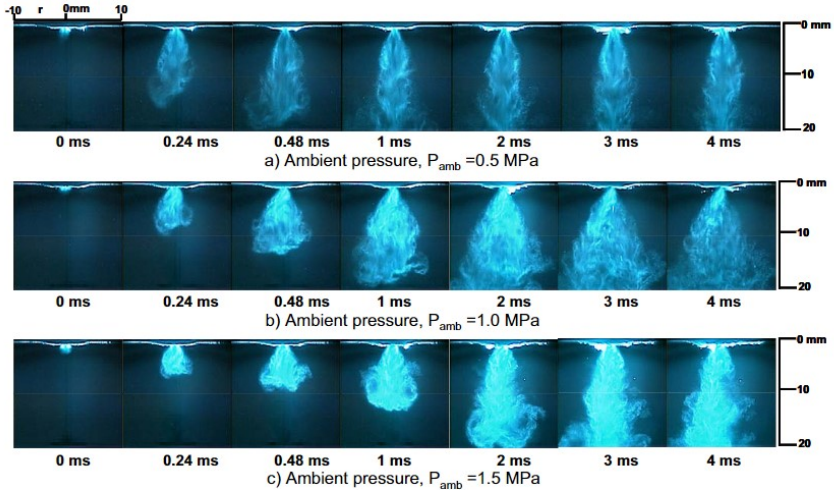

Figure 2.4: High-speed direct images of a 3-MPa injection pressure hydrogen jet into three different ambient pressure N_2-filled chambers[23].

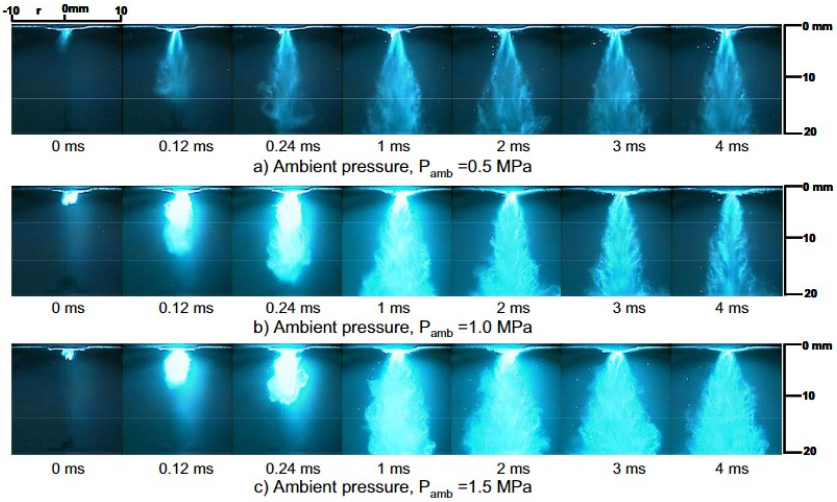

Figure 2.5: High-speed direct images of a 5-MPa injection pressure hydrogen jet into three different ambient pressure N_2-filled chambers[23].

Although high-pressure injection can better adapt to the combustion process of hydrogen-fueled engines, the low viscosity and poor lubrication properties of hydrogen can lead to increased wear of combustion chamber components under high-pressure conditions. This increased wear can significantly shorten the engine's lifespan. Additionally, as working pressure increases over time, the mass proportion of hydrogen fuel will decrease, reducing the vessel's travel range. Considering these issues, opting for low-pressure injection seems to be a better option.

Low-pressure injection mainly uses lower pressure, such as a pressure below 50 bar, compared to a high-pressure injection with 300 bar pressure. The injection strategy using low-pressure injection can avoid the problem of reducing the life of engine components and ship mileage. However, two issues need to be paid attention to. First, due to the reduction of injection pressure, the power density of hydrogen fuel will decrease, which requires increasing the low-pressure throat area of the injector nozzle to maintain the same mass flow rate and power output as the high-pressure injector. Secondly, the injection cannot be carried out at the end of the compression stroke due to

the low-pressure injection. However, premature injection will cause the hydrogen fuel to enter the cylinder and move with the piston, which increases the risk of accidental ignition, so a suitable injection time should be higher than the pressure in the cylinder at all times, which requires finding a proper balance between the benefits and risks injected during the compression stroke.

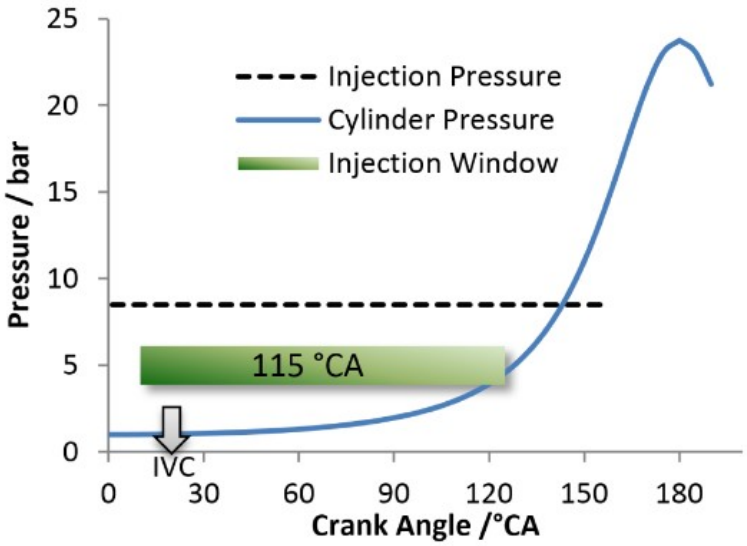

Figure 2.6: Calculated cylinder pressure with $\varepsilon = 9.6$ and the possible injection window with $850kPa$ fuel pressure[24].

Figure 2.6 shows the injection window where low-pressure injection starts after the intake valve closes and injection stops when the in-cylinder pressure and injection pressure are equal. Finding a balance between injection pressure and in-cylinder pressure is necessary for different engines and injectors.

2.5 INJECTION TIMING

Regarding the injection timing, choosing different injection timing will directly affect the injection strategy and combustion process of

the hydrogen engine. Direct injection technology has three mainstream injection timing: intake period injection, early injection, and late injection.

Early injection is carried out at the beginning of the compression stroke. At this time, the slight pressure in the cylinder allows for the use of a lower injection pressure. By fully utilizing the injection window, the power density of the hydrogen fuel in the cylinder can reach a reasonable level, resulting in better power output. However, since the early injection is performed at the beginning of the compression stroke, the hydrogen fuel injected into the cylinder will reciprocate with the piston. Suppose the temperature in the cylinder is too high, or there is residual exhaust gas from the previous stroke. In that case, it will easily meet hydrogen's low ignition energy requirements, causing pre-ignition and engine knocking. Therefore, low-temperature liquid hydrogen is often selected so that when the fuel is injected into the cylinder, the temperature in the cylinder can be cooled by low-temperature liquid hydrogen, reducing the risk of accidental ignition.

2.6 ABNORMAL COMBUSTION IN HYDROGEN ENGINE

Due to the thermophysical properties of hydrogen as a fuel, low ignition energy requirements, high diffusivity, and fast laminar flame speed, hydrogen fuel engines are prone to abnormal combustion problems, such as pre-ignition, backfire, and engine knock. Those problems will significantly impact the working efficiency and output power of the hydrogen fuel engine, which may even shorten the engine's lifecycle and reduce the engine's reliability.

2.6.1 *Pre-ignition*

Pre-ignition is a significant problem when developing hydrogen fuel engines, whether using port or direct injection. Pre-ignition is defined as combustion before ignition timing begins during the engine's com-

pression stroke. Since pre-ignition is a difficult-to-predict event, its reasons are complex, and no clear conclusion exists. Generally speaking, due to the nature of low ignition energy requirements, during the compression stroke, the high temperature inside the combustion chamber and the residual combustion products from the previous stroke may lead to pre-ignition. The minimum ignition energy depends on the equivalence ratio. When the mixture of hydrogen and air in the combustion chamber approaches the stoichiometric ratio, the risk of early ignition will also increase significantly. In addition, the increase in engine load will also increase the temperature of the combustion chamber, thereby increasing the risk of pre-ignition.

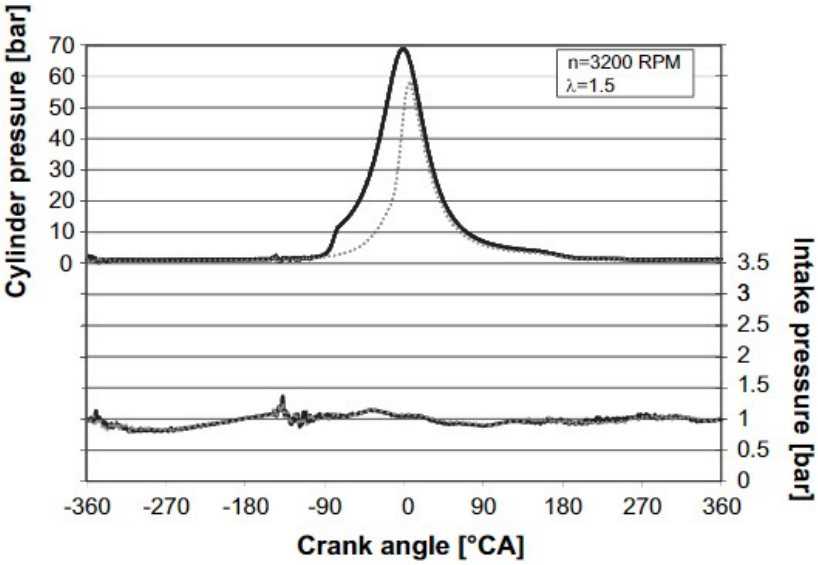

Figure 2.7: Typical cylinder and intake manifold pressure traces with pre-ignition(solid lines),compared to regular pressure traces(dotted lines)[25]

Figure 2.7 shows data obtained from a car-sized single-cylinder hydrogen engine, where the dotted line is the pressure curve for normal combustion and the solid line is the pressure curve when pre-combustion occurs. It can be seen that the peak pressure when pre-ignition occurs is higher than standard ignition. The time of early

ignition occurs about 80 degrees before the top dead center[25]. It can be seen that the pressure in the cylinder begins to rise, and the pressure curve trend of early ignition occurs. Compared with the pressure curve trend of standard combustion, there is no significant difference, indicating that pre-ignition occurs after the intake valve is closed.

As for current measures to reduce the risk of pre-ignition, engines using port injection are generally designed to ventilate the crankcase, reduce the temperature of the combustion chamber, or optimize the engine cooling design. However, the emerging method is direct injection technology, effectively reducing the risk of pre-ignition.

2.6.2 *Backfire*

Backfire refers to abnormal combustion that occurs during the engine's intake stroke. When the intake valve opens, fresh air and hydrogen mixture enter the combustion chamber from the intake manifold. If there are residual combustion products or hot spots from the previous stroke inside the combustion chamber at this time, the charged hydrogen fuel will be ignited. At the same time, the flame speed of hydrogen fuel is fast, which will cause the hydrogen fuel to ignite from the combustion chamber and propagate to the intake valve. This process is similar to pre-ignition, but the main difference is when it occurs. Pre-ignition occurs after the intake valve closes and the compression stroke begins, while backfire occurs when the intake valve opens, and the intake stroke begins. When a backfire occurs, the pressure and temperature in the intake manifold will rise sharply, damaging the intake system and seriously affecting the life of the engine.

Figure 2.8 compares the pressure curves of a car-sized single-cylinder hydrogen fuel engine during backfire and regular operation. It can be seen that when the engine backfires, the peak pressure in the cylinder is much smaller than the pressure in regular operation, and the intake air pressure is much higher than normal pressure. Because a large amount of fuel is burned during the intake stroke,

which leads to an increase in the intake pressure, and only part of the fuel enters the inside of the cylinder, the pressure in the cylinder is much lower than the normal pressure after the ignition timing, which also reduces the output power. , indicating that backfire will seriously affect the engine's output power and working efficiency.

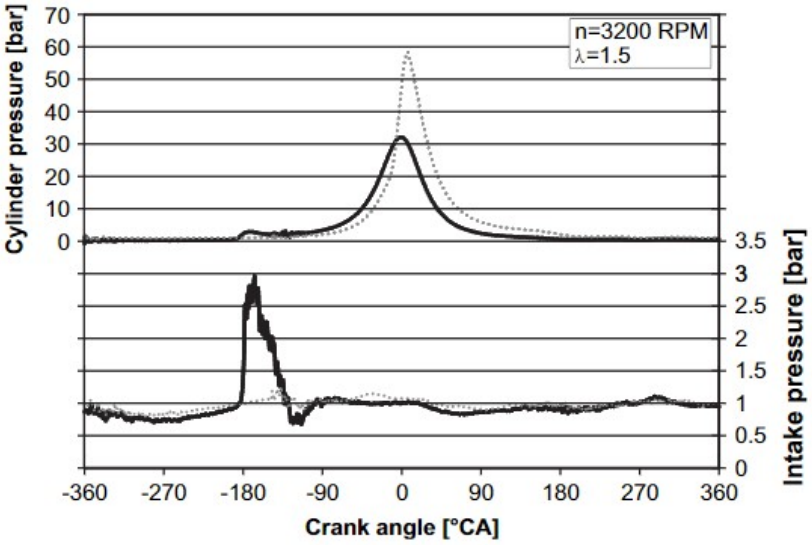

Figure 2.8: Typical cylinder and intake pressure traces for backfiring cycle (solid lines), compared to regular pressure traces (dotted lines)[25]

After a backfire occurs, the ignited fuel will also increase the temperature in the cylinder, thereby increasing the risk of pre-ignition and causing backfires in a continuous cycle, which can be said that backfire is a precursor to pre-ignition. So, the measure that can reduce the risk of backfire can also reduce the risk of pre-ignition. For engines using port injection, the main goal of reducing the risk of backfire is to solve the residual hydrogen concentration in the intake inlet. When the mixture of hydrogen and air reaches the stoichiometric ratio, it is easy to burn, so the lower the residual hydrogen concentration, the lower the possibility of backfire. Of course, more current research is on the direct use of direct injection technology

because the mixture of hydrogen and air is directly injected into the cylinder, completely solving the backfire problem at the intake port.

2.6.3 *Engine knock*

Engine knocking occurs when the exhaust gas meets spontaneous combustion conditions. The remaining energy of the exhaust gas is quickly released, generating a high-amplitude pressure wave. This, combined with the increased mechanical and thermal stress on the engine, results in knocking and can even cause engine damage. The risk of engine knocking is closely related to the octane number of the fuel. Traditional internal combustion engines study the anti-knock properties of fuels by studying the octane number of the fuel and the anti-knock properties of mixtures with normal heptane and isooctane. Comparison shows that this method is not suitable for engines using hydrogen fuel. Figure 2.9 shows the in-cylinder pressure curve of a single-cylinder hydrogen fuel engine of car size when knocking occurs. It can be seen that the peak in-cylinder pressure during normal operation is 90 bar. After detonation, the maximum peak pressure is as high as 150 bar and decays over time[25].

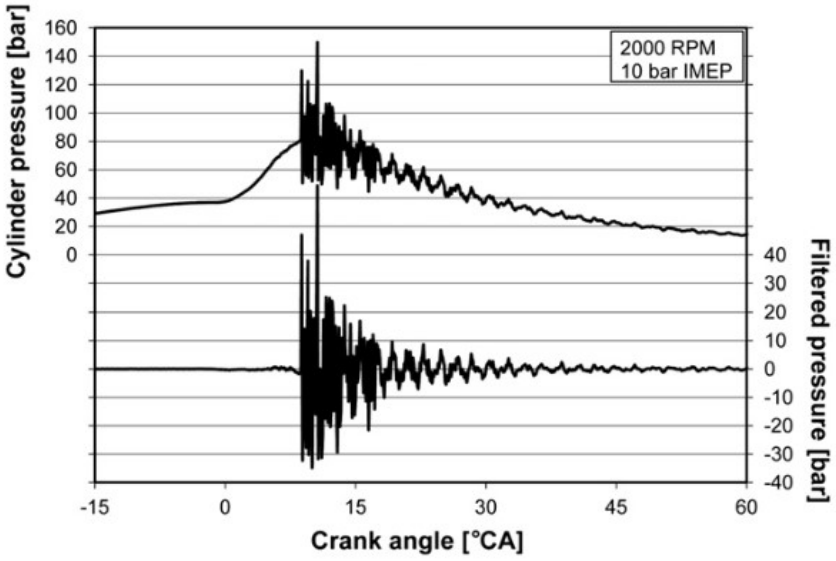

Figure 2.9: Typical cylinder pressure trace for heavy knocking cycle[25]

2.6.4 *Avoiding abnormal combustion*

Using direct injection technology instead of port injection technology can minimize pre-ignition risk and backfire. At the same time, finding the optimal injection timing is necessary. The early injection can cause hydrogen fuel to flow back from the cylinder to the intake air at the end of the intake stroke. If injected too late, the hydrogen fuel will not have enough time to reach the cylinder. It will eventually remain at the intake valve, increasing the next cycle's fuel-air mixture ratio and the risk of abnormal combustion in the next stroke. Whether pre-ignition, backfire, or detonation, the core principle behind it is the fuel-air equivalence ratio. Reducing the fuel-air equivalence ratio avoids abnormal combustion in hydrogen-fuel engines, so hydrogen-fuel engines often use a lean combustion strategy. Excess air in lean operation reduces combustion chamber temperature, reducing the presence of hot spots and reducing the risk of knocking. However, lean combustion will limit the power output of the engine. Balancing

the engine power output and the risk of abnormal combustion has become worth studying.

2.7 CONCLUSION

After examining the physical properties of hydrogen, it is observed that it has a high autoignition temperature, leading to the selection of spark ignition. Due to the extremely fast flame propagation speed of hydrogen, port injection technology would result in engine backfire and uncontrolled pre-ignition events. Therefore, direct injection technology was chosen to mitigate these risks. Additionally, low-pressure injection was selected over high-pressure injection because the latter would shorten engine lifespan and increase engine costs. Thus, the chosen approach is a low-pressure direct injection spark-ignition hydrogen-fueled engine.

3

INJECTOR PROTOTYPE

Since the present work aims to study the injection control system in a low-pressure direct injection engine powered by hydrogen fuel, selecting the injector is crucial. The patent number of the injector prototype is DE102020127020B3. The characteristic of this injector is that it can achieve injection with an injection pressure lower than 50 bar, as shown in the Figure 3.1.

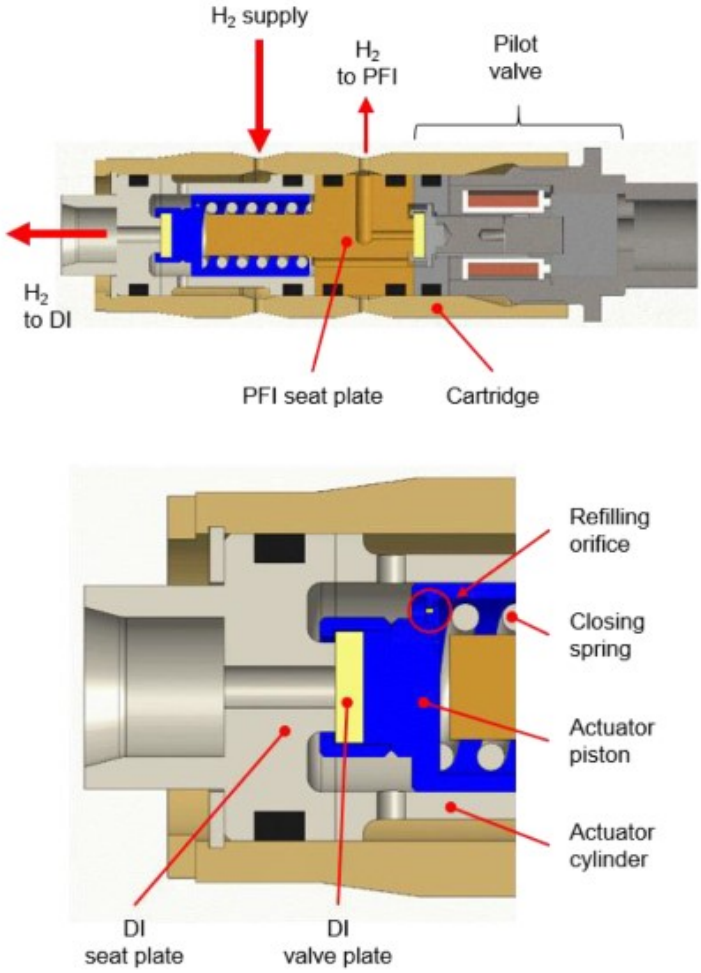

Figure 3.1: Injector Prototype[14]

The primary function of the direct injection injector is to open and close regularly and ensure no fuel leakage. When the injector is closed, the fuel flow should be infinitely close to zero, while when the injector is open, the fuel flow should reach the desired flow rate. The injector selected this time adopts a poppet valve design in terms of fuel flow control, and the opening direction of the poppet valve is designed to open the valve inward. The reason why poppet valves are used instead of rotary valves in the first place is that the valves are

often exposed to high-temperature combustion gases. Rotary valves can get stuck and leak, while poppet valves will avoid such problems. Secondly, the opening direction of the poppet valve is set to open inward rather than outward because in a low-pressure direct injection engine, except for the intake stroke and early compression stroke, the in-cylinder pressure will be less than the injection pressure. At other times, the in-cylinder pressure will be greater than the injection pressure, and the pressure difference is concentrated in the valve closing stage. As shown in the Figure 3.2, the inward opening valve will benefit from the self-sealing effect so that hydrogen fuel leakage will not occur if the valve spring fails.

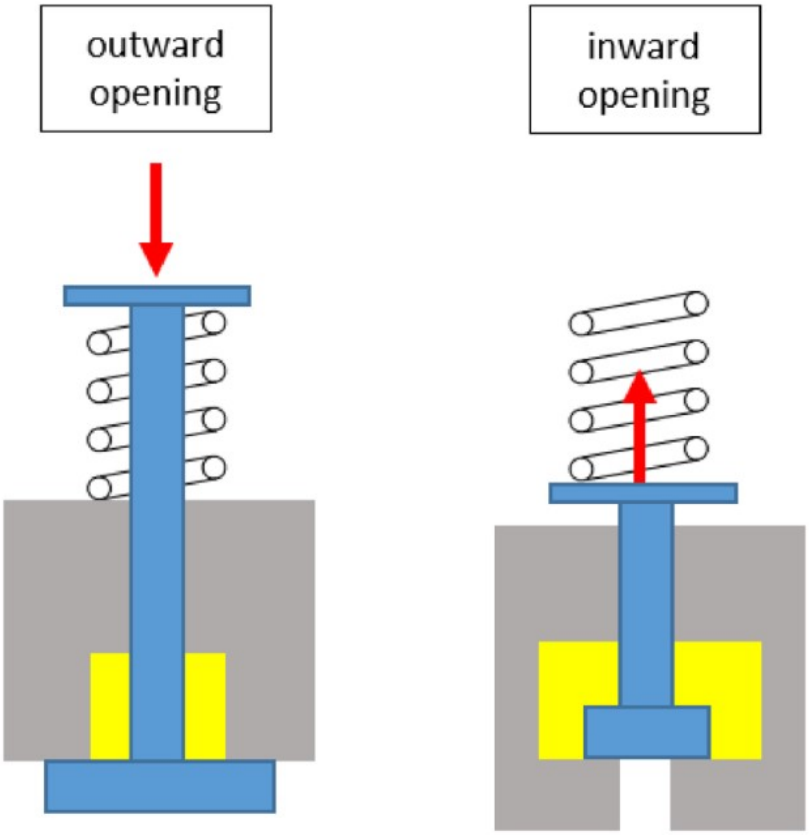

Figure 3.2: Outward opening and inward opening[14]

3.1 BASIC WORKING PRINCIPLE OF INJECTOR

The injector used in this study is a newly developed patent. It is mainly composed of a pneumatic valve and a solenoid pilot valve. The basic working principle is that the solenoid pilot valve controls the opening and closing of the ball valve, thereby controlling the pressure decrease and increase inside the pneumatic valve(acutuator cylinder), which ultimately functions to control the opening and closing of the valve plate, thereby controlling the switch of this injector. As shown in the Figure 3.3.

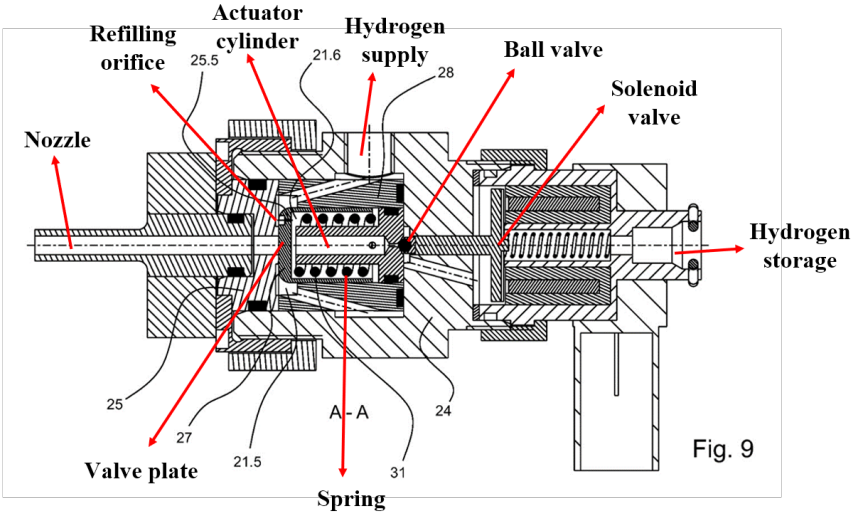

Figure 3.3: Injector section view[26]

In order to better understand the working principle of this new injector, the pressure change in the actuator cylinder of this injector will be introduced in detail. The pressure change diagram in the actuator cylinder is shown in the Figure 3.4.

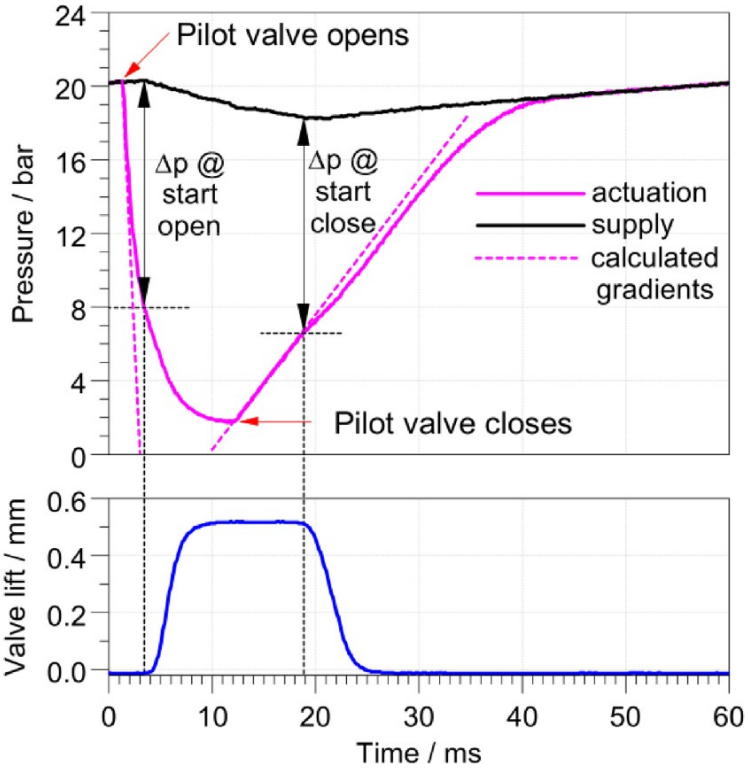

Figure 3.4: The pressure change diagram in the actuator cylinder[14]

According to the pressure change diagram in the actuator cylinder, it can be divided into six phases:

- Receive signal to start injection
- The valve plate lifts and reaches the set lift value
- Maintain the lifted height
- Receive signal to end injection
- The valve plate drops and returns to the valve seat
- The internal pressure of the actuator cylinder rises to the supply pressure

3.1.1 *Receive signal to start injection*

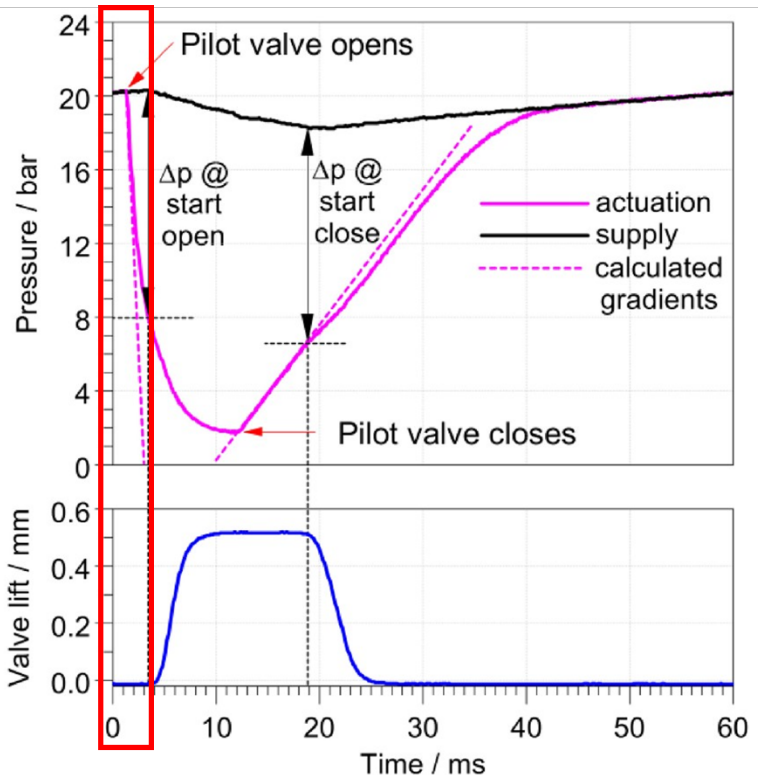

Figure 3.5: Pressure change after receiving signal to start injection[14]

Before the start of injection, the refilling orifice remains open, thereby connecting the actuator cylinder to the supply pipeline, resulting in equalized pressure between the actuator cylinder and the supply pressure. Upon receiving the injection signal, the solenoid valve lifts, which, due to its metallic connection to the ball valve, causes the ball valve to lift simultaneously. Consequently, the hydrogen within the actuator cylinder is connected via the pipeline to the hydrogen storage space, where the pressure is significantly lower than that within the actuator cylinder. This leads to a decrease in pressure within the actuator cylinder. As the pressure in the actuator cylinder drops, a pressure differential emerges across the surface of the valve

plate, specifically between the supply pressure and the actuator cylinder pressure. However, at this juncture, the pressure differential is insufficient to counteract the spring force, thus preventing the valve plate from lifting. Therefore, following the injection signal's receipt, the injector cannot immediately initiate hydrogen injection. At this phase, the valve plate remains stationary, and the volume within the actuator cylinder does not change. According to the ideal gas law under constant volume conditions, the pressure gradient within the actuator cylinder is solely dependent on the variation in the mass of the gas contained within:

$$\frac{\mathrm{d}p}{\mathrm{d}t} = \frac{R \cdot T}{V_0} \cdot \frac{\mathrm{d}m}{\mathrm{d}t} \tag{3.1}$$

Where T is the gas temperature, R is the specific gas constant of hydrogen, and V_0 is the volume of the actuator cylinder when the valve plate is not moving.
The change in gas mass in the actuator cylinder can be written as a mass balance equation:

$$\frac{\mathrm{d}m}{\mathrm{d}t} = \dot{m}_{in} - \dot{m}_{out} \tag{3.2}$$

Where $\dot{m}_{in}$ is the mass flow passing the refilling orifice and $\dot{m}_{out}$ is the mass flow passing the ball valve.Since the cross-sectional area of the refilling orifice is $A_{eff,RO} = 0.07mm^2$[14] and the cross-sectional area of the ball valve outlet is $A_{eff,BV} = 0.79mm^2$[14], the difference between the two values is more than ten times. To facilitate calculation, $\dot{m}_{in}$ is ignored at this stage and only $\dot{m}_{out}$ is considered:

$$\frac{\mathrm{d}m}{\mathrm{d}t} = -\dot{m}_{out} \tag{3.3}$$

The mass flow of a compressible fluid through a valve can be calculated by Saint-Venant-Wantzel-equation[14]:

$$\dot{m} = A_{eff} \cdot \psi \cdot \sqrt{2 \cdot P_{sup} \cdot \rho_{sup}} \tag{3.4}$$

In order to facilitate calculation, the ideal gas equation is used to transform:

$$\dot{m} = A_{eff} \cdot \psi \cdot P_{sup} \cdot \sqrt{\frac{2}{R \cdot T_{sup}}} \tag{3.5}$$

Where A_{eff} is the effective flow cross-sectional area of the ball valve and P_{sup} is the supply pressure.ψ is the isentropic flow function,which depends only on the pressure ratio over the valve gap $\frac{P_{cyl}}{P_{sup}}$ and the ratio of the specific heats:

$$\psi = \sqrt{\frac{\kappa}{\kappa - 1} \cdot \left[\left(\frac{P_{cyl}}{P_{sup}} \right)^{\frac{2}{\kappa}} - \left(\frac{P_{cyl}}{P_{sup}} \right)^{\frac{\kappa+1}{\kappa}} \right]} \tag{3.6}$$

Where P_{cyl} is the downstream pressure of the valve and P_{sup} is the upstream pressure of the valve. To ensure the smooth flow of hydrogen through the valve, the pressure ratio between the upstream and downstream of the valve must satisfy the critical pressure ratio; otherwise, the valve will choke. The critical pressure ratio depends solely on the ratio of specific heats of the fluid. For computational convenience, the compression process of hydrogen is considered isentropic, with the ratio of specific heats assumed to be constant at $\kappa = 1.4$.

$$\frac{P_{cyl}}{P_{sup}} = \left(\frac{2}{\kappa + 1} \right)^{\frac{\kappa}{\kappa+1}} = 0.528 \tag{3.7}$$

Once the critical pressure ratio is met, the flow function ψ_{max} also reaches its maximum value $\psi_{max} = 0.484$. Thus, for the normal flow of hydrogen, the value of the flow function must be at its maximum. Then, the expression of the $\dot{m}_{out}$:

$$\dot{m}_{out} = A_{eff,BV} \cdot \psi_{max} \cdot P \cdot \sqrt{\frac{2}{R \cdot T_{sup}}} \tag{3.8}$$

Then the expression of the pressure change $\frac{\mathrm{d}p}{\mathrm{d}t}$:

$$\frac{\mathrm{d}p}{\mathrm{d}t} = -\psi_{max} \cdot \sqrt{2 \cdot R \cdot T_{sup}} \cdot \frac{A_{eff,BV}}{V_0} \cdot P \tag{3.9}$$

3.1.2 *The valve plate lifts and reaches the set lift value*

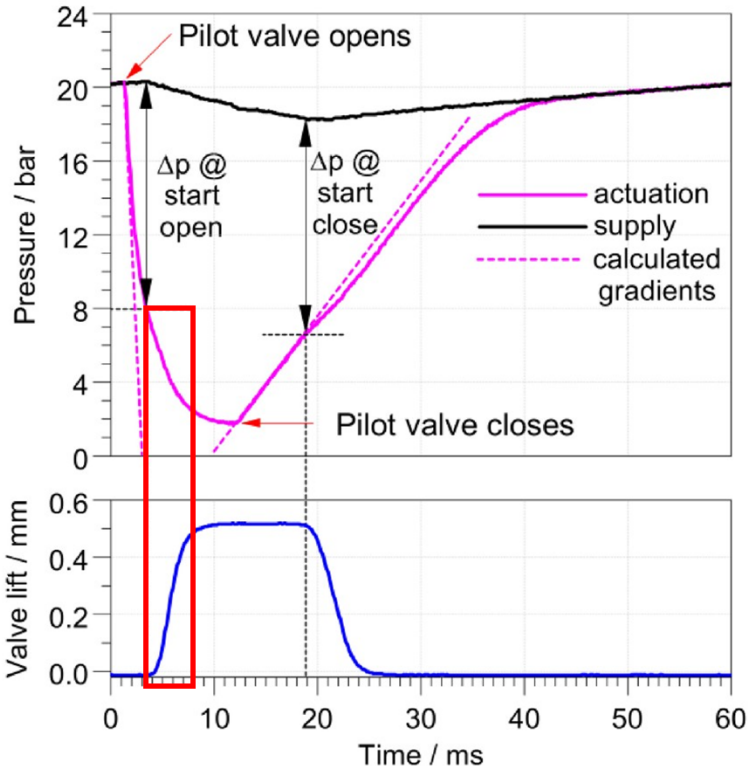

Figure 3.6: The valve plate lifts and reaches the set lift value[14]

When the pressure differential across the surface of the valve plate gradually increases to the point where it can open the valve, the valve plate begins to lift, allowing hydrogen to be injected into the engine cylinder through the nozzle. Since the valve plate is integrated with the actuator cylinder, the volume of the actuator cylinder also changes. The expression for the pressure change within the actuator cylinder remains the same as in the previous phase:

$$\frac{\mathrm{d}p}{\mathrm{d}t} = -\psi_{max} \cdot \sqrt{2 \cdot R \cdot T_{sup}} \cdot \frac{A_{eff,BV}}{V(t)} \cdot P \tag{3.10}$$

Because the valve plate is lifted, the volume inside the actuator cylinder changes:

$$V(t) = V_0 - \frac{\pi}{4} \cdot d_1^2 \cdot h(t) \tag{3.11}$$

Where $V(t)$ is the actuator cylinder volume as a function of time,d_1 is the diameter of the actuator cylinder and $h(t)$ is the valve plate lift as a function of time. Since the valve plate moves, Newton's second law is used to analyze its force.

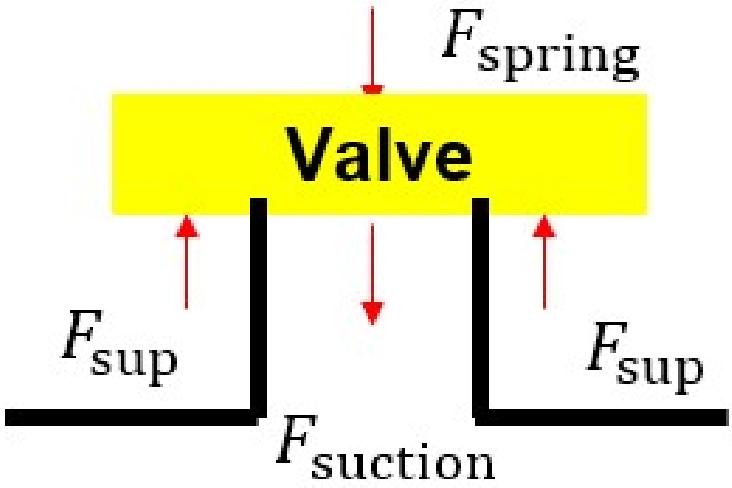

Figure 3.7: Force analysis of valve plate

F_{sup} is the difference between the supply pressure and the actuator cylinder pressure,and $F_{suction}$ exists because the pressure in the engine cylinder is always less than the injection pressure during the injection process,which means that the pressure difference F_{sup} must overcome the spring force F_{spring} and the suction force $F_{suction}$ to make the valve lift.

$$F_{sup} = (P - P_{sup}) \cdot \frac{\pi}{4} \cdot (d_1^2 - D^2) \tag{3.12}$$

$$F_{suction} = (P - P_{cyl}) \cdot s \tag{3.13}$$

$$F_{spring} = k \cdot (L_0 + h) \tag{3.14}$$

Then the expression of the valve plate lift $h(t)$:

$$\frac{\mathrm{d}^2 h}{\mathrm{d}t^2} = \frac{1}{m} \cdot ((P - P_{sup}) \cdot \frac{\pi}{4} \cdot (d_1^2 - D^2) - (P - P_{cyl}) \cdot s - k \cdot (L_0 + h)) \tag{3.15}$$

Where m is the mass of the actuator piston,D is the diameter of curtain area,k is the spring stiffness,and s is the nozzle effective area,L_0 is the length that the spring is compressed to maintain the preload force of the seal.
After lifting, the valve plate will rise to a maximum value, which is closely related to the injection timing. The corresponding curtain area diameter, spring stiffness, effective cross-sectional area of the nozzle, and the spring's preload force are also related to the injection timing. Therefore, this section will focus on the derivation of the mathematical model, while the specific parameters will be detailed and introduced in subsequent chapters.

3.1.3 *Maintain the lifted height*

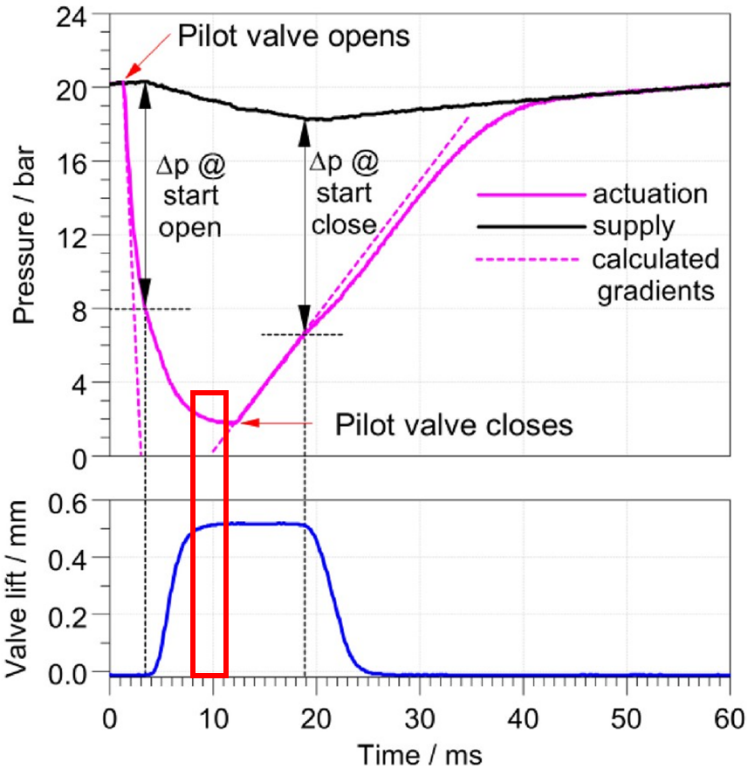

Figure 3.8: Maintain the lifted height[14]

After the valve plate reaches its maximum value, the solenoid valve has not received a signal to stop the injection, so the ball valve remains open. The hydrogen in the actuator cylinder continues to flow into the hydrogen storage space. Therefore, the expression for the pressure change within the actuator cylinder remains the same as in the previous phase. However, unlike the previous phase, since the valve plate has reached its maximum position and will not change, the volume inside the actuator cylinder also remains constant. At

this point, the volume of the actuator cylinder is a fixed value and no longer varies with time.

$$\frac{\mathrm{d}p}{\mathrm{d}t} = -\psi_{max} \cdot \sqrt{2 \cdot R \cdot T_{sup}} \cdot \frac{A_{eff,BV}}{V_1} \cdot P \tag{3.16}$$

$$V_1 = V_0 - \frac{\pi}{4} \cdot d_1^2 \cdot h_{max} \tag{3.17}$$

Where V_1 is the volume after the valve plate is lifted to the maximum value.

3.1.4 *Receive signal to end injection*

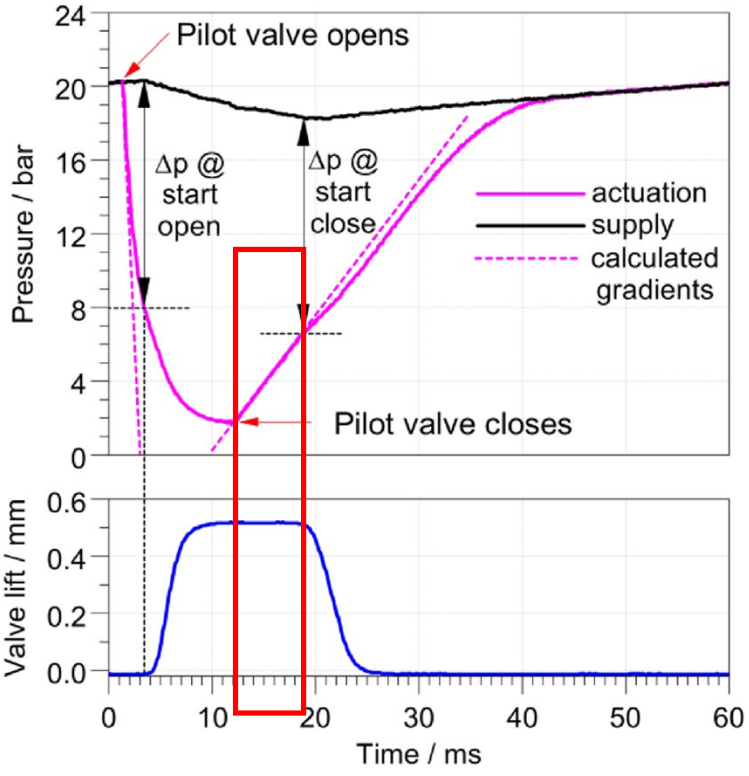

Figure 3.9: Receive signal to end injection[14]

When the solenoid valve receives the signal to stop injection, it stops working and the ball valve immediately falls back to the valve seat. At this time, no mass flow passes through the ball valve anymore,then the mass balance equation:

$$\frac{\mathrm{d}m}{\mathrm{d}t} = \dot{m}_{in} \tag{3.18}$$

The corresponding expression for the pressure change in the actuator cylinder is as follows:

$$\frac{\mathrm{d}p}{\mathrm{d}t} = \psi_{max} \cdot \sqrt{2 \cdot R \cdot T_{sup}} \cdot \frac{A_{eff,RO}}{V_1} \cdot P_{sup} \tag{3.19}$$

Where $A_{eff,RO}$ is refilling orifice effective cross-section area. The rationale behind using V_1 as the volume parameter in the calculations stems from the persistent pressure differential across the valve plate, despite the actuator cylinder commencing refilling via the refilling orifice subsequent to the closure of the ball valve and the initiation of internal pressure rise. This pressure differential is insufficient to lower the valve plate, so the volume of the actuator cylinder remains constant, the same as in the previous phase.

3.1.5 *The valve plate drops and returns to the valve seat*

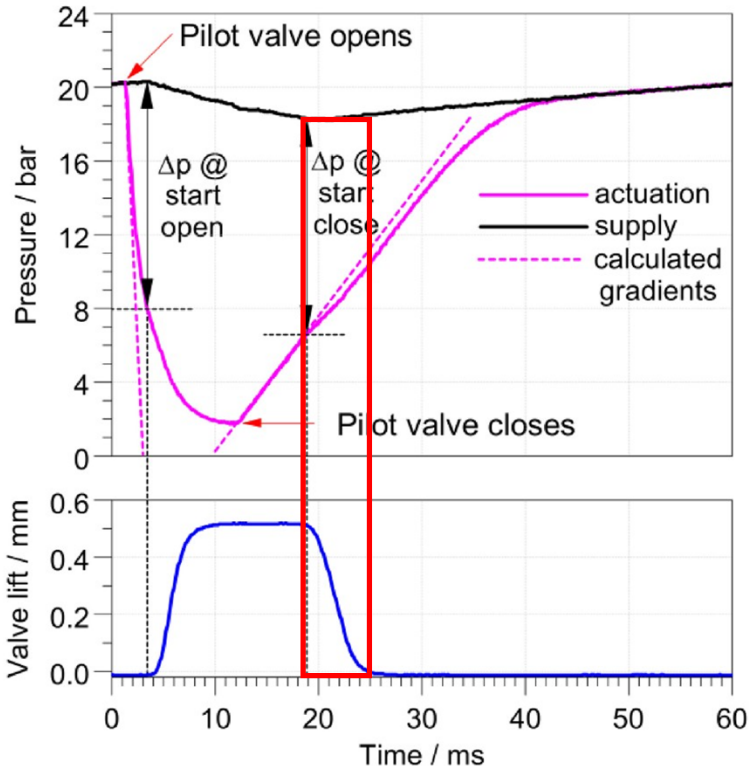

Figure 3.10: The valve plate drops and returns to the valve seat[14]

In this phase, the pressure differential across the valve plate is no longer sufficient to overcome the spring force and suction force, causing the valve plate to begin to fall back to the valve seat, thereby leading to a change in the volume of the actuator cylinder. The pressure change equation in this phase differs from the previous phase. Firstly, the supply pressure is a constant value; secondly, the volume is no longer constant but is a time-dependent function.

$$\frac{\mathrm{d}p}{\mathrm{d}t} = \psi_{max} \cdot \sqrt{2 \cdot R \cdot T_{sup}} \cdot \frac{A_{eff,RO}}{V(t)} \cdot P_{sup} \tag{3.20}$$

$$V(t) = V_0 - \frac{\pi}{4} \cdot d_1^2 \cdot h(t) \tag{3.21}$$

Then the expression of the $h(t)$:

$$\frac{\mathrm{d}^2 h}{\mathrm{d}t^2} = \frac{1}{m} \cdot ((P - P_{sup}) \cdot \frac{\pi}{4} \cdot (d_1^2 - D^2) - (P - P_{cyl}) \cdot s - k \cdot (L_0 + h)) \tag{3.22}$$

3.1.6 *The internal pressure of the actuator cylinder rises to the supply pressure*

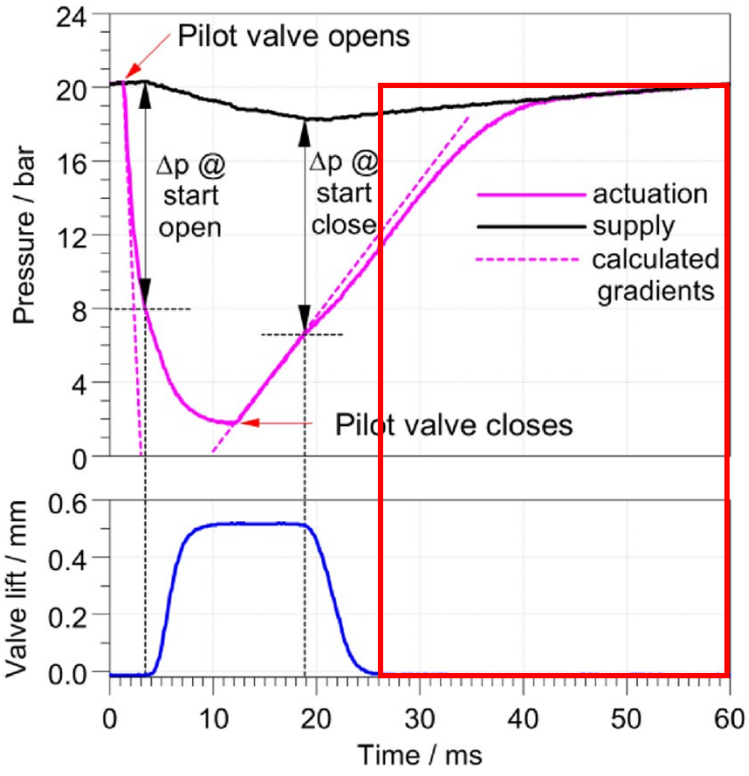

Figure 3.11: The internal pressure of the actuator cylinder rises to the supply pressure[14]

This phase is the refilling phase. Since the ball valve is already closed, the pressure change within the actuator cylinder is solely caused by the refilling process. Therefore, the pressure change equation is the same as in the previous stage.

$$\frac{\mathrm{d}p}{\mathrm{d}t} = \psi_{max} \cdot \sqrt{2 \cdot R \cdot T_{sup}} \cdot \frac{A_{eff,RO}}{V_0} \cdot P_{sup} \tag{3.23}$$

The only difference in this phase is that the valve plate has also returned to the valve seat, so the volume of the actuator cylinder is at its initial value V_0. When the pressure in the actuator cylinder gradually rises to match the supply pressure, the pressure in the actuator cylinder no longer changes.

3.2 INJECTOR PARAMETER DESIGN

In the chapter that discusses the working principle of injector, various geometric parameters of the injectors, such as A_{eff}, s, and D, are introduced. These parameters, which are crucial for redesigning the injectors to match the engine's requirements, play a vital role in ensuring the proper functioning of both the injector and the engine. Based on the mathematical derivation of the working principle of injector, it can be seen that the overall mathematical model is established on this equation:

$$\dot{m} = A_{eff} \cdot \psi \cdot P_{sup} \cdot \sqrt{\frac{2}{R \cdot T_{sup}}} \tag{3.24}$$

For the convenience of establishing the mathematical model, corresponding values for supply pressure P_{sup} and temperature T_{sup} have been set, while the specific gas constant R and isentropic flow function ψ are also known. Therefore, in this equation, undetermined parameters are only the mass flow $\dot{m}$ and the effective flow cross-sectional area A_{eff}.
To determine the geometric parameters of the fuel injector, namely the effective flow cross-sectional area A_{eff}, it is necessary to first establish the mass flow $\dot{m}$. This begins with determining the total

mass of hydrogen consumed by the engine within one operating cycle.

3.2.1 *Static Mass Flow*

The total mass of hydrogen required to be injected during each operating cycle is determined by the following equation:

$$m_{H_2} = \frac{\omega_i \cdot V_h}{\eta_i \cdot H_u} \tag{3.25}$$

Where ω_i is the indicated specific piston work,V_h is the displacement per cylinder,η_i is the indicated engine efficiency and H_u is the lower heating value.
The mass of hydrogen must be injected into the cylinder within the available injection window time $\triangle t_{inj}$

$$\triangle t_{inj} = \frac{1}{n} \cdot \frac{\triangle \alpha_{inj}}{360} \tag{3.26}$$

Where n is the engine speed,$\triangle \alpha_{inj}$ is the available injection crank angle.The available injection crank angle is related to the pressure variation inside the engine cylinder, which will be detailed in the subsequent chapters of mathematical modeling. For the theoretical derivation convenience, it is considered as a known value at this stage.
After deriving the total mass of hydrogen and the available injection time, the static mass flow within this time period can be derived:

$$\dot{m}_{static} = \frac{m_{H_2}}{\triangle t_{inj}} = \frac{\omega_i}{\eta_i \cdot H_u} \cdot V_h \cdot n \cdot \frac{360}{\triangle \alpha_{inj}} \tag{3.27}$$

3.2.2 *Effective Flow Cross-Sectional Area*

Before deriving the effective flow cross-sectional area, it is necessary to introduce its geometric model, primarily consisting of the

area where the valve plate contacts the nozzle, as illustrated in the Figure 3.12.

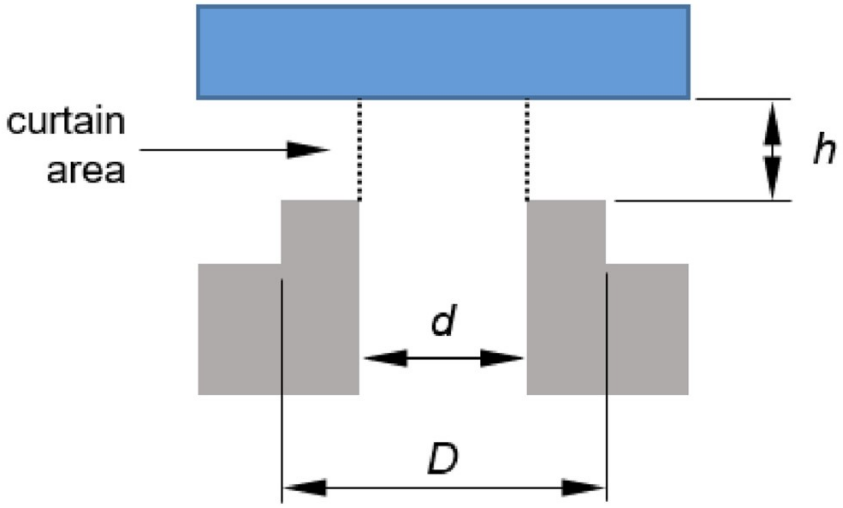

Figure 3.12: Geometric design parameters at the inward opening flat seat[14]

Once the static mass flow rate has been determined, the effective flow cross-sectional area can be expressed as follows:

$$A_{eff} = \frac{\dot{m}_{static}}{\psi \cdot P_{sup} \cdot \sqrt{\frac{2}{R \cdot T_{sup}}}} \tag{3.28}$$

Due to friction and flow jet contraction, the effective flow cross-sectional area is smaller than the actual flow cross-sectional area. The relationship between them is typically achieved by multiplying the actual flow cross-sectional area by an appropriate coefficient to obtain the effective flow cross-sectional area:

$$A_{eff} = A_{ref} \cdot C_D \tag{3.29}$$

Where A_{ref} is the reference flow cross-sectional area,which is the actual flow cross-sectional area, C_D is the discharge coefficient, taking

$C_D = 0.6$ as the coefficient value.
As can be seen from the Figure 3.12, the curtain area is:

$$A_{curtain} = \pi \cdot d \cdot h \tag{3.30}$$

This includes two undetermined design parameters: the nozzle diameter d and the valve lift height h. To determine these parameters, it is necessary to establish relational equations between these parameters and the known quantities. The curtain area is general defined as the area when the valve lift height does not exceed one-quarter of the nozzle diameter. Therefore, the relationship between the valve lift height and the nozzle diameter is:

$$h = \frac{d}{4} \tag{3.31}$$

For convenience in modeling, the nozzle cross-sectional area is set equal to the reference flow cross-sectional area:

$$A_{ref} = A_{nozzle} = \frac{\pi}{4} \cdot d^2 \tag{3.32}$$

At this point, the valve lift height h and the nozzle diameter d have both been determined.

3.2.3 *Spring Force*

In the basic working principle of the fuel injector, it can be seen that the spring force, which has a significant impact on the operation of the new type of fuel injector, primarily serves the following functions during its operation:

- Ensuring that the valve plate is not forced open by the supply pressure when the injector is closed
- Ensuring that the valve plate is not forced open by the cylinder pressure after the injection ends

Essentially, this is due to the spring being part of the pneumatic valve. Changes in the internal pressure of the pneumatic valve result in variations in the pressure differential across the surface of the valve plate. Similarly, fluctuations in the cylinder pressure also affect the pressure differential on the valve plate surface. Therefore, to ensure effective sealing, the spring force must exceed the pressure differential on the valve plate surface when the solenoid valve is not operating.

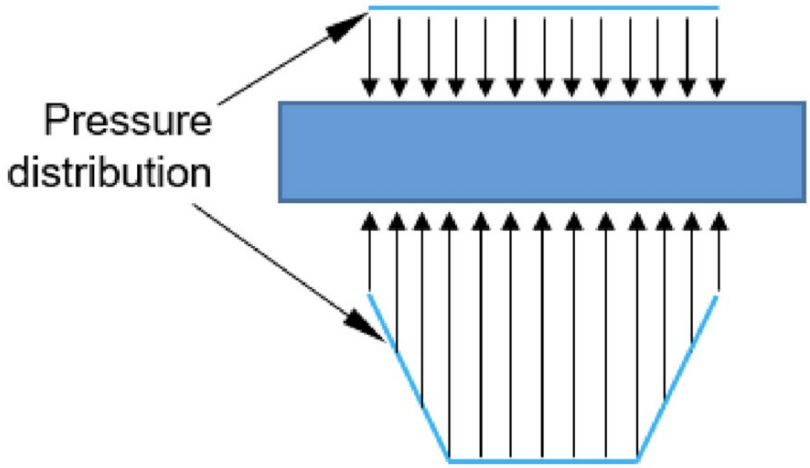

Figure 3.13: Pressure distribution of the valve plate[14]

For the convenience of modeling, the pressure distribution on the valve plate surface is assumed as shown in the Figure 3.13. The upper side of the valve plate is subjected to the supply pressure, while the lower side is subjected to the cylinder pressure. When the injector ceases operation, the valve plate begins to fall back to the valve seat. The pressure across the entire contact area of the valve seat decreases linearly, and can be mathematically expressed as follows:

$$F_{spring} = \left[\frac{\pi}{4} \cdot d^2 + \pi \cdot \triangle r^2 \cdot \left(\frac{d}{2 \cdot \triangle r} + \frac{1}{3}\right)\right] \cdot \triangle P \tag{3.33}$$

$$\triangle P = P_{cyl} - P_{sup} \tag{3.34}$$

Where $\triangle r$ is the radial width of the contact area $\triangle r = \frac{D}{2} - \frac{d}{2}$.The spring force per pressure difference is plotted in Figure 3.14 as a function of the nozzle cross-sectional area for different contact area.

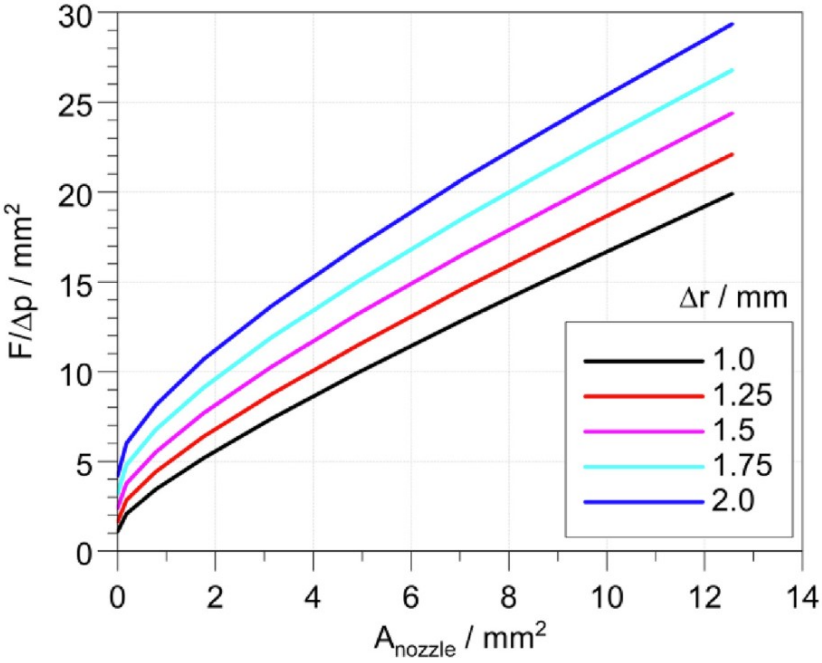

Figure 3.14: Spring force per pressure difference acting on the valve plate[14]

It can be seen that their relationship approximately increases linearly, so choose $\triangle r = 1.7mm$.Once the spring stiffness k is determined, the spring force can be established.

4

MODELLING APPROACH

As introduced above, high-pressure hydrogen injection systems will shorten engine life and reduce fuel availability. On the contrary, low-pressure hydrogen injection systems can solve these problems well. Direct injection can reduce backfire and leakage risks compared to the port injection. At the same time, it can easily meet the engine power demand, so for the application of hydrogen fuel in ship engines, the low-pressure direct injection system will become a better choice.

4.1 ENGINE VERIFICATION

We chose the X92-DF dual-fuel engine of WinGD Company as the simulator, and the parameters of this model engine are as follows:

X92-DF(two stroke)	
Cylinder Bore	**920mm**
Piston Stroke	**3468mm**
Speed	**80rpm**
Mean effective pressure at R1	**17.3bar**
Stroke/Bore	**3.77**
Number of Cylinders	**12**
BSGC(Gas)	**134.6g/kWh**
BSFC(Fuel)	**173.9g/kWh**
Output Power	**63840kW**
Compresstion Ratio for LNG	**12.4**
Stoichiometric air-fuel Ratio for hydrogen	**34.3**
Fuel of LHV	**42.7MJ/kg**
LNG of LHV	**50MJ/kg**
Hydrogen of LHV	**120MJ/kg**

4.1.1 *Engine efficiency*

The effective engine efficiency is defined as brake power divided by the overall heat flow corresponding to the fuel input:

$$\eta_e = \frac{P_b}{\dot{Q}_f} \tag{4.1}$$

Heat flow and fuel flow are related by the lower heat value of the fuel:

$$\dot{Q}_f = \dot{m}_f \cdot h^L \tag{4.2}$$

And fuel consumption related to the brake power(in this case is BSGC or BSFC):

$$BSGC(BSFC) = \frac{\dot{m}_f}{P_b} \tag{4.3}$$

Now the total efficiency of the engine can be expressed approximately as:

$$\eta_e = \frac{1}{BSGC(BSFC) \cdot h^L} \tag{4.4}$$

In case LHV is expressed in kJ/kg and BSGC(BSFC) is in g/kWh,the expression is:

$$\eta_e = \frac{3600000}{BSGC(BSFC) \cdot h^L} \tag{4.5}$$

Substituting the data in the above table, the efficiency of this type of engine in gas mode can be obtained as:

$$\begin{aligned} \eta_e &= \frac{3600000}{(134.6 \times 50000} \\ &= 53.45\% \\ &= 53.5\% \end{aligned} \tag{4.6}$$

the efficiency of this type of engine in fuel mode can be obtained as:

$$\begin{aligned} \eta_e &= \frac{3600000}{173.9 \times 42700} \\ &= 48.3\% \end{aligned} \tag{4.7}$$

From this, we can get that the efficiency of this type of engine in gas mode is higher than that of traditional fuel mode.

4.1.2 *Compression Ratio*

We already know the efficiency of the engine in the gas mode is 53.5%, and the overall efficiency of the engine is work output divided by heat input:

$$\eta_e = \frac{W_e}{Q_f} \tag{4.8}$$

Then the brake power is linked to the effective work ouput of a discrete cycle as follows:

$$W_e = \frac{P_b}{f} \tag{4.9}$$

The cycle frequency for a 2-stroke 12 cylinders engine equals:

$$\begin{aligned} f &= \frac{i \cdot N}{k} \\ &= \frac{n_e \cdot 12}{60 \cdot k} \\ &= \frac{80 \times 12}{60 \times 1} \\ &= 16Hz \end{aligned} \tag{4.10}$$

Then the work done by each cylinder is:

$$\begin{aligned} W_e &= \frac{P_b}{f} \\ &= \frac{63840}{16} \\ &= 3990kJ \end{aligned} \tag{4.11}$$

Then the heat input by each cylinder is:

$$\begin{aligned} Q_f &= \frac{W_e}{\eta_e} \\ &= \frac{3990}{53.5\%} \\ &= 7457.97kJ \end{aligned} \tag{4.12}$$

For the overall heat input, the following amount of hydrogen per cycle is necessary:

$$\begin{aligned} m_f &= \frac{Q_f}{h^L} \\ &= \frac{7457.97}{120000} \\ &= 0.062kg \end{aligned} \tag{4.13}$$

Next, use the Seiliger process to analyze whether the compression ratio of this type of engine is appropriate. The current compression ratio is 12.4.
The stroke volume:

$$\begin{aligned} V_s &= L_s \cdot A_B \\ &= 3468 \times \frac{\pi}{4} \times 920^2 \\ &= 2.31m^3 \end{aligned} \tag{4.14}$$

The combustion volume at top dead centre:

$$\begin{aligned} V_{TDC} &= \frac{V_s}{\epsilon - 1} \\ &= \frac{2.31}{12.4 - 1} \\ &= 0.203m^3 \end{aligned} \tag{4.15}$$

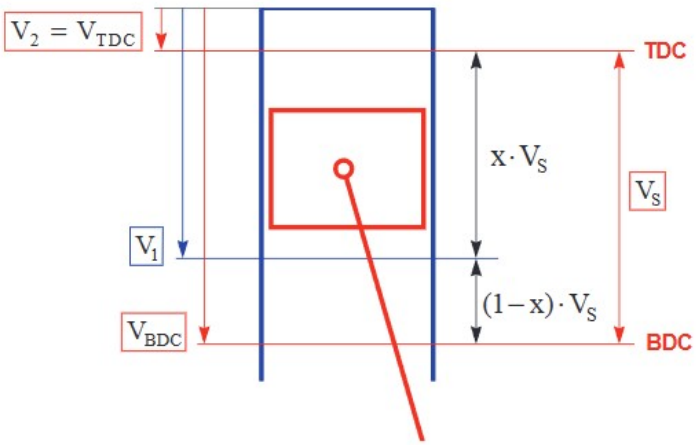

Figure 4.1: Stroke volume

The trapped volume on the other hand is not equal to the volume at BDC since the inlet valve normally close after BDC.

$$V_1 = x \times V_s + V_{TDC} \tag{4.16}$$

And the effect that compression does not start at BDC gives rise to the idea of introducing an effective compression ratio:

$$\begin{aligned} r_C &= \frac{V_1}{V_{TDC}} \\ &= x \cdot (\epsilon - 1) + 1 \end{aligned} \tag{4.17}$$

For the 2-stroke engine the inlet ports close at 45 to 55 degrees after BDC to allow time for the scavenging process: an x-value around 0.82 to 0.79 is more realistic for this type of engine. In our case, choose 0.8 as the value of x.

$$\begin{aligned} V_1 &= 0.8 \times 2.31 + 0.203 \\ &= 2.05m^3 \\ r_C &= 0.8 \times (12.4 - 1) + 1 \\ &= 10.12 \end{aligned} \tag{4.18}$$

Use the Seiliger process to analyze whether hydrogen can be ignited in the compression stage 1 to 2. These data are valid for nominal ambient conditions: air temperature 298K, and auto-ignition temperature is 858K.

$$\begin{aligned} \frac{T_2}{T_1} &= r_C^{n_C-1} \\ \frac{858}{298} &= 10.12^{n_C-1} \\ n_c &= 1.46 \end{aligned} \tag{4.19}$$

The specific heat ratio of hydrogen is:

$$\begin{aligned} \gamma &= \frac{c_P}{c_V} \\ &= 1.4 \end{aligned} \tag{4.20}$$

It can be seen that the value of the variable index n is greater than the specific heat ratio of hydrogen in the compression stage, but it should be smaller, which means that the currently selected compression ratio cannot meet the compression ignition hydrogen. In order to obtain the minimum required compression ratio, the value of n_C is set to 1.4, and the effective compression ratio can be obtained by substituting it into the calculation:

$$\begin{aligned} \frac{858}{298} &= r_C^{n_C-1} \\ 2.88 &= r_C^{0.4} \\ r_C &= 14.1 \\ \epsilon &= 17.38 \end{aligned} \tag{4.21}$$

The compression ratio obtained here is 17.38. Through the Seiliger process, we can conclude that it is OK to use compression ignition when the initial pressure is not higher than 1.23 bar. However, due to the low-density nature of hydrogen, to meet the power output requirements of the engine, a turbocharger is often added to compress the hydrogen to provide sufficient volumetric energy density. To

avoid backfire, we use direct injection technology, which means that the initial pressure is generally 2 to 3 bar and is unlikely to be lower than 1.23 bar. The engine model currently used is already the largest two-stroke engine in the world. If naturally aspirated, the engine will be three to four times larger than it is now, which is not worth it for compression ignition.

4.2 AVAILABLE INJECTION WINDOW

After modeling the basic operating principles of the injector mathematically, it is necessary to determine the appropriate injection timing. Given that this study involves the largest dual-fuel two-stroke engine in the world, it is essential to match the engine parameters with the injector parameters. Since this study uses compressed hydrogen as fuel, it is necessary to analyze the cylinder pressure change during the compression stroke to better match the engine with the injector. The analysis of cylinder pressure change will focus on the period from the beginning of the compression stroke to just before the combustion stroke, as the engine uses compressed hydrogen as fuel and an early injection strategy.

4.2.1 *Crank-Slider Kinematics*

Since the research focuses on the compression stroke, the Seliger process is used to analyze it, as in the engine verification chapter, and combined with the geometric model of the crank slider mechanism to obtain the cylinder pressure as a function of the crank angle. In the derivation process of this section, hydrogen is regarded as an ideal gas. The compression stroke is also considered isentropic compression, and the influence of the change of the polytropic index of hydrogen in the compression stroke is not considered.

$$\frac{V_1}{V_2} = r_C \tag{4.22}$$

$$\frac{P_2}{P_1} = r_C^{n_C} \tag{4.23}$$

$$P_2 = P_1 \cdot (\frac{V_1}{V_2})^{n_C} \tag{4.24}$$

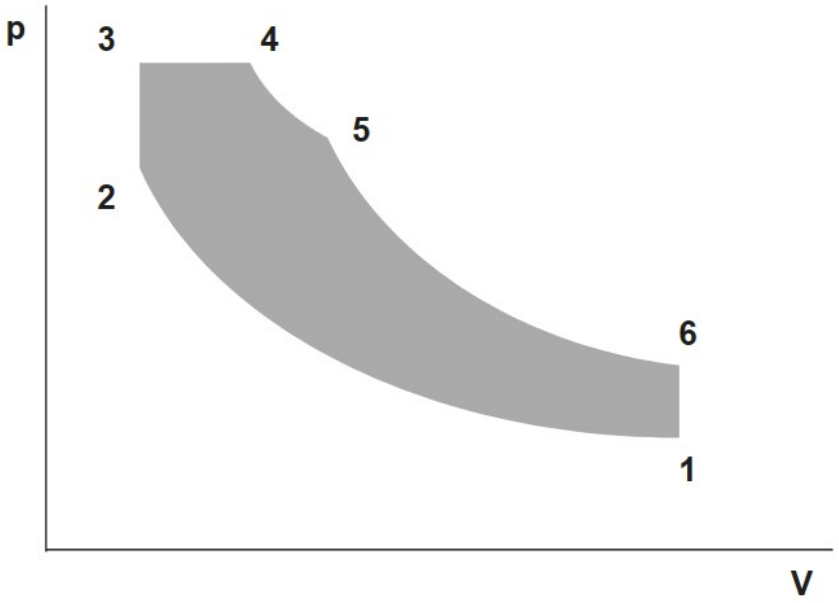

Figure 4.2: Ideal Seiliger process

Where V_1 and V_2 correspond to the cylinder volumes at the beginning and the end of the compression stroke respectively,P_1 and P_2 correspond to the cylinder pressure at the beginning and the end of the compression stroke respectively.r_C is the effective compression ratio,and n_C is the polytropic index for the compression stroke.
At this point, it can be seen that to derive the equation for the cylinder pressure variation, an analysis of the cylinder volume changes is necessary. For the convenience of modeling, the geometric model of a crank-slider mechanism is used, as shown in the Figure 4.3.

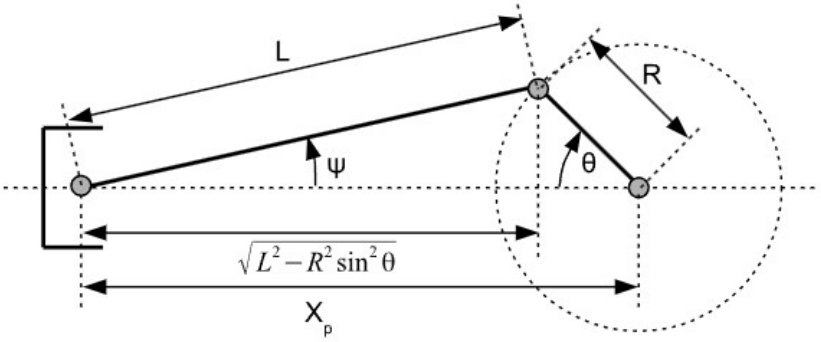

Figure 4.3: Schematic overview of a crank-cylinder mechanism[27]

Where R is the crank radius,L is the connecting rod length,θ is crank angle and X_P is the piston position.The mathematical relationship between piston position and crank angle is as follows:

$$X_P(\theta) = R + L - \left[(L^2 - R^2\sin^2\theta)^{\frac{1}{2}} + R\cdot\cos\theta\right] \tag{4.25}$$

After determining the piston position, the corresponding cylinder volume can be determined:

$$V(\theta) = \frac{\pi}{4}\cdot d^2\cdot X_P(\theta) \tag{4.26}$$

Therefore the relationship between the cylinder pressure and the crank angle is as follows:

$$P_2 = P_1\cdot(\frac{V(\theta_1)}{V(\theta_2)})^{n_C} \tag{4.27}$$

4.3 MATHEMATICAL MODEL

The working principle and parameter design of the hydrogen injector, as well as the mathematical modeling of the cylinder pressure change during the compression stroke, have been previously discussed. This

chapter introduces several specific and critical assumptions for the mathematical modeling of this project, namely the linkage process between the injector solenoid valve and the pneumatic valve, the positioning of the fuel injector, and the setting of the spring force for the pneumatic valve.

4.3.1 *Solenoid Valve*

In the chapter introducing the prototype of the hydrogen injector, the working principle of this new type of injector is detailed. Essentially, when the solenoid valve is energized, the ball valve opens, causing a change in the internal pressure of the pneumatic valve, which in turn opens the valve plate and start injection. From the introduction of the working principle, it can be seen that when the solenoid valve is energized, the expression for the pressure variation inside the pneumatic valve is:

$$\frac{\mathrm{d}p}{\mathrm{d}t} = -\psi_{max} \cdot \sqrt{2 \cdot R \cdot T_{sup}} \cdot \frac{A_{eff,BV}}{V(t)} \cdot P \tag{4.28}$$

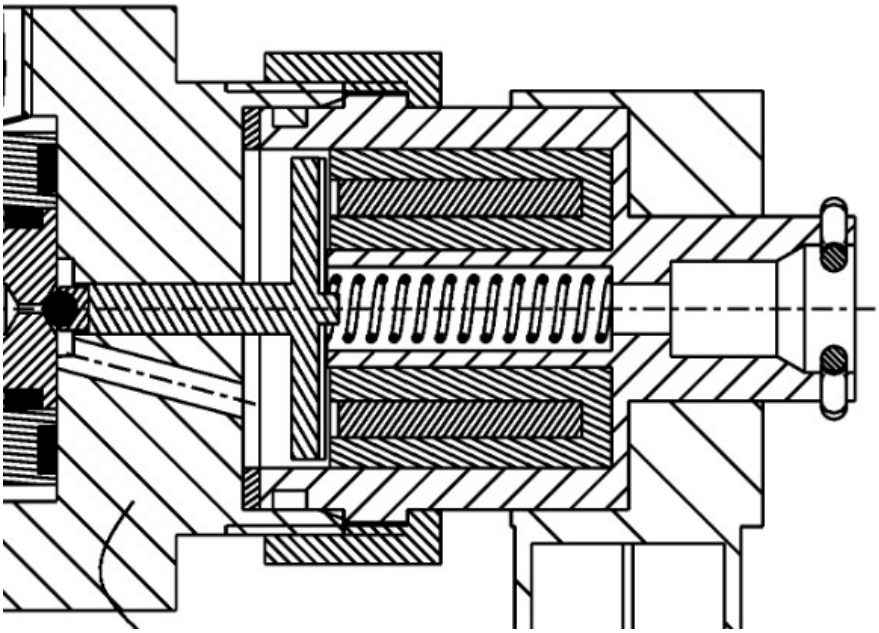

Figure 4.4: Solenoid valve and ball valve [26]

When the solenoid valve is de-energized, the expression for the pressure variation inside the pneumatic valve is:

$$\frac{\mathrm{d}p}{\mathrm{d}t} = \psi_{max} \cdot \sqrt{2 \cdot R \cdot T_{sup}} \cdot \frac{A_{eff,RO}}{V(t)} \cdot P_{sup} \tag{4.29}$$

It can be observed that these two equations are quite similar, with the main differences being:

- When energized, the pressure variation inside the pneumatic valve results in a decrease,when de-energized, the pressure variation inside the pneumatic valve results in an increase.
- Different effective flow cross-sectional areas
- When energized, only gas flows out, and when de-energized, only gas flows in. Therefore, the instantaneous pressure change inside when energized needs to be considered, while the pressure of the gas flowing in when de-energized is constant.

Therefore, to simplify the modeling, the mathematical expression of the solenoid valve operation is not derived in detail. Instead, switching between different pressure variation equations and the corresponding parameter changes represents the process of the solenoid valve being energized and de-energized.

4.3.2 *Injector Position*

In most large two-stroke engines, the injector is often placed at the top of the engine cylinder, that is, at the cylinder head. The benefits of this placement are obvious: it can mix better with the air, leading to improved combustion efficiency. However, this also imposes higher requirements on engine design, most notably the significantly increased sealing requirements for the injector. Firstly, during the compression stroke, after injection ends, the valve plate needs to remain closed, but the cylinder pressure at the end of the compression stroke is often quite high. Secondly, during the engine's operation, there is a peak pressure point within the cylinder, usually occurring shortly after fuel combustion. During this time, the injector must also maintain its seal, or it may lead to continuous explosions causing engine knocking.

Therefore, in this study, the injector is placed in the middle of the cylinder, approximately 40% to 50% of the distance from the top dead center. As shown in the Figure 4.5.

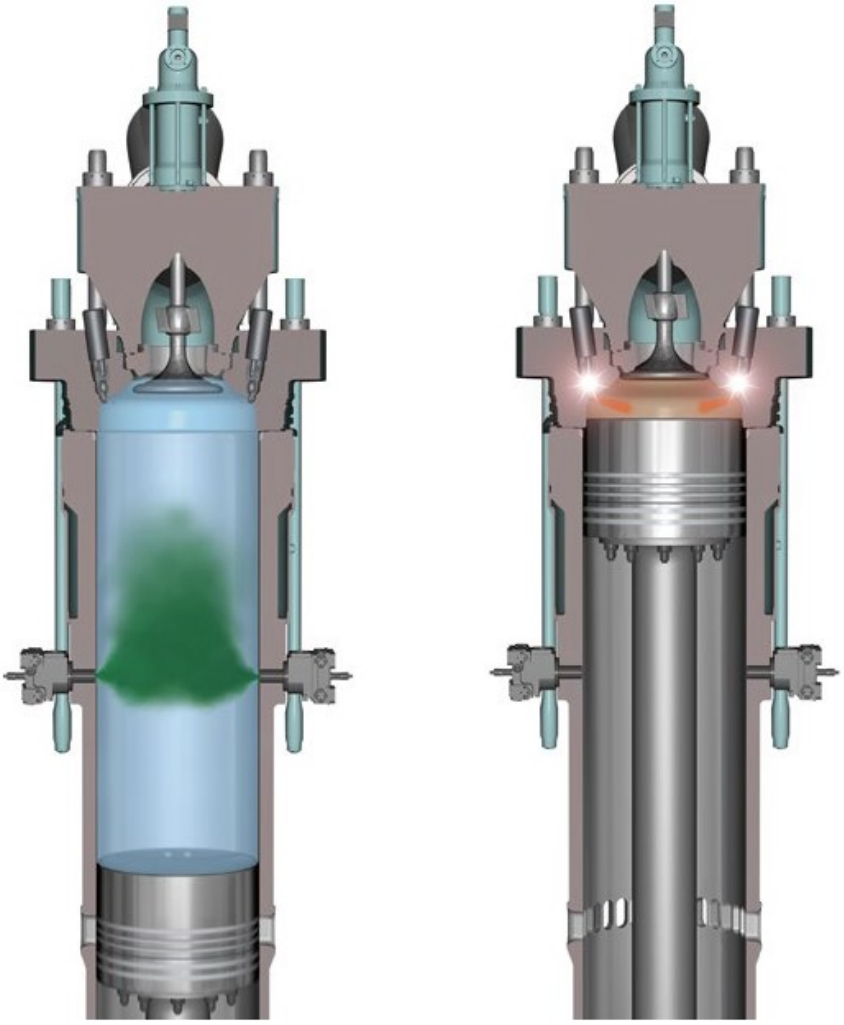

Figure 4.5: Injector position[28]

When the injector is placed in the middle of the cylinder, the sealing requirements for the injector are significantly reduced. Firstly, during the compression stroke, the cylinder pressure does not increase significantly before the piston head passes the nozzle, and it is often lower than the injection pressure. This creates a pressure differential on the valve plate that acts as suction, which can even help seal

the injector. Secondly, after the piston head passes the nozzle, the pressure connected between the nozzle and the inside of the cylinder becomes the crankcase pressure. At this time, the pressure is much lower than the cylinder pressure when the piston head reaches the top dead center, meaning that the peak pressure of the engine no longer needs to be considered in the injector's sealing design, greatly reducing the sealing requirements.

4.3.3 *Spring Force*

In the hydrogen injector, the primary component that is responsible for the sealing function is the spring in the pneumatic valve, making the setting of the spring force a crucial point. As mentioned in the chapter on the injector prototype, the spring force, which must ensure that the valve plate does not open accidentally, is calculated using a formula from the literature that considers the peak pressure inside the cylinder. This means that $P_{cyl,max}$, which is used in the calculation, represents the peak cylinder pressure.

$$\triangle P = P_{cyl,max} - P_{sup} \tag{4.30}$$

This results in a relatively large calculated spring force. However, in this research, the injector is placed in the middle of the cylinder. Before the piston head rises to the nozzle, the cylinder pressure does not change significantly. Therefore, the cylinder pressure is approximated to be equal to the pressure of the air after turbo compression. For simplicity in calculations, a constant cylinder pressure $P_{cyl} = 3\text{bar}$ is chosen.

4.4 MODEL VALIDATION

The mathematical model is derived based on the original literature[14]. However, since the original literature does not describe the physical process of the valve plate's lifting and falling, it is necessary to validate this mathematical model. By substituting the parameters

from the original literature (as shown in the Table 5.1) into the model, the following figures were obtained.

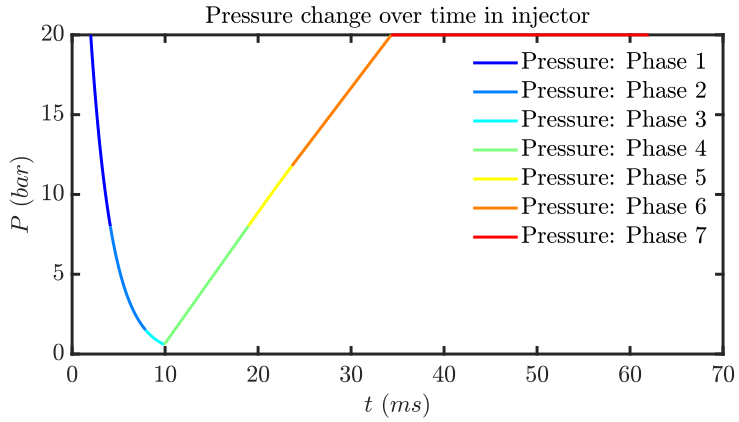

Figure 4.6: Pressure change based on literature parameters

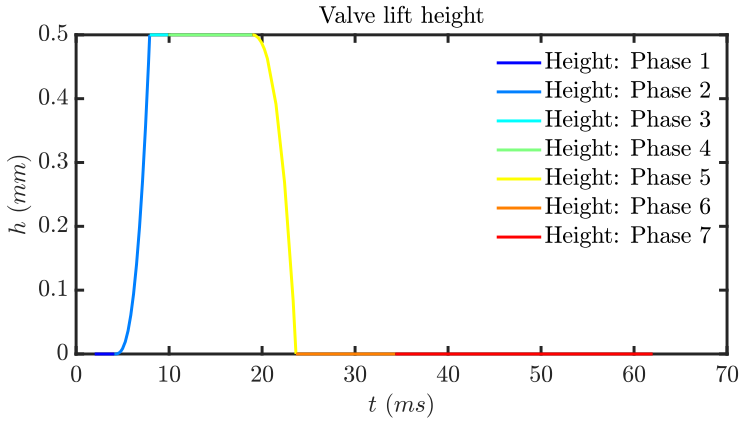

Figure 4.7: Valve lift based on literature parameters

From Figure 4.6 and Figure 4.7, it can be observed that the overall trend is very similar to that in the original literature. It is important to note that the first six phases shown in the figure correspond to the six phases described in the Section 3.1. The seventh phase in the figure represents the phase where hydrogen is refilling to the supply pressure, and this pressure is maintained until the process

ends. The purpose of including this phase is to better illustrate the physical process. Therefore, the sixth and seventh phases in the figure essentially represent the final phase described in the Section 3.1.

This page intentionally left blank

5

SIMULATION AND RESULTS

This chapter primarily uses the formulas introduced in the previous mathematical modeling section for simulation. Since the main parameters of the engine have already been discussed in the engine verification section, the focus will be on the parameter design of the hydrogen injector.

5.1 SIMULATION PARAMETERS

5.1.1 *In-cylinder pressure changes during the compression stroke*

As previously mentioned, it is necessary to first determine an appropriate injection window. Therefore, the engine was modeled using the kinematics of the crank-slider mechanism, focusing on the cylinder pressure change during the compression stroke. Consequently, the cylinder pressure change shown in the simulation results mainly exhibits an upward trend.as shown in the Figure 5.1.

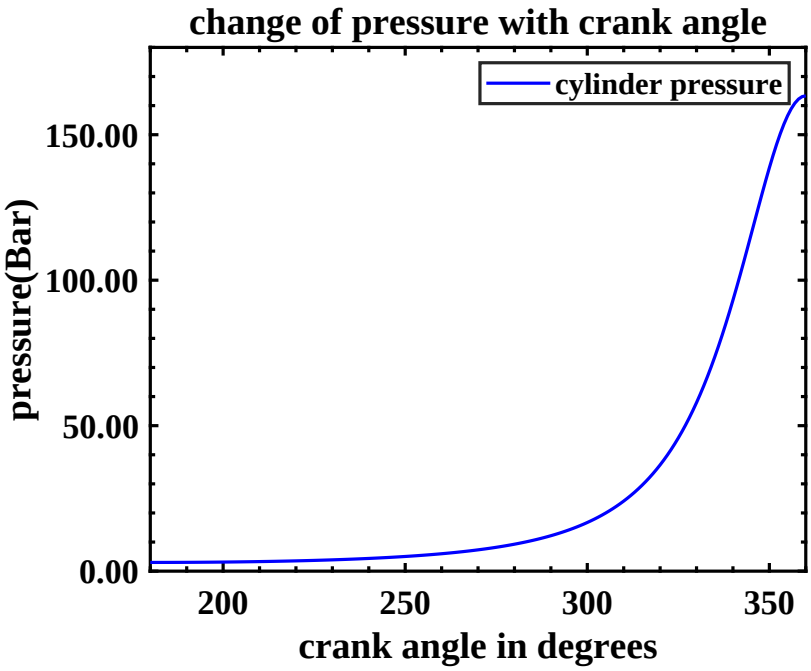

Figure 5.1: Cylinder pressure during compression stroke

Figure 5.2 shows the cylinder pressure variation during the compression stroke, with an initial cylinder pressure of $P_{cyl} = 3bar$, in the crank angle range of 180° to 360°. As discussed in the previous section regarding the injector prototype, it's necessary to consider the critical pressure ratio during injection. If the pressure at the nozzle exceeds the critical pressure ratio, the nozzle may become chocked, leading to stop injection. Since this study focuses on low-pressure injection, the injection pressure is set at $P_{sup} = 50bar$.Then,calculate the critical pressure ratio:

$$\frac{P_{cyl}}{P_{sup}} = (\frac{2}{\kappa + 1})^{\frac{\kappa}{\kappa - 1}} = 0.528 \tag{5.1}$$

Where κ is the hydrogen specific heats,$\kappa = 1.4$.After setting the injection pressure to $P_{sup} = 50bar$, the critical pressure in the cylinder

is:

$$P_{cyl,critical} = P_{sup} \cdot (\frac{2}{\kappa+1})^{\frac{\kappa}{\kappa-1}} = 26.4 \tag{5.2}$$

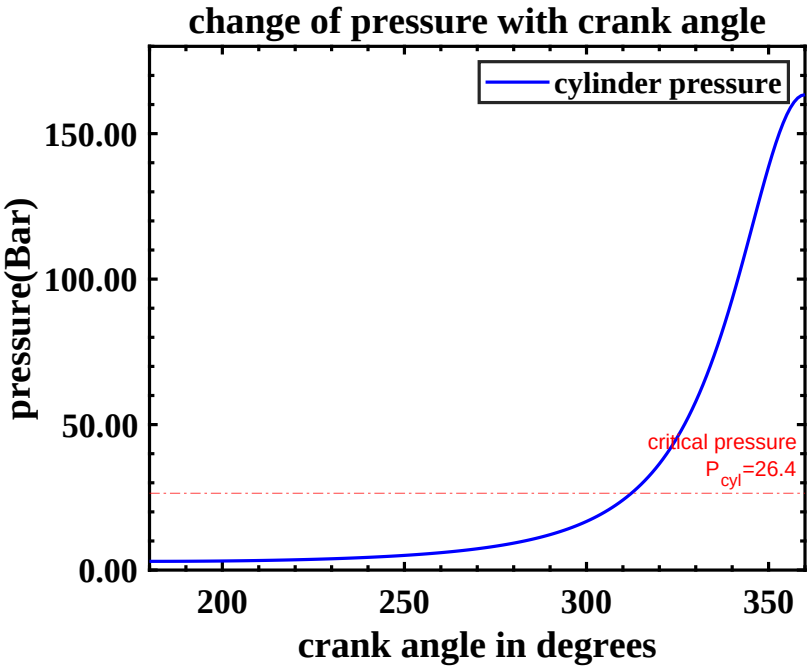

Figure 5.2: Critical pressure

However, since this study adopts the approach of placing the injector in the middle of the cylinder, injection should end when the piston head passes the nozzle. This means that the total volume of the cylinder cannot be applied, implying that injection should stop earlier than when reaching the critical pressure. Therefore, it is necessary to obtain the relationship between the piston's motion and the crankshaft angle, as shown in the Figure 5.3.

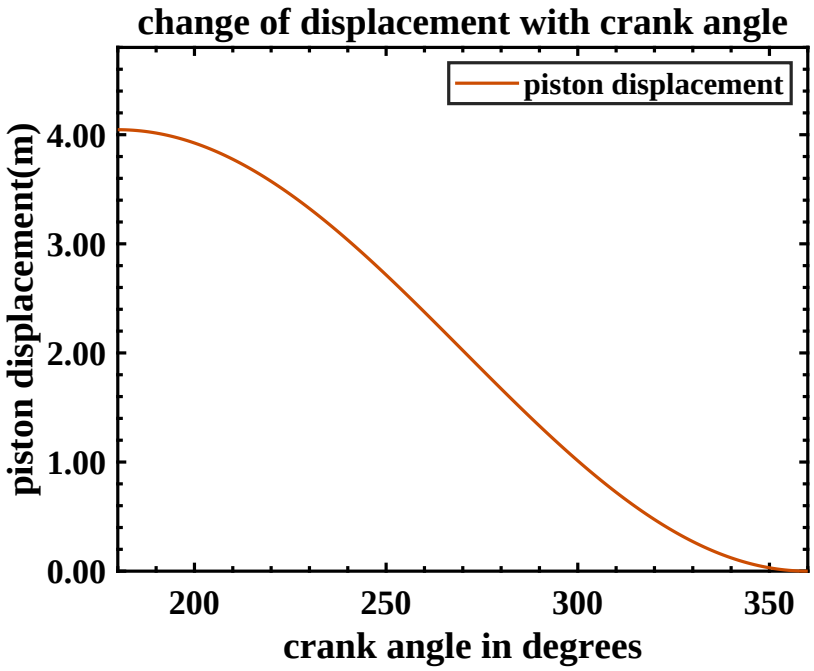

Figure 5.3: Piston displacement

Figure 5.3 shows the variation of the distance from the piston head to the top dead center with the change of crank angle. Since it's the compression stroke, the overall trend is a decrease. For simulation convenience, the position of the injector is set at half of the total displacement of the piston head, which is 50% of its position, as shown in the Figure 5.4.

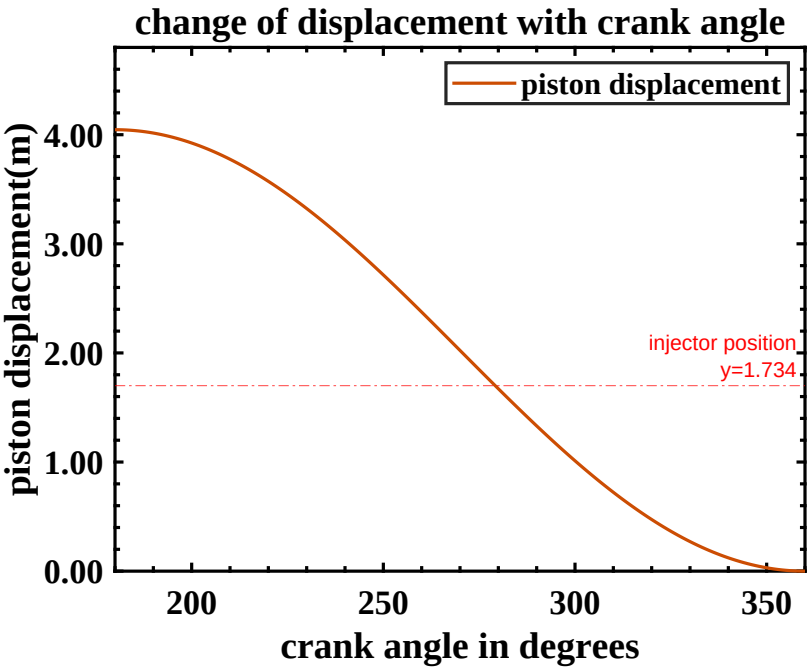

Figure 5.4: Crank angle when the piston head moves to the middle of the cylinder

As depicted in the Figure 5.4, when the piston head displaces to the middle of the cylinder, which corresponds to the location of the injector, the corresponding crank angle is approximately 279°. This angle is smaller than the crank angle of 322° when the cylinder pressure reaches the critical pressure. Therefore, the available injection window should be from 180° to 279°, indicating an angular range of approximately $\triangle\alpha_{inj} = 100°$ for the available injection window. As illustrated in the Figure 5.5.

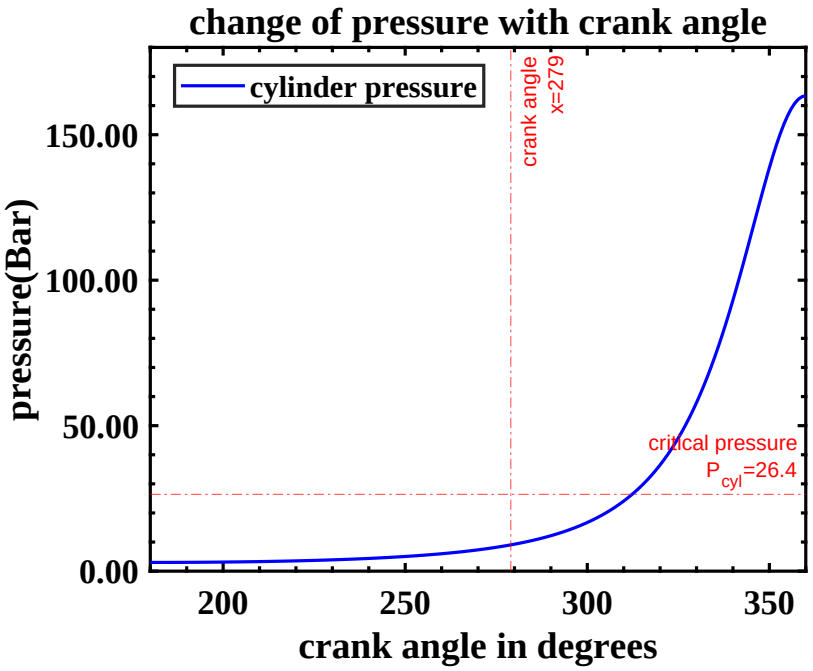

Figure 5.5: The available injection window

5.1.2 *Injector Parameters*

Once the available injection window is determined, the parameters of the injector can be designed to match the engine. The first step is to calculate the total static mass flow rate $\dot{m}_{static}$ required during injection:

$$\dot{m}_{static} = \frac{m_{H_2}}{\triangle t_{inj}} = \frac{\omega_i}{\eta_i \cdot H_u} \cdot V_h \cdot n \cdot \frac{360}{\triangle \alpha_{inj}} \tag{5.3}$$

$$\dot{m}_{static} = \frac{3990kJ}{0.535 \times 120000kJ/kg} \times 80 \times 60 \times \frac{360}{100} = 1074kg/h \tag{5.4}$$

The corresponding effective flow cross-sectional area $A_{eff}$is:

$$A_{eff} = \frac{\dot{m}_{static}}{\psi \cdot P_{sup} \cdot \sqrt{\frac{2}{R \cdot T_{sup}}}} \tag{5.5}$$

$$A_{eff} = \frac{1074kg/h}{0.484 \times 50bar \times \sqrt{\frac{2}{4125.6J/kg \cdot k \times 293.15K}}} = 96mm^2 \tag{5.6}$$

Then the reference flow cross-sectional area A_{ref} is:

$$A_{eff} = C_D \cdot A_{ref} \tag{5.7}$$

$$A_{ref} = \frac{A_{eff}}{0.6} = 160mm^2 \tag{5.8}$$

Then the nozzle diameter is:

$$A_{nozzle} = A_{ref} = \frac{\pi}{4} \cdot d^2 \tag{5.9}$$

$$d = 14.27mm \tag{5.10}$$

Then the valve lift height h is:

$$h = \frac{1}{4} \cdot d = 3.6mm \tag{5.11}$$

After obtaining the above injector parameters, the formula used in the literature to calculate the spring force is as follows:

$$F_{spring} = \left[\frac{\pi}{4} \cdot d^2 + \pi \cdot \triangle r^2 \cdot (\frac{d}{2 \cdot \triangle r} + \frac{1}{3}) \right] \cdot \triangle P \tag{5.12}$$

$$\triangle P = P_{cyl} - P_{sup} \tag{5.13}$$

Where $\triangle r = \frac{D}{2} - \frac{d}{2}$ is the maximal contact surface diameter.Since the injector is placed in the middle of the cylinder, the cylinder pressure does not need to account for peak pressure. Additionally, through the observation of cylinder pressure changes, it can be seen that when the piston head passes the nozzle, the cylinder pressure is much lower than the injection pressure, which results in the cylinder pressure creating a suction force on the valve plate surface. This means that when calculating the spring force, there is no need to consider the risk of the valve opening accidentally due to cylinder pressure changes. The spring force only needs to ensure that the valve plate is not pushed open by the supply pressure when the injector is closed.

Calculating the spring force requires analyzing the forces acting on the valve plate. As introduced in the section on the injector's working principle, the effective area of the valve plate in contact with the valve seat is:

$$S_{eff} = \frac{\pi}{4} \cdot (d_2^2 - D^2) \tag{5.14}$$

Where d_2 is the radial width of the valve plate. In the literature[14], a diameter of $d_{2,lit} = 15mm$ was used. However, since the engine used in this study is a large two-stroke engine, the nozzle diameter is approximately five times that in the literature. After considering the strength of the metal structure,choose $d_2 = 75mm$ for this study. Accordingly, the value of $\triangle r$ is also increased fivefold. In the literature, $\triangle r = 1.7$ was used, so in this study, $\triangle r = 8.5$ is adopted as the parameter, resulting in $D = 31.27mm$. Then $F_{spring} = 875N$,considering the effect of the suction force generated by the cylinder pressure on the valve plate surface.

The Table 5.1 presents a comparison of the injector parameters used in this study and those in the literature.

Geometric parameters	literature	Research
$\dot{m}_{static}$	$17.43kg/h$	$1074kg/h$
A_{eff}	$3.9mm^2$	$96mm^2$
A_{ref}	$6.5mm^2$	$160mm^2$
d	$3mm$	$14.27mm$
h	$0.75mm$	$3.6mm$
$\triangle r$	1.7	8.5
d_2	$15mm$	$75mm$
D	$6.4mm$	$31.27mm$
F_{spring}	$214N$	$875N$

Table 5.1: Comparison of design parameters of the injector in the original literature and this study[14]

It can be observed that the injector parameters matching the engine selected for this study, derived using the same method as in the literature, show a clear multiple relationship with the parameters in the original literature. Part of this is due to proportional scaling after considering the strength of the metal material, but the main reason is that the chosen engine is currently the largest two-stroke dual-fuel engine in the world. Therefore, there are significant differences in the design parameters.

5.2 RESULTS

The focus of this study is primarily on the compression stroke phase, so it is necessary to calculate the time required for one cylinder of the engine to complete one working cycle.

$$f = \frac{i \cdot N}{k} \tag{5.15}$$

$$f = \frac{80 \times 12}{60 \times 1} = 16Hz \tag{5.16}$$

Then,the cycle time T is:

$$T = \frac{1}{f} = 750ms \tag{5.17}$$

In the engine verification chapter, the mass of hydrogen required for one cylinder to complete one working cycle under 100% work load conditions was calculated as follows:

$$m_f = \frac{Q_f}{h^L} = 0.062kg \tag{5.18}$$

Thus, the injection duration can be calculated as follows:

$$t_{inj} = \frac{m_f}{\dot{m}_{static}} = 208ms \tag{5.19}$$

Set injection pressure $P_{sup} = 50bar$,and the simulation results are shown in the figure below.

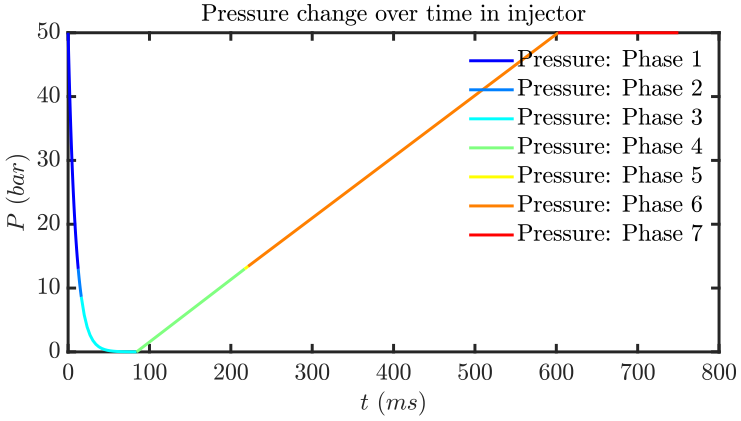

Figure 5.6: Injector operation at 100 % engine working load

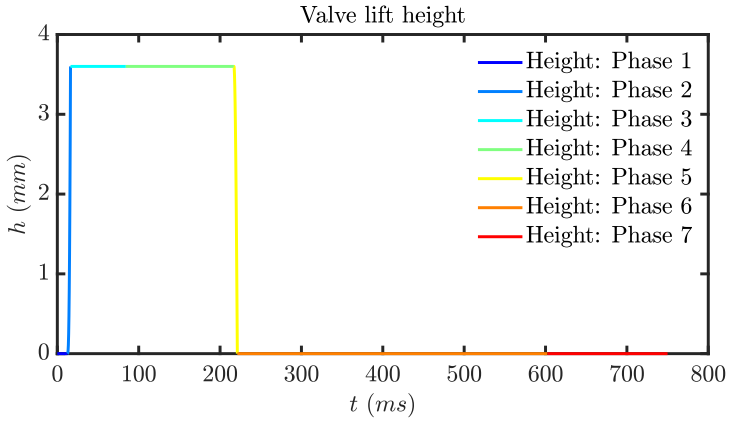

Figure 5.7: Injector operation at 100 % engine working load

From the Figure 5.6 and Figure 5.7, it can be observed that the trend of internal pressure variation and valve displacement of the injector resembles that of the trends in the original literature, indicating that the mathematical model effectively simulates the operation of this new injector. At 100 % engine working load, the valve lift height reaches the calculated height from the theoretical calculations, indicating that sufficient hydrogen is injected during the available injection window to meet the engine's output power requirements. Additionally, the trend of pressure variation within the injector matches the derivation in the section describing the injector's operational principles.

This model can also achieve the function of controlling engine conditions by adjusting the injection duration. With the injector parameters determined and the injection pressure unchanged, the static mass flow rate at the nozzle remains constant. Through the following equation, it can be observed that adjusting the injection duration allows for the adjustment of the total hydrogen mass injected into the cylinder, ultimately achieving the function of adjusting engine conditions:

$$m_f = t_{inj} \cdot \dot{m}_{static} \tag{5.20}$$

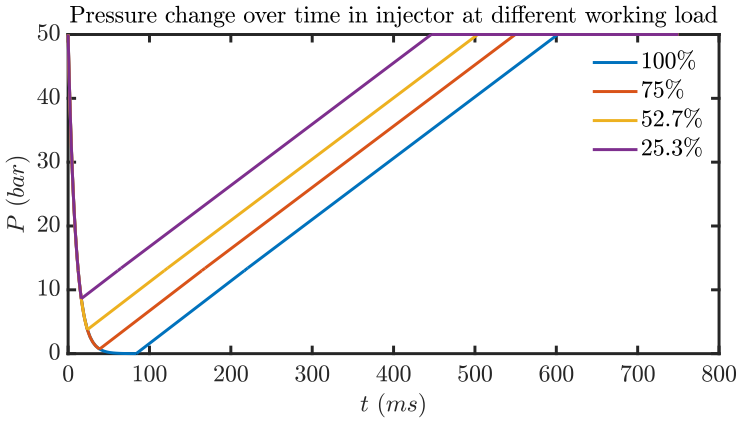

Figure 5.8: Comparison of pressure changes under different working loads

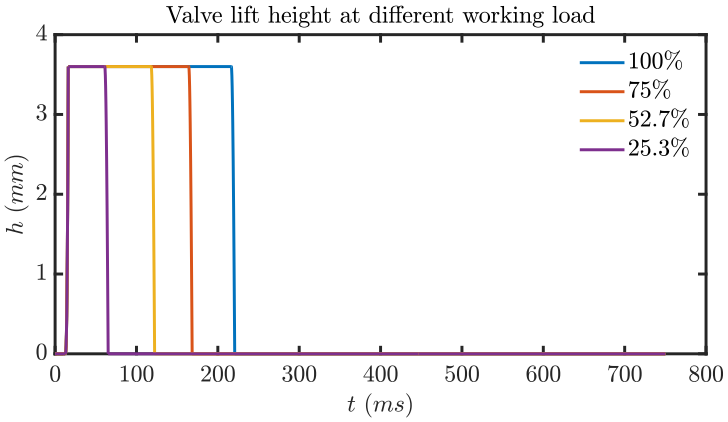

Figure 5.9: Comparison of valve lifts under different working loads

From Figure 5.8 and Figure 5.9, it can be seen that by adjusting the injection timing, the engine's working load can be controlled. This is most evident in the significant difference in the duration of the valve plate's lift under different working load. The lifting and closing of the valve plate are controlled by the energization and de-energization of the solenoid valve. When the solenoid valve is energized, the ball valve lifts, causing a rapid drop in internal pressure, which results in the valve plate lifting. When the solenoid valve is de-energized,

the ball valve closes, leading to an increase in internal pressure, causing the valve plate to close. There is a delay time associated with the opening and closing of the ball valve, meaning that when the solenoid valve is energized or de-energized, the action of opening or closing the ball valve takes some time to complete. This period is referred to as the delay time.

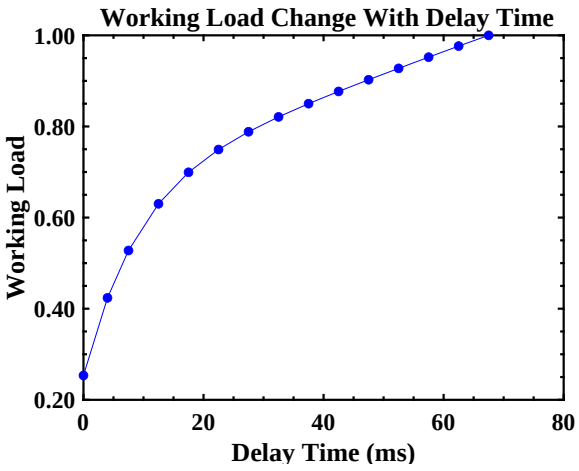

Figure 5.10: Variation in working load with changes in delay time

Figure 5.10 illustrates the relationship between delay time and engine working load. Combining this with the results discussed earlier, it can be understood that by adjusting the delay time, the duration of the valve plate's lift can be influenced, which in turn affects the duration of the injection and, ultimately, the amount of hydrogen injected. This subsequently changes the engine working load. Figure 5.11 illustrates the relationship between delay time and total consumed hydrogen mass.

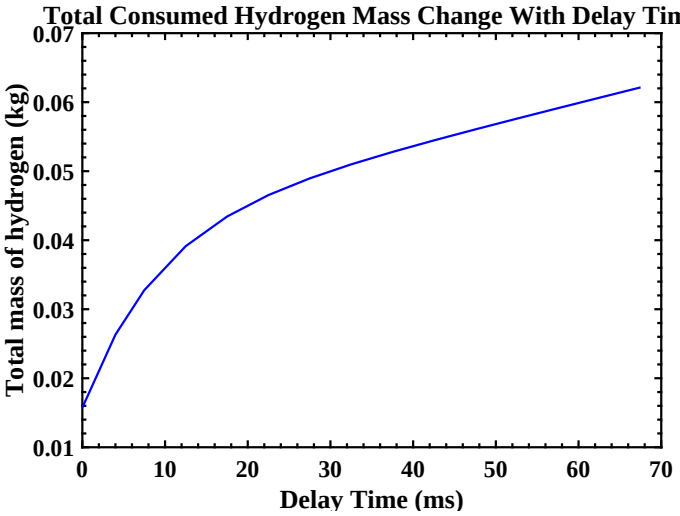

Figure 5.11: Variation in total hydrogen consumption with changes in delay time

6

CONCLUDING REMARKS

Based on the simulation results above, the following conclusions can be drawn from this study:

- The parameter design of the injector is closely related to the engine parameters. Directly related parameters include the static mass flow rate of hydrogen and the available injection window. Indirectly related parameters include the effective flow area and nozzle diameter. Additionally, some parameters, such as the radial diameter of the valve plate, need to be correspondingly enlarged to match the engine.
- The mathematical model established in this study theoretically demonstrates that with well-matched injector parameter design, this new type of injector can be applied to low-pressure direct injection hydrogen fuel engines, even in large two-stroke engines.
- When the injector is placed in the middle of the cylinder, the peak pressure of the cylinder can be disregarded, which simplifies the design of the injector. However, it is necessary to consider the crank angle when the piston head passes over the nozzle and adjust the injection duration accordingly.
- The mathematical model also demonstrates that by changing the injection duration, it is possible to adjust the engine's operating conditions. This has a positive impact on improving fuel efficiency during a ship's voyage.

This page intentionally left blank

7

DISCUSSION

The focus of this study is to theoretically simulate the operation of this new type of injector in a large two-stroke engine and to explore its feasibility for application. During the research process, certain assumptions and simplifications were made for convenience, which may affect practical applications.

- In analyzing the working principle of the injector, numerical simulation of the solenoid valve was not performed. Instead, switching mathematical equations were used to represent the process of the solenoid valve receiving the start or end injection signal. Although the model's delay is reflected in the numerical simulation results, it cannot fully replicate the actual working process.
- When designing injector parameters based on engine parameters, some parameters, such as the selection of the valve plate's radial diameter, are chosen as approximate values after considering the practical design feasibility and metal strength. Although the numerical simulation results have effectively realized the working process of the injector, more detailed research is required.
- Placing the injector in the middle of the cylinder can reduce the difficulty of injector design, but whether this affects the uniformity of fuel mixing has not been thoroughly explored in this study. Future research could utilize CFD to analyze the diffusion and mixing degree of hydrogen during the injection

process and compare the impact of different injector positions on engine performance.

- In this modeling process, the focus was on the compression stroke, which was theoretically considered as an isentropic compression, with the specific heat ratio of hydrogen assumed to be constant. However, this is not feasible in practical applications, so the simulation results are for reference only. At the very least, results demonstrate the theoretical feasibility of applying this injector to a two-stroke engine.

- In this study, only the injection duration was considered as a variable for adjusting engine working load, while other variables were not taken into account. In the future, research could explore changing the injection angle of the nozzle or the injection pressure of the injector.

In summary, the main focus of this study was on theoretically deriving the working process of the new injector and exploring its feasibility for application in large two-stroke engines. The analysis was conducted solely through mathematical modeling and numerical simulation, without experimental validation due to time constraints and facility limitations. Hence, only theoretical possibilities were provided. Future research should consider experimental validation to obtain more accurate results.

APPENDICES

A

ENGINE PARAMETERS

X92DF-2.0

IMO Tier III in gas mode

Cylinder bore	920 mm
Piston stroke	3 468 mm
Speed	70-80 rpm
Mean effective pressure at R1	17.3 bar
Stroke / bore	3.77

RATED POWER, PRINCIPAL DIMENSIONS AND WEIGHTS

Cyl.	Output in kW at 80 rpm R1	R2	70 rpm R3	R4	Length A mm	Weight tonnes
6	31 920	26 580	27 930	23 250	11 755	1 120
7	37 240	31 010	32 585	27 125	13 345	1 260
8	42 560	35 440	37 240	31 000	14 935	1 380
9	47 880	39 870	41 895	34 875	17 960	1 630
10	53 200	44 300	46 550	38 750	19 550	1 790
11	58 520	48 730	51 205	42 625	21 215	1 960
12	63 840	53 160	55 860	46 500	22 875	2 140

Dimensions (mm)	B	C	D	
	5 550	1 900	13 140	
	F1	F2	F3	G
	15 520	15 530	14 260	2 970

BRAKE SPECIFIC CONSUMPTIONS IN GAS MODE

Rating point		R1	R2	R3	R4
BSEC (energy)	kJ/kWh	6 760	6 512	6 858	6 615
BSGC (gas)	g/kWh	134.6	129.6	136.6	131.6
BSPC (pilot fuel)	g/kWh	0.7	0.8	0.7	0.8

BRAKE SPECIFIC FUEL CONSUMPTION IN DIESEL MODE

Rating point		R1	R2	R3	R4
BSFC (diesel Tier II)	g/kWh	173.9	167.9	175.9	171.9

For definitions see page 60.

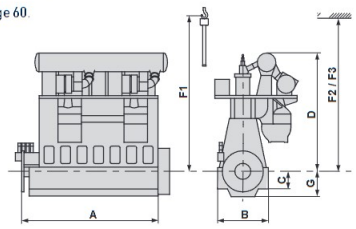

Figure A.1: Engine parameters[29]

B

MATLAB CODE

Listing B.1: MATLAB Code

```
%% Initial
clc
clear
close all
%% Constant parameter
phi_max = 0.484; %the maximum value for the flow function
R = 4125.6; % the specific gas constant of hydrogen(J/(kg*K)=kg*
    m^2/(s^2*K))
P_sup = 50e5; % supply pressure(Pa = kg/(m*s^2))
T_sup = 293.15; % supply temperature(K)
A_effBV = 0.79e-6*25; % the effective cross-sectional flow area
    of the pilot valve(m^2)
A_effRO = 0.07e-6*5; % the effective flow cross-sectional area
    of the refilling orifice(m^2)
k = 25.46e3;% spring stiffnes(N/m=kg/(s^2))
% F = 350; %cclsosing spring force(kg*m/(s^2))
% L0 = F/k*2.5; % initial displacement
d2 = 75e-3*0.4; % The diameter of the actuator piston(m)
s = 160e-6;  % the nozzle cross-sectional area(m^2)
D = 31.27e-3*0.7; % the diameter of curtain(mm)
P_cyl = 3e5; % cylinder pressure
V0 = 34.3e-6*4; %  the initial volume of the piston (m^3)
m_va = 0.825/4; % mass of valve (kg)
h_max = 3.6e-3; % maximum of height (m)
delta_t = 0e-3; %s
%% calculate constants
s1 = 3.468; %stroke in meters
```

```
d_bore = 0.92; %diameter in meters
we = 3990;%the work done by each cylinder(kJ)
u = 0.535;%efficiency of the engine in gas mode
h1 = 120000;%fuel lower heating value(kJ/kg)
n1 = 80; %rpm
alpha = 100; %available angular injection window

v = (pi/4*d_bore^2*s1)*1000;%displacement per cylinder(dm^3)
w = we/v;%Indicated specific piston work(kJ/dm^3)
m1 = (w/(u*h1))*v*n1*60*360/alpha; %total mass flow(kg/h)
x = m1/v;%specific static flow (kg/(h*dm^3))
x1 = x*v/3600000;%mass flow rate(kg/ms)

Fontsize = 16;
LineWidth = 2;
color = jet(7);
%% Phase 1: pressure drops to the critical value and the valve
    starts to move
% Critical point: F_spring + p*pi/4*d2^2 = P_cyl*pi/4*d^2 + P_
    sup * pi/4 *
% (d2^2 - D^2)
t0 = 0;
P0 = P_sup;
P1 = P_cyl + 10e5;
F = P_cyl * s + P_sup * pi/4 * (d2^2 - D^2) - P1 * (pi/4 * d2^2)
    ;
L0 = F/k;
% P1 = (P_cyl * s + P_sup * pi/4 * (d2^2 - D^2) - F)/ (pi/4 * d
    2^2); % s = pi/4*d^2;
G1 = phi_max * sqrt(2*R*T_sup) * A_effBV/V0;
t1 = -1/G1*log(P1/P0);
h1 = 0;
t_all = linspace(t0, t1, 20)';
P_all = P0 * exp(-G1*t_all);
h_all = 0*t_all;
hfig1=figure(1);
plot(t_all*1e3, P_all*1e-5, 'LineWidth',LineWidth, ...
        'Color', color(1, :), ...
        'DisplayName', 'Pressure: Phase 1')
hold on
picturewidth = 20;
hw_ratio = 0.3;
```

```
% title('Phase 1 Pressure')
ylabel('$P$ $(bar)$')
xlabel('$t$ $(ms)$')
set(findall(hfig1,'-property','FontSize'),'FontSize',Fontsize)
set(findall(hfig1,'-property','FontName'),'FontName','
    TimesNewRoman')
set(findall(hfig1,'-property','Interpreter'),'Interpreter','
    latex')
set(findall(hfig1,'-property','TickLabelInterpreter'),'
    TickLabelInterpreter','latex')
set(gca, 'Box','on','LineWidth',2)
set(hfig1,'Units','centimeters','Position',[3 3 picturewidth hw_
    ratio*picturewidth])
legend('Interpreter','latex','FontSize',Fontsize, ...
    'Location','northeast', 'AutoUpdate','on',...
    'NumColumns',1, 'Orientation','horizontal', ...
    'Box','off')

hfig2=figure(2);
plot(t_all*1e3, h_all*1e3, 'LineWidth',LineWidth, ...
        'Color', color(1, :), ...
        'DisplayName', 'Height: Phase 1')
hold on
picturewidth = 20;
hw_ratio = 0.3;
% title('Phase 1 Height')
ylabel('$h$ $(mm)$')
xlabel('$t$ $(ms)$')
set(findall(hfig2,'-property','FontSize'),'FontSize',Fontsize)
set(findall(hfig2,'-property','FontName'),'FontName','
    TimesNewRoman')
set(findall(hfig2,'-property','Interpreter'),'Interpreter','
    latex')
set(findall(hfig2,'-property','TickLabelInterpreter'),'
    TickLabelInterpreter','latex')
set(gca, 'Box','on','LineWidth',2)
set(hfig2,'Units','centimeters','Position',[3 3 picturewidth hw_
    ratio*picturewidth])
legend('Interpreter','latex','FontSize',Fontsize, ...
    'Location','northeast', 'AutoUpdate','on',...
    'NumColumns',1, 'Orientation','horizontal', ...
    'Box','off')
```

```
%% Phase 2:
tspan = [t1 0.1];
[tsol2, varsol2] = ode45(@(t, var) phase2(t, var, V0, d2, phi_
    max, R, T_sup, ...
    A_effBV, m_va, P_sup, s, k, L0, P_cyl, D), tspan, [P1; 0;
        0]);
Psol2 = varsol2(:, 1);
hsol2 = varsol2(:, 2);
vsol2 = varsol2(:,3);
index = find(hsol2>h_max,1, 'first');
t2 = interp1(hsol2, tsol2, h_max);
P2 = interp1(tsol2, Psol2, t2);
h2 = h_max;
tsol2 = tsol2(1:index);
Psol2 = Psol2(1:index);
hsol2 = hsol2(1:index);
tsol2(end) = t2;
Psol2(end) = P2;
hsol2(end) = h2;
t_all = [t_all; tsol2];
P_all = [P_all; Psol2];
h_all = [h_all; hsol2];
hfig1 = figure(1);
plot(tsol2*1e3, Psol2*1e-5,'LineWidth',LineWidth, ...
        'Color', color(2, :), ...
        'DisplayName', 'Pressure: Phase 2')
hold on
picturewidth = 20;
hw_ratio = 0.3;
%title('Phase 1+2')
ylabel('$P$ $(bar)$')
xlabel('$t$ $(ms)$')
set(findall(hfig1,'-property','FontSize'),'FontSize',Fontsize)
set(findall(hfig1,'-property','FontName'),'FontName','
    TimesNewRoman')
set(findall(hfig1,'-property','Interpreter'),'Interpreter','
    latex')
set(findall(hfig1,'-property','TickLabelInterpreter'),'
    TickLabelInterpreter','latex')
set(gca, 'Box','on','LineWidth',2)
```

```
set(hfig1,'Units','centimeters','Position',[3 3 picturewidth hw_
    ratio*picturewidth])
legend('Interpreter','latex','FontSize',Fontsize, ...
    'Location','northeast', 'AutoUpdate','on',...
    'NumColumns',1, 'Orientation','horizontal', ...
    'Box','off')
hfig2 = figure(2);
plot(tsol2*1e3, hsol2*1e3,'LineWidth',LineWidth, ...
        'Color', color(2, :), ...
        'DisplayName', 'Height: Phase 2')
hold on
picturewidth = 20;
hw_ratio = 0.3;
%title('Phase 1+2')
ylabel('$h$ $(mm)$')
xlabel('$t$ $(ms)$')
set(findall(hfig2,'-property','FontSize'),'FontSize',Fontsize)
set(findall(hfig2,'-property','FontName'),'FontName','
    TimesNewRoman')
set(findall(hfig2,'-property','Interpreter'),'Interpreter','
    latex')
set(findall(hfig2,'-property','TickLabelInterpreter'),'
    TickLabelInterpreter','latex')
set(gca, 'Box','on','LineWidth',2)
set(hfig2,'Units','centimeters','Position',[3 3 picturewidth hw_
    ratio*picturewidth])
legend('Interpreter','latex','FontSize',Fontsize, ...
    'Location','northeast', 'AutoUpdate','on',...
    'NumColumns',1, 'Orientation','horizontal', ...
    'Box','off')
% figure(3)
% dhdtdt = 1/m_va*(P_cyl * s + P_sup * pi/4 * (d2^2 - D^2) - k*(
    L0+hsol2) - Psol2 * (pi/4 * d2^2));
% plot(tsol2*1e3, dhdtdt/1e3)
% title('acceleration')
% ylabel('$\frac{d^2h}{dt^2}$',Interpreter='latex')
% xlabel('t')
%% Phase 3:
V3 = V0 - pi/4*d2^2*h2;
G3 = phi_max * sqrt(2*R*T_sup) * A_effBV/V3;
t3  = t2 + delta_t;
h3 = h2;
```

```
P3 =exp(-G3*(t3-t2))*P2;
tsol3 = linspace(t2, t3, 20);
Psol3 = P2*exp(-G3*(tsol3 - t2));
hsol3 = 0*tsol3 + h2;
hfig1 = figure(1);
plot(tsol3*1e3, Psol3*1e-5,'LineWidth',LineWidth, ...
        'Color', color(3, :), ...
        'DisplayName', 'Pressure: Phase 3')
hold on
picturewidth = 20;
hw_ratio = 0.3;
%title('Phase 1+2+3')
ylabel('$P$ $(bar)$')
xlabel('$t$ $(ms)$')
set(findall(hfig1,'-property','FontSize'),'FontSize',Fontsize)
set(findall(hfig1,'-property','FontName'),'FontName','
    TimesNewRoman')
set(findall(hfig1,'-property','Interpreter'),'Interpreter','
    latex')
set(findall(hfig1,'-property','TickLabelInterpreter'),'
    TickLabelInterpreter','latex')
set(gca, 'Box','on','LineWidth',2)
set(hfig1,'Units','centimeters','Position',[3 3 picturewidth hw_
    ratio*picturewidth])
legend('Interpreter','latex','FontSize',Fontsize, ...
    'Location','northeast', 'AutoUpdate','on',...
    'NumColumns',1, 'Orientation','horizontal', ...
    'Box','off')
hfig2 = figure(2);
plot(tsol3*1e3, hsol3*1e3,'LineWidth',LineWidth, ...
        'Color', color(3, :), ...
        'DisplayName', 'Height: Phase 3')
hold on
picturewidth = 20;
hw_ratio = 0.3;
%title('Phase 1+2+3')
ylabel('$h$ $(mm)$')
xlabel('$t$ $(ms)$')
set(findall(hfig2,'-property','FontSize'),'FontSize',Fontsize)
set(findall(hfig2,'-property','FontName'),'FontName','
    TimesNewRoman')
```

```
set(findall(hfig2,'-property','Interpreter'),'Interpreter','
    latex')
set(findall(hfig2,'-property','TickLabelInterpreter'),'
    TickLabelInterpreter','latex')
set(gca, 'Box','on','LineWidth',2)
set(hfig2,'Units','centimeters','Position',[3 3 picturewidth hw_
    ratio*picturewidth])
legend('Interpreter','latex','FontSize',Fontsize, ...
    'Location','northeast', 'AutoUpdate','on',...
    'NumColumns',1, 'Orientation','horizontal', ...
    'Box','off')
%% Phase 4:
V4 = V3;
h4 = h3;
G4 = phi_max * sqrt(2*R*T_sup) * A_effRO/V4;
P4 = (P_cyl * s + P_sup * pi/4 * (d2^2 - D^2) - F)/ (pi/4 * d
    2^2);
t4 = (P4-P3)/G4/P_sup+t3;
% P4 = P3 * exp(G4*(t4-t3));
% t4 = t2+200e-3;
tsol4 = linspace(t3, t4, 200);
Psol4 = P3 + G4*P_sup*(tsol4-t3);
hsol4 = 0*tsol4 + h3;
hfig1 = figure(1);
plot(tsol4*1e3, Psol4*1e-5,'LineWidth',LineWidth, ...
        'Color', color(4, :), ...
        'DisplayName', 'Pressure: Phase 4')
hold on
picturewidth = 20;
hw_ratio = 0.3;
%title('Phase 1+2+3+4')
ylabel('$P$ $(bar)$')
xlabel('$t$ $(ms)$')
set(findall(hfig1,'-property','FontSize'),'FontSize',Fontsize)
set(findall(hfig1,'-property','FontName'),'FontName','
    TimesNewRoman')
set(findall(hfig1,'-property','Interpreter'),'Interpreter','
    latex')
set(findall(hfig1,'-property','TickLabelInterpreter'),'
    TickLabelInterpreter','latex')
set(gca, 'Box','on','LineWidth',2)
```

```
set(hfig1,'Units','centimeters','Position',[3 3 picturewidth hw_
    ratio*picturewidth])
legend('Interpreter','latex','FontSize',Fontsize, ...
    'Location','northeast', 'AutoUpdate','on',...
    'NumColumns',1, 'Orientation','horizontal', ...
    'Box','off')
hfig2 = figure(2);
plot(tsol4*1e3, hsol4*1e3,'LineWidth',LineWidth, ...
        'Color', color(4, :), ...
        'DisplayName', 'Height: Phase 4')
hold on
picturewidth = 20;
hw_ratio = 0.3;
%title('Phase 1+2+3+4')
ylabel('$h$ $(mm)$')
xlabel('$t$ $(ms)$')
set(findall(hfig2,'-property','FontSize'),'FontSize',Fontsize)
set(findall(hfig2,'-property','FontName'),'FontName','
    TimesNewRoman')
set(findall(hfig2,'-property','Interpreter'),'Interpreter','
    latex')
set(findall(hfig2,'-property','TickLabelInterpreter'),'
    TickLabelInterpreter','latex')
set(gca, 'Box','on','LineWidth',2)
set(hfig2,'Units','centimeters','Position',[3 3 picturewidth hw_
    ratio*picturewidth])
legend('Interpreter','latex','FontSize',Fontsize, ...
    'Location','northeast', 'AutoUpdate','on',...
    'NumColumns',1, 'Orientation','horizontal', ...
    'Box','off')
%% Phase 5:
tspan = [t4 0.5];
[tsol5, varsol5] = ode45(@(t, var) phase5(t, var, V0, d2, phi_
    max, R, T_sup, ...
    A_effRO, m_va, P_sup, s, k, L0, P_cyl, D), tspan, [P4; h4;
        0]);
Psol5 = varsol5(:, 1);
hsol5 = varsol5(:, 2);
vsol5 = varsol5(:,3);
index = find(hsol5<0,1, 'first');
t5 = interp1(hsol5, tsol5, 0);
P5 = interp1(tsol5, Psol5, t5);
```

```
h5 = 0;
tsol5 = tsol5(1:index);
Psol5 = Psol5(1:index);
hsol5 = hsol5(1:index);
tsol5(end) = t5;
Psol5(end) = P5;
hsol5(end) = h5;
hfig1 = figure(1);
plot(tsol5*1e3, Psol5*1e-5,'LineWidth',LineWidth, ...
        'Color', color(5, :), ...
        'DisplayName', 'Pressure: Phase 5')
hold on
picturewidth = 20;
hw_ratio = 0.3;
%title('Phase 1+2+3+4+5')
ylabel('$P$ $(bar)$')
xlabel('$t$ $(ms)$')
set(findall(hfig1,'-property','FontSize'),'FontSize',Fontsize)
set(findall(hfig1,'-property','FontName'),'FontName','
    TimesNewRoman')
set(findall(hfig1,'-property','Interpreter'),'Interpreter','
    latex')
set(findall(hfig1,'-property','TickLabelInterpreter'),'
    TickLabelInterpreter','latex')
set(gca, 'Box','on','LineWidth',2)
set(hfig1,'Units','centimeters','Position',[3 3 picturewidth hw_
    ratio*picturewidth])
legend('Interpreter','latex','FontSize',Fontsize, ...
    'Location','northeast', 'AutoUpdate','on',...
    'NumColumns',1, 'Orientation','horizontal', ...
    'Box','off')
hfig2 = figure(2);
plot(tsol5*1e3, hsol5*1e3,'LineWidth',LineWidth, ...
        'Color', color(5, :), ...
        'DisplayName', 'Height: Phase 5')
hold on
picturewidth = 20;
hw_ratio = 0.3;
%title('Phase 1+2+3+4+5')
ylabel('$h$ $(mm)$')
xlabel('$t$ $(ms)$')
set(findall(hfig2,'-property','FontSize'),'FontSize',Fontsize)
```

```
set(findall(hfig2,'-property','FontName'),'FontName','
    TimesNewRoman')
set(findall(hfig2,'-property','Interpreter'),'Interpreter','
    latex')
set(findall(hfig2,'-property','TickLabelInterpreter'),'
    TickLabelInterpreter','latex')
set(gca, 'Box','on','LineWidth',2)
set(hfig2,'Units','centimeters','Position',[3 3 picturewidth hw_
    ratio*picturewidth])
legend('Interpreter','latex','FontSize',Fontsize, ...
    'Location','northeast', 'AutoUpdate','on',...
    'NumColumns',1, 'Orientation','horizontal', ...
    'Box','off')
%% Phase 6:
V6 = V0;
P6 = P_sup;
G6 = phi_max * sqrt(2*R*T_sup) * A_effRO/V0;
t6 = (P6-P5)/(G6*P_sup)+t5;
tsol6 = linspace(t5, t6, 50);
Psol6 = P5 + G6*P_sup*(tsol6 - t5);
hsol6 = 0*tsol6;
hfig1 = figure(1);
plot(tsol6*1e3, Psol6*1e-5,'LineWidth',LineWidth, ...
        'Color', color(6, :), ...
        'DisplayName', 'Pressure: Phase 6')
hold on
picturewidth = 20;
hw_ratio = 0.3;
%title('Phase 1+2+3+4+5+6')
ylabel('$P$ $(bar)$')
xlabel('$t$ $(ms)$')
set(findall(hfig1,'-property','FontSize'),'FontSize',Fontsize)
set(findall(hfig1,'-property','FontName'),'FontName','
    TimesNewRoman')
set(findall(hfig1,'-property','Interpreter'),'Interpreter','
    latex')
set(findall(hfig1,'-property','TickLabelInterpreter'),'
    TickLabelInterpreter','latex')
set(gca, 'Box','on','LineWidth',2)
set(hfig1,'Units','centimeters','Position',[3 3 picturewidth hw_
    ratio*picturewidth])
legend('Interpreter','latex','FontSize',Fontsize, ...
```

```
    'Location','northeast', 'AutoUpdate','on',...
    'NumColumns',1, 'Orientation','horizontal', ...
    'Box','off')
hfig2 = figure(2);
plot(tsol6*1e3, hsol6*1e3,'LineWidth',LineWidth, ...
        'Color', color(6, :), ...
        'DisplayName', 'Height: Phase 6')
hold on
picturewidth = 20;
hw_ratio = 0.3;
%title('Phase 1+2+3+4+5+6')
ylabel('$h$ $(mm)$')
xlabel('$t$ $(ms)$')
set(findall(hfig2,'-property','FontSize'),'FontSize',Fontsize)
set(findall(hfig2,'-property','FontName'),'FontName','
    TimesNewRoman')
set(findall(hfig2,'-property','Interpreter'),'Interpreter','
    latex')
set(findall(hfig2,'-property','TickLabelInterpreter'),'
    TickLabelInterpreter','latex')
set(gca, 'Box','on','LineWidth',2)
set(hfig2,'Units','centimeters','Position',[3 3 picturewidth hw_
    ratio*picturewidth])
legend('Interpreter','latex','FontSize',Fontsize, ...
    'Location','northeast', 'AutoUpdate','on',...
    'NumColumns',1, 'Orientation','horizontal', ...
    'Box','off')
%% Phase 7:
t7 =0.75;
tsol7 = linspace(t6,t7, 50);
Psol7 = 0*tsol7 + P_sup;
hsol7 = 0*tsol7;
figure(1)
plot(tsol7*1e3, Psol7*1e-5,'LineWidth',LineWidth, ...
        'Color', color(7, :), ...
        'DisplayName', 'Pressure: Phase 7')
hold on
picturewidth = 20;
hw_ratio = 0.5;
title('Pressure change over time in injector')
ylabel('$P$ $(bar)$')
xlabel('$t$ $(ms)$')
```

```
set(findall(hfig1,'-property','FontSize'),'FontSize',Fontsize)
set(findall(hfig1,'-property','FontName'),'FontName','
    TimesNewRoman')
set(findall(hfig1,'-property','Interpreter'),'Interpreter','
    latex')
set(findall(hfig1,'-property','TickLabelInterpreter'),'
    TickLabelInterpreter','latex')
set(gca, 'Box','on','LineWidth',2)
set(hfig1,'Units','centimeters','Position',[3 3 picturewidth hw_
    ratio*picturewidth])
legend('Interpreter','latex','FontSize',Fontsize, ...
    'Location','northeast', 'AutoUpdate','on',...
    'NumColumns',1, 'Orientation','horizontal', ...
    'Box','off')
hfig2 = figure(2);
plot(tsol7*1e3, hsol7*1e3,'LineWidth',LineWidth, ...
        'Color', color(7, :), ...
        'DisplayName', 'Height: Phase 7')
hold on
picturewidth = 20;
hw_ratio = 0.5;
title('Valve lift height')
ylabel('$h$ $(mm)$')
xlabel('$t$ $(ms)$')
set(findall(hfig2,'-property','FontSize'),'FontSize',Fontsize)
set(findall(hfig2,'-property','FontName'),'FontName','
    TimesNewRoman')
set(findall(hfig2,'-property','Interpreter'),'Interpreter','
    latex')
set(findall(hfig2,'-property','TickLabelInterpreter'),'
    TickLabelInterpreter','latex')
set(gca, 'Box','on','LineWidth',2)
set(hfig2,'Units','centimeters','Position',[3 3 picturewidth hw_
    ratio*picturewidth])
legend('Interpreter','latex','FontSize',Fontsize, ...
    'Location','northeast', 'AutoUpdate','on',...
    'NumColumns',1, 'Orientation','horizontal', ...
    'Box','off')
```

Listing B.2: odephase2

```
    function diffeqs=ode_phase2(t,var, V0, d2, phi_max, R, T_sup
        , ...
    A_effPV, m_va, P_sup, s, k, L0, P_cyl, D)
P = var(1);
h = var(2);
hdot= var(3);

% V(t)
V = V0 - pi/4*d2^2*h;
%dp/dt
dPdt = -phi_max*sqrt(2*R*T_sup)*(A_effPV/V)*(P-P_cyl);

% dh/dt
dhdt = hdot;

%d^2h/dt^2
dhdtdt = 1/m_va*((P_sup - P))*(d2^2 - D^2)*pi/4 - k*(L0 + h)-((P
    - P_cyl)*s);
if (h==0)  && (dhdtdt<=0)
    dhdtdt = 0;
end
diffeqs = [dPdt; dhdt; dhdtdt];
end
```

Listing B.3: odephase3

```
    function dPdt = ode_phase3(t, P, phi_max, R, T_sup, A_effRO,
         V_h,P_cyl)
dPdt = -phi_max*sqrt(2*R*T_sup)*(A_effRO/V_h)*(P);
end
```

Listing B.4: odephase4

```
    function diffeqs=ode_phase4(t,var, V0, d2, phi_max, R, T_sup
        , ...
    A_effRO, m_va, P_sup, s, k, L0, P_cyl, D)
P = var(1);
h = var(2);
hdot= var(3);


if P>= 50e5
```

```
    P= 50e5;
end
if h<= 0
    h=0;
    hdot=0;
end

% dh/dt
dhdt = hdot;
%d^2h/dt^2
dhdtdt = -(1/m_va*((P_sup - P)*(d2^2 - D^2)*pi/4 - k*(L0 + h)
    ...
    - (P - P_cyl)*s));
if h<= 0
    dhdtdt = 0;
end

% V(t)
 V = V0 - pi/4*d2^2*h;
%dp/dt
dPdt = phi_max*sqrt(2*R*T_sup)*(A_effRO/V)*P_sup;

if P>= 50e5
    dPdt = 0;
end




diffeqs = [dPdt; dhdt; dhdtdt];
end
```

Listing B.5: working load

```
%% Initial
clc
clear
close all
%% data
Delay_time =
    [0,4,7.5,12.5,17.5,22.5,27.5,32.5,37.5,42.5,47.5,52.5,57.5,62.5,67.5];
```

```
TM =
    [0.015744,0.026317,0.032776,0.039138,0.043433,0.046539,0.04896,0.050987,0.05278

WL =
    [0.25351,0.42377,0.52777,0.63021,0.69937,0.74939,0.78838,0.82101,0.85,0.87687,0

%% figure
figure()
%scatter(Delay_time,WL,'filled')
%hold on
plot(Delay_time,WL,'-o','Color','b','MarkerFaceColor', 'b')
title(' Working Load Change With Delay Time')
ylabel('Working Load')
xlabel('Delay Time (ms)')
ax = gca; ax.FontName = 'Century Gothic'; ax.FontSize=16; ax.
    FontWeight='bold'; ax.GridAlpha=0.07; ax.GridLineStyle='--';
     ax.LineWidth=1.5; ax.XColor=[0 0 0]; ax.XMinorTick='on'; ax
    .YColor=[0 0 0]; ax.YMinorTick='on';
 xtickformat('%.0f')
 ytickformat('%.2f');
 set(gca,'fontname','times');
 set(gcf,'Color','w');


figure()
plot(Delay_time,TM,'b','LineWidth',1.5,'LineStyle','-','Marker
    ','none','MarkerSize',15)
title('Total Consumed Hydrogen Mass Change With Delay Time')
ylabel('Total mass of hydrogen (kg)')
xlabel('Delay Time (ms)')
ax = gca; ax.FontName = 'Century Gothic'; ax.FontSize=16; ax.
    FontWeight='bold'; ax.GridAlpha=0.07; ax.GridLineStyle='--';
     ax.LineWidth=1.5; ax.XColor=[0 0 0]; ax.XMinorTick='on'; ax
    .YColor=[0 0 0]; ax.YMinorTick='on';
 xtickformat('%.0f')
 ytickformat('%.2f');
 set(gca,'fontname','times');
 set(gcf,'Color','w');
```

Listing B.6: compare

```
%% Initial
```

```
clc
clear
%close all
%% Constant parameter
phi_max = 0.484; %the maximum value for the flow function
R = 4125.6; % the specific gas constant of hydrogen(J/(kg*K)=kg*
    m^2/(s^2*K))
P_sup = 50e5; % supply pressure(Pa = kg/(m*s^2))
T_sup = 293.15; % supply temperature(K)
A_effBV = 0.79e-6*25; % the effective cross-sectional flow area
    of the pilot valve(m^2)
A_effRO = 0.07e-6*5; % the effective flow cross-sectional area
    of the refilling orifice(m^2)
k = 25.46e3;% spring stiffnes(N/m=kg/(s^2))
% F = 350; %cclsosing spring force(kg*m/(s^2))
% L0 = F/k*2.5; % initial displacement
d2 = 75e-3*0.4; % The diameter of the actuator piston(m)
s = 160e-6;  % the nozzle cross-sectional area(m^2)
D = 31.27e-3*0.7; % the diameter of curtain(mm)
P_cyl = 3e5; % cylinder pressure
V0 = 34.3e-6*4; %  the initial volume of the piston (m^3)
m_va = 0.825/4; % mass of valve (kg)
h_max = 3.6e-3; % maximum of height (m)
delta_t = 0e-3; %s
color_ss = "#7E2F8E";
WL = 25.3;
%% calculate constants
s1 = 3.468; %stroke in meters
d_bore = 0.92; %diameter in meters
we = 3990;%the work done by each cylinder(kJ)
u = 0.535;%efficiency of the engine in gas mode
h1 = 120000;%fuel lower heating value(kJ/kg)
n1 = 80; %rpm
alpha = 100; %available angular injection window

v = (pi/4*d_bore^2*s1)*1000;%displacement per cylinder(dm^3)
w = we/v;%Indicated specific piston work(kJ/dm^3)
m1 = (w/(u*h1))*v*n1*60*360/alpha; %total mass flow(kg/h)
x = m1/v;%specific static flow (kg/(h*dm^3))
x1 = x*v/3600000;%mass flow rate(kg/ms)

Fontsize = 16;
```

```
LineWidth = 2;
%% Phase 1: pressure drops to the critical value and the valve
    starts to move
% Critical point: F_spring + p*pi/4*d2^2 = P_cyl*pi/4*d^2 + P_
    sup * pi/4 *
% (d2^2 - D^2)
t0 = 0;
P0 = P_sup;
P1 = P_cyl + 10e5;
F = P_cyl * s + P_sup * pi/4 * (d2^2 - D^2) - P1 * (pi/4 * d2^2)
    ;
L0 = F/k;
% P1 = (P_cyl * s + P_sup * pi/4 * (d2^2 - D^2) - F)/ (pi/4 * d
    2^2); % s = pi/4*d^2;
G1 = phi_max * sqrt(2*R*T_sup) * A_effBV/V0;
t1 = -1/G1*log(P1/P0);
h1 = 0;
t_all = linspace(t0, t1, 20)';
P_all = P0 * exp(-G1*t_all);
h_all = 0*t_all;
hfig1=figure(1);
plot(t_all*1e3, P_all*1e-5, 'LineWidth',LineWidth, ...
        'Color', color_ss, ...
        'DisplayName', '$'+string(WL)+' \%$')
hold on
picturewidth = 20;
hw_ratio = 0.3;
% title('Phase 1 Pressure')
ylabel('$P$ $(bar)$')
xlabel('$t$ $(ms)$')
set(findall(hfig1,'-property','FontSize'),'FontSize',Fontsize)
set(findall(hfig1,'-property','FontName'),'FontName','
    TimesNewRoman')
set(findall(hfig1,'-property','Interpreter'),'Interpreter','
    latex')
set(findall(hfig1,'-property','TickLabelInterpreter'),'
    TickLabelInterpreter','latex')
set(gca, 'Box','on','LineWidth',2)
set(hfig1,'Units','centimeters','Position',[3 3 picturewidth hw_
    ratio*picturewidth])
legend('Interpreter','latex','FontSize',Fontsize, ...
    'Location','northeast', 'AutoUpdate','off',...
```

```
    'NumColumns',1, 'Orientation','horizontal', ...
    'Box','off')

hfig2=figure(2);
plot(t_all*1e3, h_all*1e3, 'LineWidth',LineWidth, ...
        'Color', color_ss, ...
        'DisplayName', '$'+string(WL)+' \%$')
hold on
picturewidth = 20;
hw_ratio = 0.3;
% title('Phase 1 Height')
ylabel('$h$ $(mm)$')
xlabel('$t$ $(ms)$')
set(findall(hfig2,'-property','FontSize'),'FontSize',Fontsize)
set(findall(hfig2,'-property','FontName'),'FontName','
    TimesNewRoman')
set(findall(hfig2,'-property','Interpreter'),'Interpreter','
    latex')
set(findall(hfig2,'-property','TickLabelInterpreter'),'
    TickLabelInterpreter','latex')
set(gca, 'Box','on','LineWidth',2)
set(hfig2,'Units','centimeters','Position',[3 3 picturewidth hw_
    ratio*picturewidth])
legend('Interpreter','latex','FontSize',Fontsize, ...
    'Location','northeast', 'AutoUpdate','off',...
    'NumColumns',1, 'Orientation','horizontal', ...
    'Box','off')

%% Phase 2:
tspan = [t1 0.1];
[tsol2, varsol2] = ode45(@(t, var) phase2(t, var, V0, d2, phi_
    max, R, T_sup, ...
    A_effBV, m_va, P_sup, s, k, L0, P_cyl, D), tspan, [P1; 0;
        0]);
Psol2 = varsol2(:, 1);
hsol2 = varsol2(:, 2);
vsol2 = varsol2(:,3);
index = find(hsol2>h_max,1, 'first');
t2 = interp1(hsol2, tsol2, h_max);
P2 = interp1(tsol2, Psol2, t2);
h2 = h_max;
tsol2 = tsol2(1:index);
```

```
Psol2 = Psol2(1:index);
hsol2 = hsol2(1:index);
tsol2(end) = t2;
Psol2(end) = P2;
hsol2(end) = h2;
t_all = [t_all; tsol2];
P_all = [P_all; Psol2];
h_all = [h_all; hsol2];
hfig1 = figure(1);
plot(tsol2*1e3, Psol2*1e-5,'LineWidth',LineWidth, ...
        'Color', color_ss)
hold on
picturewidth = 20;
hw_ratio = 0.3;
%title('Phase 1+2')
ylabel('$P$ $(bar)$')
xlabel('$t$ $(ms)$')
set(findall(hfig1,'-property','FontSize'),'FontSize',Fontsize)
set(findall(hfig1,'-property','FontName'),'FontName','
    TimesNewRoman')
set(findall(hfig1,'-property','Interpreter'),'Interpreter','
    latex')
set(findall(hfig1,'-property','TickLabelInterpreter'),'
    TickLabelInterpreter','latex')
set(gca, 'Box','on','LineWidth',2)
set(hfig1,'Units','centimeters','Position',[3 3 picturewidth hw_
    ratio*picturewidth])
legend('Interpreter','latex','FontSize',Fontsize, ...
    'Location','northeast', 'AutoUpdate','off',...
    'NumColumns',1, 'Orientation','horizontal', ...
    'Box','off')
hfig2 = figure(2);
plot(tsol2*1e3, hsol2*1e3,'LineWidth',LineWidth, ...
        'Color', color_ss)
hold on
picturewidth = 20;
hw_ratio = 0.3;
%title('Phase 1+2')
ylabel('$h$ $(mm)$')
xlabel('$t$ $(ms)$')
set(findall(hfig2,'-property','FontSize'),'FontSize',Fontsize)
```

```
set(findall(hfig2,'-property','FontName'),'FontName','
    TimesNewRoman')
set(findall(hfig2,'-property','Interpreter'),'Interpreter','
    latex')
set(findall(hfig2,'-property','TickLabelInterpreter'),'
    TickLabelInterpreter','latex')
set(gca, 'Box','on','LineWidth',2)
set(hfig2,'Units','centimeters','Position',[3 3 picturewidth hw_
    ratio*picturewidth])
legend('Interpreter','latex','FontSize',Fontsize, ...
    'Location','northeast', 'AutoUpdate','off',...
    'NumColumns',1, 'Orientation','horizontal', ...
    'Box','off')
% figure(3)
% dhdtdt = 1/m_va*(P_cyl * s + P_sup * pi/4 * (d2^2 - D^2) - k*(
    L0+hsol2) - Psol2 * (pi/4 * d2^2));
% plot(tsol2*1e3, dhdtdt/1e3)
% title('acceleration')
% ylabel('$\frac{d^2h}{dt^2}$',Interpreter='latex')
% xlabel('t')
%% Phase 3:
V3 = V0 - pi/4*d2^2*h2;
G3 = phi_max * sqrt(2*R*T_sup) * A_effBV/V3;
t3  = t2 + delta_t;
h3 = h2;
P3 =exp(-G3*(t3-t2))*P2;
tsol3 = linspace(t2, t3, 20);
Psol3 = P2*exp(-G3*(tsol3 - t2));
hsol3 = 0*tsol3 + h2;
hfig1 = figure(1);
plot(tsol3*1e3, Psol3*1e-5,'LineWidth',LineWidth, ...
        'Color', color_ss)
hold on
picturewidth = 20;
hw_ratio = 0.3;
%title('Phase 1+2+3')
ylabel('$P$ $(bar)$')
xlabel('$t$ $(ms)$')
set(findall(hfig1,'-property','FontSize'),'FontSize',Fontsize)
set(findall(hfig1,'-property','FontName'),'FontName','
    TimesNewRoman')
```

```
set(findall(hfig1,'-property','Interpreter'),'Interpreter','
    latex')
set(findall(hfig1,'-property','TickLabelInterpreter'),'
    TickLabelInterpreter','latex')
set(gca, 'Box','on','LineWidth',2)
set(hfig1,'Units','centimeters','Position',[3 3 picturewidth hw_
    ratio*picturewidth])
legend('Interpreter','latex','FontSize',Fontsize, ...
    'Location','northeast', 'AutoUpdate','off',...
    'NumColumns',1, 'Orientation','horizontal', ...
    'Box','off')
hfig2 = figure(2);
plot(tsol3*1e3, hsol3*1e3,'LineWidth',LineWidth, ...
        'Color', color_ss)
hold on
picturewidth = 20;
hw_ratio = 0.3;
%title('Phase 1+2+3')
ylabel('$h$ $(mm)$')
xlabel('$t$ $(ms)$')
set(findall(hfig2,'-property','FontSize'),'FontSize',Fontsize)
set(findall(hfig2,'-property','FontName'),'FontName','
    TimesNewRoman')
set(findall(hfig2,'-property','Interpreter'),'Interpreter','
    latex')
set(findall(hfig2,'-property','TickLabelInterpreter'),'
    TickLabelInterpreter','latex')
set(gca, 'Box','on','LineWidth',2)
set(hfig2,'Units','centimeters','Position',[3 3 picturewidth hw_
    ratio*picturewidth])
legend('Interpreter','latex','FontSize',Fontsize, ...
    'Location','northeast', 'AutoUpdate','off',...
    'NumColumns',1, 'Orientation','horizontal', ...
    'Box','off')
%% Phase 4:
V4 = V3;
h4 = h3;
G4 = phi_max * sqrt(2*R*T_sup) * A_effRO/V4;
P4 = (P_cyl * s + P_sup * pi/4 * (d2^2 - D^2) - F)/ (pi/4 * d
    2^2);
t4 = (P4-P3)/G4/P_sup+t3;
% P4 = P3 * exp(G4*(t4-t3));
```

```
% t4 = t2+200e-3;
tsol4 = linspace(t3, t4, 200);
Psol4 = P3 + G4*P_sup*(tsol4-t3);
hsol4 = 0*tsol4 + h3;
hfig1 = figure(1);
plot(tsol4*1e3, Psol4*1e-5,'LineWidth',LineWidth, ...
        'Color', color_ss)
hold on
picturewidth = 20;
hw_ratio = 0.3;
%title('Phase 1+2+3+4')
ylabel('$P$ $(bar)$')
xlabel('$t$ $(ms)$')
set(findall(hfig1,'-property','FontSize'),'FontSize',Fontsize)
set(findall(hfig1,'-property','FontName'),'FontName','
    TimesNewRoman')
set(findall(hfig1,'-property','Interpreter'),'Interpreter','
    latex')
set(findall(hfig1,'-property','TickLabelInterpreter'),'
    TickLabelInterpreter','latex')
set(gca, 'Box','on','LineWidth',2)
set(hfig1,'Units','centimeters','Position',[3 3 picturewidth hw_
    ratio*picturewidth])
legend('Interpreter','latex','FontSize',Fontsize, ...
    'Location','northeast', 'AutoUpdate','off',...
    'NumColumns',1, 'Orientation','horizontal', ...
    'Box','off')
hfig2 = figure(2);
plot(tsol4*1e3, hsol4*1e3,'LineWidth',LineWidth, ...
        'Color', color_ss)
hold on
picturewidth = 20;
hw_ratio = 0.3;
%title('Phase 1+2+3+4')
ylabel('$h$ $(mm)$')
xlabel('$t$ $(ms)$')
set(findall(hfig2,'-property','FontSize'),'FontSize',Fontsize)
set(findall(hfig2,'-property','FontName'),'FontName','
    TimesNewRoman')
set(findall(hfig2,'-property','Interpreter'),'Interpreter','
    latex')
```

```
set(findall(hfig2,'-property','TickLabelInterpreter'),'
    TickLabelInterpreter','latex')
set(gca, 'Box','on','LineWidth',2)
set(hfig2,'Units','centimeters','Position',[3 3 picturewidth hw_
    ratio*picturewidth])
legend('Interpreter','latex','FontSize',Fontsize, ...
    'Location','northeast', 'AutoUpdate','off',...
    'NumColumns',1, 'Orientation','horizontal', ...
    'Box','off')
%% Phase 5:
tspan = [t4 0.5];
[tsol5, varsol5] = ode45(@(t, var) phase5(t, var, V0, d2, phi_
    max, R, T_sup, ...
    A_effRO, m_va, P_sup, s, k, L0, P_cyl, D), tspan, [P4; h4;
        0]);
Psol5 = varsol5(:, 1);
hsol5 = varsol5(:, 2);
vsol5 = varsol5(:,3);
index = find(hsol5<0,1, 'first');
t5 = interp1(hsol5, tsol5, 0);
P5 = interp1(tsol5, Psol5, t5);
h5 = 0;
tsol5 = tsol5(1:index);
Psol5 = Psol5(1:index);
hsol5 = hsol5(1:index);
tsol5(end) = t5;
Psol5(end) = P5;
hsol5(end) = h5;
hfig1 = figure(1);
plot(tsol5*1e3, Psol5*1e-5,'LineWidth',LineWidth, ...
        'Color', color_ss)
hold on
picturewidth = 20;
hw_ratio = 0.3;
%title('Phase 1+2+3+4+5')
ylabel('$P$ $(bar)$')
xlabel('$t$ $(ms)$')
set(findall(hfig1,'-property','FontSize'),'FontSize',Fontsize)
set(findall(hfig1,'-property','FontName'),'FontName','
    TimesNewRoman')
set(findall(hfig1,'-property','Interpreter'),'Interpreter','
    latex')
```

```
set(findall(hfig1,'-property','TickLabelInterpreter'),'
    TickLabelInterpreter','latex')
set(gca, 'Box','on','LineWidth',2)
set(hfig1,'Units','centimeters','Position',[3 3 picturewidth hw_
    ratio*picturewidth])
legend('Interpreter','latex','FontSize',Fontsize, ...
    'Location','northeast', 'AutoUpdate','off',...
    'NumColumns',1, 'Orientation','horizontal', ...
    'Box','off')
hfig2 = figure(2);
plot(tsol5*1e3, hsol5*1e3,'LineWidth',LineWidth, ...
        'Color', color_ss)
hold on
picturewidth = 20;
hw_ratio = 0.3;
%title('Phase 1+2+3+4+5')
ylabel('$h$ $(mm)$')
xlabel('$t$ $(ms)$')
set(findall(hfig2,'-property','FontSize'),'FontSize',Fontsize)
set(findall(hfig2,'-property','FontName'),'FontName','
    TimesNewRoman')
set(findall(hfig2,'-property','Interpreter'),'Interpreter','
    latex')
set(findall(hfig2,'-property','TickLabelInterpreter'),'
    TickLabelInterpreter','latex')
set(gca, 'Box','on','LineWidth',2)
set(hfig2,'Units','centimeters','Position',[3 3 picturewidth hw_
    ratio*picturewidth])
legend('Interpreter','latex','FontSize',Fontsize, ...
    'Location','northeast', 'AutoUpdate','off',...
    'NumColumns',1, 'Orientation','horizontal', ...
    'Box','off')
%% Phase 6:
V6 = V0;
P6 = P_sup;
G6 = phi_max * sqrt(2*R*T_sup) * A_effRO/V0;
t6 = (P6-P5)/(G6*P_sup)+t5;
tsol6 = linspace(t5, t6, 50);
Psol6 = P5 + G6*P_sup*(tsol6 - t5);
hsol6 = 0*tsol6;
hfig1 = figure(1);
plot(tsol6*1e3, Psol6*1e-5,'LineWidth',LineWidth, ...
```

```
        'Color', color_ss)
hold on
picturewidth = 20;
hw_ratio = 0.3;
%title('Phase 1+2+3+4+5+6')
ylabel('$P$ $(bar)$')
xlabel('$t$ $(ms)$')
set(findall(hfig1,'-property','FontSize'),'FontSize',Fontsize)
set(findall(hfig1,'-property','FontName'),'FontName','
    TimesNewRoman')
set(findall(hfig1,'-property','Interpreter'),'Interpreter','
    latex')
set(findall(hfig1,'-property','TickLabelInterpreter'),'
    TickLabelInterpreter','latex')
set(gca, 'Box','on','LineWidth',2)
set(hfig1,'Units','centimeters','Position',[3 3 picturewidth hw_
    ratio*picturewidth])
legend('Interpreter','latex','FontSize',Fontsize, ...
    'Location','northeast', 'AutoUpdate','off',...
    'NumColumns',1, 'Orientation','horizontal', ...
    'Box','off')
hfig2 = figure(2);
plot(tsol6*1e3, hsol6*1e3,'LineWidth',LineWidth, ...
        'Color', color_ss)
hold on
picturewidth = 20;
hw_ratio = 0.3;
%title('Phase 1+2+3+4+5+6')
ylabel('$h$ $(mm)$')
xlabel('$t$ $(ms)$')
set(findall(hfig2,'-property','FontSize'),'FontSize',Fontsize)
set(findall(hfig2,'-property','FontName'),'FontName','
    TimesNewRoman')
set(findall(hfig2,'-property','Interpreter'),'Interpreter','
    latex')
set(findall(hfig2,'-property','TickLabelInterpreter'),'
    TickLabelInterpreter','latex')
set(gca, 'Box','on','LineWidth',2)
set(hfig2,'Units','centimeters','Position',[3 3 picturewidth hw_
    ratio*picturewidth])
legend('Interpreter','latex','FontSize',Fontsize, ...
    'Location','northeast', 'AutoUpdate','off',...
```

```
    'NumColumns',1, 'Orientation','horizontal', ...
    'Box','off')
%% Phase 7:
t7 =0.75;
tsol7 = linspace(t6,t7, 50);
Psol7 = 0*tsol7 + P_sup;
hsol7 = 0*tsol7;
figure(1)
plot(tsol7*1e3, Psol7*1e-5,'LineWidth',LineWidth, ...
        'Color', color_ss)
hold on
picturewidth = 20;
hw_ratio = 0.5;
title('Pressure change over time in injector at different
    working load')
ylabel('$P$ $(bar)$')
xlabel('$t$ $(ms)$')
set(findall(hfig1,'-property','FontSize'),'FontSize',Fontsize)
set(findall(hfig1,'-property','FontName'),'FontName','
    TimesNewRoman')
set(findall(hfig1,'-property','Interpreter'),'Interpreter','
    latex')
set(findall(hfig1,'-property','TickLabelInterpreter'),'
    TickLabelInterpreter','latex')
set(gca, 'Box','on','LineWidth',2)
set(hfig1,'Units','centimeters','Position',[3 3 picturewidth hw_
    ratio*picturewidth])
legend('Interpreter','latex','FontSize',Fontsize, ...
    'Location','northeast', 'AutoUpdate','on',...
    'NumColumns',1, 'Orientation','horizontal', ...
    'Box','off')
hfig2 = figure(2);
plot(tsol7*1e3, hsol7*1e3,'LineWidth',LineWidth, ...
        'Color', color_ss)
hold on
picturewidth = 20;
hw_ratio = 0.5;
title('Valve lift height at different working load')
ylabel('$h$ $(mm)$')
xlabel('$t$ $(ms)$')
set(findall(hfig2,'-property','FontSize'),'FontSize',Fontsize)
```

```
set(findall(hfig2,'-property','FontName'),'FontName','
    TimesNewRoman')
set(findall(hfig2,'-property','Interpreter'),'Interpreter','
    latex')
set(findall(hfig2,'-property','TickLabelInterpreter'),'
    TickLabelInterpreter','latex')
set(gca, 'Box','on','LineWidth',2)
set(hfig2,'Units','centimeters','Position',[3 3 picturewidth hw_
    ratio*picturewidth])
legend('Interpreter','latex','FontSize',Fontsize, ...
    'Location','northeast', 'AutoUpdate','on',...
    'NumColumns',1, 'Orientation','horizontal', ...
    'Box','off')
```

This page intentionally left blank

C

DERIVATION OF ISENTROPIC FLOW FUNCTION

Nomenclature

A	cross-sectional area of flowing element
γ	weight density of fluid medium before inlet into flowing element
g	acceleration of gravity
h	height of current point at free fall
H	general height of fall
k	adiabatic exponent
L	general length of flowing element
p_0, p_h	quantities of pressure before inlet and on outlet of flowing element accordingly
$p_{st}(l)$	static head in stream
R	gas constant
T_0	thermodynamic temperature before inlet into flowing element
V_{ex}	outflow velocity (average in cross-section)
V_{max}	maximum possible outflow velocity

1 Introduction

The development of modern groundworks of gas dynamics in the field of the flowing elements and systems is bound with necessity not only to create of the physically adequate conceptual ideas and to derive on its base of new mathematical expressions, but also revise and find the final form of some existing formulae. Saint-Venant–Wantzel's formula for determining of the outflow velocity of gas stream out of flowing element, system under specified value of pressure drop is one of the formulae, which has major value in gas dynamics of flowing systems and to which it is necessary to impart the final form.

2 Approach

The considered formula is a product of long-term development. Its history was started by Torricelli and Galilei experiments with the drop water stream in 1643. Further, approximately 120 years later, Borda and Du Buat have given to it the final form for mechanics and hydraulics.

After, about 60 years later (1839), Saint-Venant and Wantzel had substituted the available work of gas expansion in the conditions of mechanical and thermal isolation instead of height of free fall in the Torricelli-Galilei-Borda-DuBuat (TGBD) formula. So, SVW formula was appeared:

$$V_{ex} = \sqrt{2g\left\{\frac{k}{k-1}RT_0\left[1-\left(\frac{p_h}{p_0}\right)^{\frac{k-1}{k}}\right]\right\}} \quad (1)$$

or

$$V_{ex} = \sqrt{\frac{2}{k-1}kgRT_0\left[1-\left(\frac{p_h}{p_0}\right)^{\frac{k-1}{k}}\right]} \quad (2)$$

Writing of SVW formula in the form (1) exactly conform to substitution in TGBD formula of the available work of gas expansion in reversible adiabatic (isentropic) process. Writing of SVW formula in the form (2) imply that the outflow velocity of gas stream out of flowing element is determined by the product of a maximum possible outflow velocity of gas (outflow in vacuum) and the dimensionless radicand containing initial p_0

Figure C.1: Derivation of isentropic flow function[30]

and final p_h pressures. In the contracted form it will match of the writing:

$$V_{ex} = V_{max}\sqrt{1-\left(\frac{p_h}{p_0}\right)^{\frac{k-1}{k}}} \qquad (3)$$

Having written TGBD formula in the form:

$$V = \sqrt{2gH\left(1-\frac{h}{H}\right)} \equiv V_{max}\sqrt{1-\frac{h}{H}} \qquad (4)$$

it is not difficult to detect that H is simultaneously both difference of potentials of the propulsive energy, and the spatial longitudinal coordinate of the motion during the free fall in it.

At comparison of the TGBD and SVW formulae also it is not difficult to note, that the spatial coordinate of motion vanishes in SVW formula when the available work of gas expansion in the reversible adiabatic process is substituted instead of the height of free fall in TGBD formula. This feature is entirely typical for thermodynamics, however the usefulness of the SVW formula becomes more than doubtful for calculation of outflow velocity out of flowing element. So, both viewed formulae are non-connected with any kind of the interaction of the moving solid, fluid medium with ambient objects and mediums. And alongside with it the spatial coordinate of motion is absent in SVW formula. At first sight the unfavourable situation becomes constructive at the approach to it from the positions of contact interaction energy. The SVW formula according to such approach is the conservation equation of energy (the weight or volume density of energy more precisely) in the simplest form. The problem is to take into account the spatially - energy connection of the flowing system the physically adequately and mathematically correctly in this conservation equation. The mathematical expression for the spatially - energy connection of gas stream with wall of flowing element is necessary to have and to know, how this connection will be inserted into considered equation for the solution of the problem.

3 Solution

The mathematical expression of the spatially - energy connection of gas stream with wall is shown in [1, 2] in the form of static head law for gas stream in flowing element. There are simultaneously the contact interaction energy of gas stream with streamline surface and power of the counter pressure in this law. This second factor has been presented in the traditional form of the writing of SVW formula. The solution of the formulated problem is reduced to replacement of p_h by $p_{st}(L)$ in the mentioned formulae (1,2). In the result we finds:

$$V_{ex} = \sqrt{\frac{2}{k-1}kgRT_0\left\{1-\left[\frac{p_{st}(L)}{p_0}\right]^{\frac{k-1}{k}}\right\}} \qquad (5)$$

or

$$V_{ex} = V_{max}\sqrt{1-\left[\frac{p_{st}(L)}{p_0}\right]^{\frac{k-1}{k}}} \qquad (6)$$

The weight-flow formula accordingly looks like:

$$G = A\gamma_0\left(\frac{p_h}{p_0}\right)^{\frac{1}{k}}V_{max}\sqrt{1-\left[\frac{p_{st}(L)}{p_0}\right]^{\frac{k-1}{k}}} \qquad (7)$$

Expressions (5,6) are the final form of the formula for the outflow velocity of gas stream out of the flowing element. The obtained expressions have generality, and SVW formula is its particular form for solution of problem concerned with the description of the gas pointwise - symmetric (spherical) expansion in gaseous medium. At the same time the mass centre of the gas is kept in rest.

4 Discussion of results

The obtained expression in the forms (5, 6) implies, that the actual outflow velocity of gas stream is determined as kinematic parameter of motion by its maximum possible quantity at outflow to empty space (V_{max}) with taking into account of energy contents of the outflowing and surrounding mediums and intensity of contact interaction of gas stream with the walls of the flowing element. Such the physical sense is much wider than sense included in it by Saint-Venant and Wantzel and consisting in the simple substitution of expression for the available work of gas expansion at reversible adiabatic (polytropic) process instead of height of free fall in TGBD formula. The new physical sense is wider as well than the traditional thermodynamic interpretation, according to which the outflow velocity is determined by difference of heat contents (enthalpies) of outflowing and surrounding mediums.

The distinguish of principle of the new formula is also what the process of the motion is presented as a mechanically irreversible process in it. This property of motion of gas stream in the flowing element is the alienable and permanent factor. The heat exchange can be absent. In this case, the out-

Figure C.2: Derivation of isentropic flow function[30]

This page intentionally left blank

BIBLIOGRAPHY

[1] Caglar Dere. "Hydrogen Fueled Engine Technology, Adaptation, and Application for Marine Engines." In: *Decarbonization of Maritime Transport*. Springer, 2023, pp. 45–63.

[2] Satista. *Shipping emissions worldwide*. https://www-statista-com.tudelft.idm.oclc.org/study/140542/global-shipping-emissions/, Last accessed on 2023-9-10. 2023.

[3] A.P.Moller-Maersk. *Sustainability Report*. https://www.maersk.com/sustainability, Last accessed on 2023-9-10. 2022.

[4] MSC. *Sustainability Report*. https://www.msc.com/en/sustainability, Last accessed on 2023-9-10. 2022.

[5] IMO. *IMO's work to cut GHG emissions from ships*. https://www.imo.org/en/MediaCentre/HotTopics/Pages/Cutting-GHG-emissions.aspx, Last accessed on 2023-9-10. 2023.

[6] Kai Zeng and Dongke Zhang. "Recent progress in alkaline water electrolysis for hydrogen production and applications." In: *Progress in energy and combustion science* 36.3 (2010), pp. 307–326.

[7] Mustafa Balat and Mehmet Balat. "Political, economic and environmental impacts of biomass-based hydrogen." In: *International journal of hydrogen energy* 34.9 (2009), pp. 3589–3603.

[8] T Petkov, TN Veziroğlu, and JW Sheffield. "An outlook of hydrogen as an automotive fuel." In: *International Journal of Hydrogen Energy* 14.7 (1989), pp. 449–474.

[9] Zbigniew Stępień. "A comprehensive overview of hydrogen-fueled internal combustion engines: Achievements and future challenges." In: *Energies* 14.20 (2021), p. 6504.

[10] IMO. *Second IMO Symposium on low- and zero-carbon fuels for shipping*. https://www.imo.org/en/MediaCentre/SecretaryGeneral/Pages/Second-IMO-Symposium-on-low--and-zero-carbon-fuels-for-shipping-Ensuring-a-just-and-inclusive-transition-towards-low-carbon.aspx, Last accessed on 2023-9-10. 2022.

[11] Jeya Jeevahan, G Mageshwaran, G Britto Joseph, RB Durai Raj, and R Thamarai Kannan. "Various strategies for reducing No x emissions of biodiesel fuel used in conventional diesel engines: A review." In: *Chemical Engineering Communications* 204.10 (2017), pp. 1202–1223.

[12] G Dnv. "Assessment of selected alternative fuels and technologies in shipping." In: *DNV GL* (2019).

[13] Wenjing Qu, Yuan Fang, Zixin Wang, Hongjie Sun, and Liyan Feng. "Optimization of injection system for a medium-speed four-stroke spark-ignition marine hydrogen engine." In: *International Journal of Hydrogen Energy* 47.44 (2022), pp. 19289–19297. ISSN: 0360-3199. DOI: https://doi.org/10.1016/j.ijhydene.2022.04.096. URL: https://www.sciencedirect.com/science/article/pii/S0360319922016093.

[14] Karsten Wittek, Vitor Cogo, and Geovane Prante. "Development of a pneumatic actuated low-pressure direct injection gas injector for hydrogen-fueled internal combustion engines." In: *International Journal of Hydrogen Energy* 48.27 (2023), pp. 10215–10234.

[15] Murat Ciniviz and Hüseyin Köse. "Hydrogen use in internal combustion engine: a review." In: *International Journal of Automotive Engineering and Technologies* 1.1 (2012), pp. 1–15.

[16] Ronak Dipakkumar Gandhi. "Use of hydrogen in internal combustion engine." In: *International Journal of Engineering and Technical Research (IJETR)* 3.2 (2015), pp. 207–216.

[17] Raphael Ryser, Michael Willmann, Gerald Müller, and Michael Gisiger. "Turbocharging and Synthetic Fuels." In: *MTZ worldwide* 82.5 (2021), pp. 44–49.

[18] GP Subash and LM Das. "An experimental investigation on the performance and emission characteristics of a hydrogen fueled spark ignition engine." In: *Int. J. Sci. Technol. Manag* 8 (2011), pp. 197–208.

[19] Stanislaw Szwaja and Karol Grab-Rogalinski. "Hydrogen combustion in a compression ignition diesel engine." In: *International journal of hydrogen energy* 34.10 (2009), pp. 4413–4421.

[20] N Saravanan and G Nagarajan. "An experimental investigation of hydrogen-enriched air induction in a diesel engine system." In: *International journal of hydrogen energy* 33.6 (2008), pp. 1769–1775.

[21] JM Gomes Antunes, Rikard Mikalsen, and AP Roskilly. "An experimental study of a direct injection compression ignition hydrogen engine." In: *International journal of hydrogen energy* 34.15 (2009), pp. 6516–6522.

[22] Madhujit Deb, Abhishek Paul, Durbadal Debroy, GRK Sastry, Raj Sekhar Panua, and PK Bose. "An experimental investigation of performance-emission trade off characteristics of a CI engine using hydrogen as dual fuel." In: *Energy* 85 (2015), pp. 569–585.

[23] Mithun Kanti Roy, Nobuyuki Kawahara, Eiji Tomita, and Takashi Fujitani. "High-pressure hydrogen jet and combustion characteristics in a direct-injection hydrogen engine." In: *SAE International Journal of Fuels and Lubricants* 5.3 (2012), pp. 1414–1425.

[24] Moritz Schumacher and Michael Wensing. *Investigations on an injector for a low pressure hydrogen direct injection*. Tech. rep. SAE Technical Paper, 2014.

[25] Sebastian Verhelst, Thomas Wallner, and Roger Sierens. "Hydrogen-Fueled internal combustion engines." In: *Handb Hydrog Energy* 35 (2014), pp. 821–902.

[26] Karsten Wittek. "Gas injection device for a reciprocating internal combustion engine." DE102020127020B3 (HOCHSCHULE

HEILBRONN Office). HOCHSCHULE HEILBRONN. Mar. 2020.

[27] Aart-Jan van der Hoeven. "Crankshaft Modeling & Identification for Cylinder Pressure Estimation-confidential." In: ().

[28] Marcel Ott, Roland Alder, and Ingemar Nylund. "Low Pressure Dual-fuel Technology for Low Speed Marine Engines." In: *ATZextra worldwide* 20.10 (2015), pp. 34–39.

[29] WinGD. *X92DF-2.0*. https://www.wingd.com/en/engines/engine-types/lng-dual-fuel-engines/x92df-2-0/, Last accessed on 2024-7-7. 2024.

[30] SL Arsenjev, IB Lozovitski, and YP Sirik. "The Flowing System Gasdynamics. Part 3: Saint-Venant-Wantzel formula modern form." In: *arXiv preprint physics/0302038* (2003).

ACKNOWLEDGMENTS

First and foremost, I would like to express my deepest gratitude to my supervisor, Prof. Peter de Vos. Without his guidance, this thesis would not have been possible. He provided me with invaluable advice and corrections throughout the research process, and his concern for my mental well-being made me feel welcomed and supported as an international student far from home.

I would also like to extend my sincere thanks to Ir. Erin Van Rheenen for her constructive feedback on my literature review and master's thesis, which greatly enhanced the quality of my work.

Furthermore, I am deeply grateful to Ir. Ning Ji and Ir. TzuYao Huang, PhD candidates at Delft, who have been great friends and mentors. Their substantial assistance during my research significantly improved my coding skills, and they helped me develop a scientific approach to writing throughout the thesis preparation process.

Lastly, I owe my heartfelt thanks to my parents and girlfriend back in China for their unwavering support during my studies abroad. Their encouragement provided me with the strength to overcome challenges and setbacks, making my academic journey possible.

Wenchao Jiao,
Delft, August 2024

This page intentionally left blank

COLOPHON

This document was typeset using the typographical look-and-feel `classicthesis` developed by André Miede and Ivo Pletikosić. The style was inspired by Robert Bringhurst's seminal book on typography *"The Elements of Typographic Style"*. `classicthesis` is available for both LaTeX and LyX:

https://bitbucket.org/amiede/classicthesis/

Final Version as of 2024-08-12 (classicthesis v4.6).